Fine Sediment Dynamics in the southern North Sea

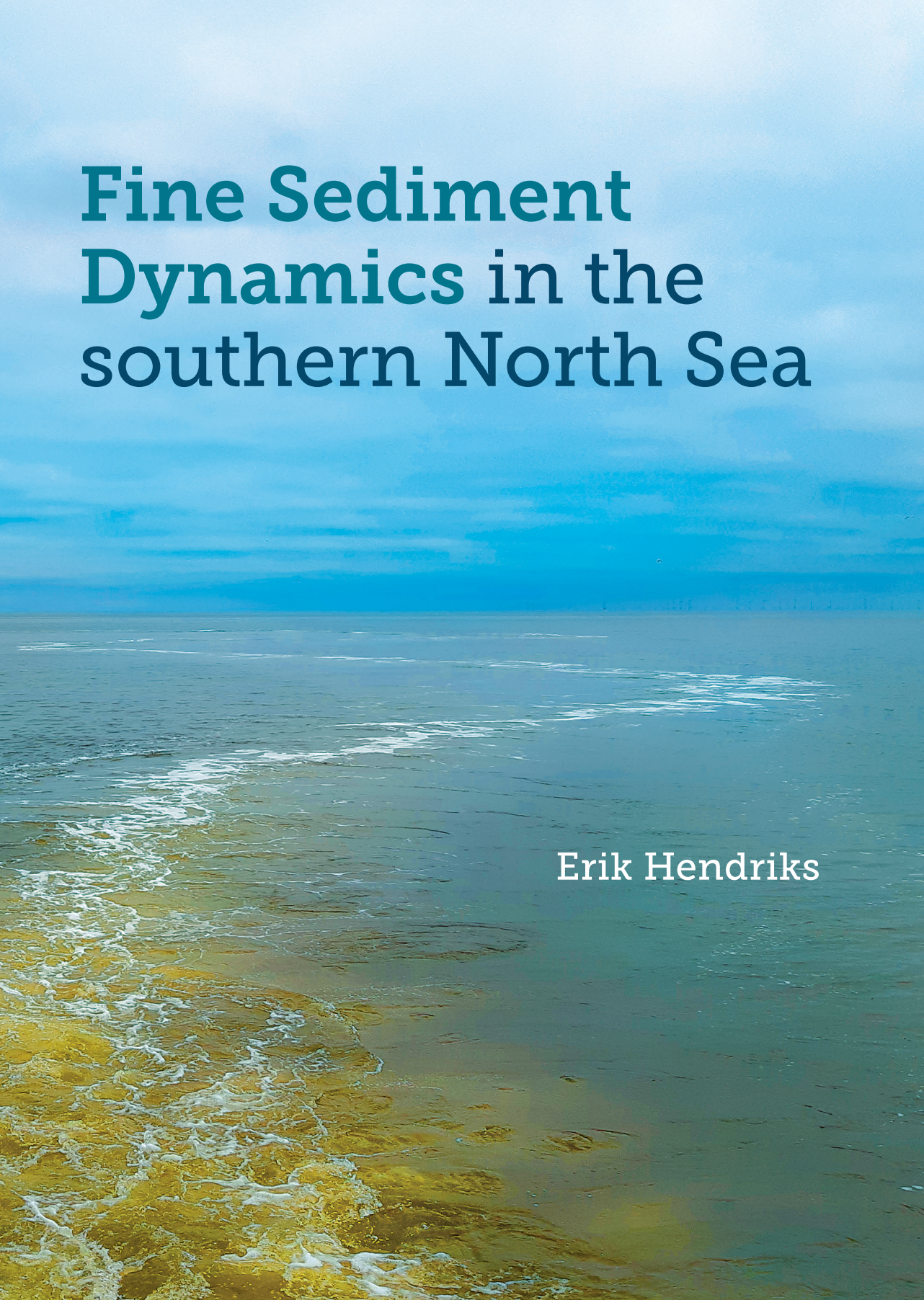

Erik Hendriks

FINE SEDIMENT DYNAMICS IN THE SOUTHERN NORTH SEA

FINE SEDIMENT DYNAMICS IN THE SOUTHERN NORTH SEA

Dissertation

for the purpose of obtaining the degree of doctor
at Delft University of Technology
by the authority of the Rector Magnificus Prof. dr. ir. H. Bijl,
chair of the Board for Doctorates
to be defended publicly on
Thursday, 5 February 2026 at 15:00 o'clock

by

Henricus Cornelis Maria HENDRIKS

Master of Science in Civil Engineering,
Delft University of Technology, The Netherlands,
born in 's-Hertogenbosch, The Netherlands.

This dissertation has been approved by the promotors.

Composition of the doctoral committee:

Rector Magnificus,	chairperson
Dr. ir. B.C. van Prooijen,	Delft University of Technology, *promotor*
Prof. dr. ir. S.G.J. Aarninkhof,	Delft University of Technology, *promotor*

Independent members:

Prof.dr. J.D. Pietrzak,	Delft University of Technology
Prof. dr. V. Van Lancker,	Institute of Natural Sciences and Ghent University, Belgium
Prof.dr. M.G. Kleinhans,	Utrecht University
Dr. M.J. Baptist,	Wageningen University and Research
Prof.dr. ir. M. van Koningsveld,	Delft University of Technology, *reserve member*

Other members:

Em. prof. dr. ir. J.C. Winterwerp,	Delft University of Technology

Em. prof. dr. ir. J.C Winterwerp of Delft University of Technology has, as supervisor, contributed significantly to the preparation of this dissertation.

This work is part of the research programme SANDBOX (Smart and sustainable design for offshore operations in a sandy seabed) with project number 871.15.011, which is (partly) financed by the Dutch Research Council (NWO).

Keywords: fine sediment, North Sea, seabed, human activities

Printed by: Ridderprint

Cover by: Joey Roberts - Ridderprint

ISBN 978-94-6518-206-3

An electronic copy of this dissertation is available at
https://repository.tudelft.nl/.

The sea, the great unifier, is man's only hope.
Now, as never before, the old phrase has a literal meaning:
we are all in the same boat.

Jacques-Yves Cousteau

CONTENTS

SUMMARY

The North Sea is one of the world's most intensively used coastal seas, supporting activities such as sand mining, fishing, offshore energy development, dredging, and shipping. It provides essential economic and societal benefits to surrounding nations. Equally important, the North Sea serves as a vital habitat for a wide variety of marine species. Assessing the impact of human activities on this ecosystem requires a clear understanding of the key physical processes at play. One such process is the transport of fine sediment, which influences turbidity, light availability, nutrient cycling, and habitat characteristics. Yet, the processes governing the exchange of fine sediment between the mostly sandy seabed and the water column remain poorly understood. This research addresses that gap by examining the spatial and temporal dynamics of fine sediment and the mechanisms of burial and remobilisation.

The main objective of this research is: How does the seabed–water column exchange of fine sediment influence the spatial and temporal distribution of fines in the southern North Sea? This question is addressed primarily through the analysis of field data. In addition to being one of the world's most intensively used coastal seas, the North Sea is also among the most extensively monitored, offering a wealth of observational data across spatial and temporal scales. To leverage this, our research draws on a large-scale sediment dataset, long-term in-situ measurements, and both conceptual and mechanistic modelling approaches. These are complemented by novel data collected during targeted field campaigns.

By analysing the large-scale sediment dataset, collected from 2005 until 2017 in the Dutch Coastal Zone, we unravelled the spatial distribution of fines in the upper seabed layer. In this area, fines are not uniformly distributed but exhibit strong spatial variability across three distinct scales: macro (tens of kilometres), meso (hundreds of metres to kilometres) and micro (centimetres to metres). To interpret these patterns, we developed a conceptual framework consisting of three components: sources of fines, transport pathways, and accumulation potential. At the macro scale, fines are primarily concentrated in a 20-kilometre-wide coastal band along the Dutch coast, governed mainly by sediment sources and transport pathways. At the meso scale, fines deposits occur near the Rhine outflow, dredged sediment disposal sites, and former estuarine channels, with mass percentages of up to 20 %. On the micro scale, fines distribution is highly patchy due to burial processes that introduce vertical and horizontal heterogeneity. Human interventions such as sand mining and land reclamation affect the meso-scale distribution by introducing new sources and changing the accumulation potential. The macro-scale distribution is only affected when either sources or transport pathways change, affecting the supply of fines.

We then examined the short-term burial of fines into the seabed. This takes place in the wake of storms, and occurs on a timescale of days to a week. It is primarily driven by

the interaction of storm-induced megaripples and current-induced ripples: as megaripples decay under calmer conditions, smaller ripples migrate into their troughs, burying fines to depths of 10–15 cm. This mechanism introduces significant vertical and horizontal variability in fines presence within the seabed. A four-phase mechanistic model was developed to describe this dynamic burial cycle, supported by sediment cores and seabed imagery. Burial efficiency depends on the balance between storm intensity and tidal current magnitude, with optimal conditions occurring under moderate currents.

Remobilisation of fines occurs when storms generate megaripples on the sandy seabed, triggering a rapid increase in suspended sediment concentration (SSC). SSC typically peaks within one to two days after the wave height maximum and returns to pre-storm levels within one to six days, resulting in an asymmetric response to hydrodynamic forcing. To quantify this process, we developed a bedform release model that links remobilisation fluxes directly to the formation and evolution of storm-induced bedforms. Validated against a 21-month in-situ dataset, the model showed a good agreement with observed SSC peaks. This process-based approach clarifies the physical basis of existing erosion formulations used in numerical models and supports the interpretation and calibration of their aggregated parameters. These findings highlight the critical role of bedform dynamics in controlling the exchange of fines between the seabed and the water column.

Our work demonstrates that fine sediment dynamics in the North Sea are governed by a tightly coupled seabed-water column system with pronounced memory effects. Small-scale processes must be taken into account to understand the exchange of fine sediment with the sandy seabed. The conceptual and mechanistic models developed here offer tools for designing effective monitoring strategies and assessing the cumulative impact of human activities. These insights are particularly relevant in the context of the ongoing energy, food, and nature transitions taking place on the North Sea. For these transitions to succeed, science-based management of the North Sea is required. Such management should rely on a combination of targeted measurements, long-term monitoring and numerical modelling. Our research provides key knowledge for research programmes such as Wozep and MONS, and contributes to safeguarding the ecological integrity of this vital marine ecosystem through informed, forward-looking decision-making.

SAMENVATTING

De Noordzee is een van de meest intensief gebruikte kustzeeën ter wereld. Ze biedt ruimte aan uiteenlopende menselijke activiteiten zoals zandwinning, visserij, offshore energieopwekking, baggeren en scheepvaart. Daarmee levert de zee essentiële economische en maatschappelijke baten aan de haar omringende landen. Een niet minder belangrijke rol van de Noordzee is dat zij een essentieel habitat vormt voor een grote verscheidenheid aan mariene soorten. Het beoordelen van de invloed van menselijke activiteiten op dit ecosysteem vereist een goed begrip van de belangrijkste fysische processen. Een van deze processen is het transport van fijn sediment (*slib*), dat invloed heeft op vertroebeling, het lichtklimaat, nutriëntentransport en habitatkenmerken. De processen die de uitwisseling van fijn sediment tussen de overwegend zandige zeebodem en de waterkolom bepalen, zijn echter nog onvoldoende begrepen. Dit onderzoek richt zich op deze kennislacune door de ruimtelijke en temporele dynamiek van fijn sediment en de mechanismen van begraving en remobilisatie te onderzoeken.

De centrale onderzoeksvraag van dit onderzoek luidt: Hoe beïnvloedt de uitwisseling tussen de zeebodem en de waterkolom de ruimtelijke en temporele verspreiding van fijn sediment in de zuidelijke Noordzee? Deze vraag wordt voornamelijk onderzocht aan de hand van in-situ gemeten data. Naast haar intensieve gebruik is de Noordzee immers ook een van de best gemonitorde kustzeeën ter wereld. Daardoor is er een schat aan data beschikbaar op verschillende ruimtelijke en temporele schalen. Om hier optimaal gebruik van te maken, benutten we in dit onderzoek een grootschalige sedimentdataset, langdurige in-situ metingen en zowel conceptuele als mechanistische modellering. Deze worden aangevuld met nieuwe gegevens die zijn verzameld tijdens gerichte veldcampagnes.

Door analyse van de sedimentdataset, verzameld tussen 2005 en 2017 in de Nederlandse kustzone, is de ruimtelijke verdeling van fijn sediment in de bovenste laag van de zeebodem in kaart gebracht. Fijn sediment is zeer heterogeen verdeeld en vertoont sterke variatie op drie ruimtelijke schalen: macro (tientallen kilometers), meso (honderden meters tot kilometers) en micro (centimeters tot meters). Om deze ruimtelijke patronen te verklaren hebben we een conceptueel raamwerk ontwikkeld met drie componenten: bronnen van fijn sediment, transportpaden en accumulatiepotentieel. Op de macroschaal is fijn sediment vooral geconcentreerd in een strook van circa 20 kilometer breed langs de Nederlandse kust, voornamelijk bepaald door sedimentbronnen en transportpaden. Op de mesoschaal komen afzettingen voor nabij de Rijnmonding, verspreidingslocaties van gebaggerd materiaal, en voormalige estuaria. Op deze locaties kunnen massapercentages slib oplopen tot 20%. Op de microschaal is de verdeling zeer grillig door begravingsprocessen die zowel verticale als horizontale variatie veroorzaken. Menselijke ingrepen zoals zandwinning en landaanwinning beïnvloeden de verdeling op mesoschaal wanneer zij nieuwe bronnen introduceren of het accumulatiepotentieel

wijzigen. De verdeling op macroschaal verandert alleen wanneer bronnen of transportpaden veranderen en daarmee de aanvoer van fijn sediment beïnvloeden.

Vervolgens hebben we de begraving van fijn sediment in de zeebodem onderzocht. Dit proces treedt op na stormen en speelt zich af op een tijdschaal van dagen tot ongeveer een week. Het wordt aangedreven door de interactie tussen door stormen gevormde megaribbels en stromingsribbels: na een storm migreren de ribbels in de troggen van afvlakkende megaribbels, waardoor fijn sediment tot 10–15 cm diep wordt begraven. Het fijn sediment dat op deze manier wordt begraven, blijft naderhand voor een periode van weken tot maanden in de zeebodem aanwezig, totdat een volgende storm het opnieuw mobiliseert. Dit mechanisme leidt tot aanzienlijke verticale en horizontale variatie in de aanwezigheid van fijn sediment in de zeebodem. Om deze dynamiek te beschrijven, is een mechanistisch model met vier fasen ontwikkeld, ondersteund door sedimentmonsters en beelden van de zeebodem. De efficiëntie van begraving hangt af van de verhouding tussen stormintensiteit en stroomsnelheid, met optimale omstandigheden bij gematigde stroomsnelheden.

Remobilisatie van fijn sediment treedt op wanneer stormen megaribbels vormen op de zandige zeebodem, wat leidt tot een snelle toename van de concentratie van zwevend sediment (*SSC*). Deze concentratie piekt doorgaans één tot twee dagen na de maximale golfhoogte en keert binnen één tot zes dagen terug naar het niveau van vóór de storm. Dit leidt tot een asymmetrische respons van SSC op hydrodynamische forcering. Om dit proces te kwantificeren, is een bedvorm-remobilisatiemodel ontwikkeld dat remobilisatiefluxen direct koppelt aan de vorming en evolutie van stormgeïnduceerde megaribbels. Het model is gevalideerd met een 21 maanden omvattende in-situ dataset en vertoont goede overeenstemming met waargenomen SSC-pieken. Deze procesgebaseerde benadering biedt een fysisch onderbouwde verklaring voor bestaande erosieformuleringen in numerieke modellen, en draagt bij aan de interpretatie en kalibratie van de daarin toegepaste parameters. Deze bevindingen bevestigen het belang van bodemvormdynamiek bij de uitwisseling van fijn sediment tussen de zeebodem en de waterkolom.

Ons onderzoek toont aan dat de dynamiek van fijn sediment in de Noordzee wordt gestuurd door een nauw gekoppeld systeem van zeebodem en waterkolom, met uitgesproken geheugeneffecten. Om de uitwisseling van fijn sediment met de zandige zeebodem goed te begrijpen, is het essentieel om kleinschalige processen mee te nemen. De ontwikkelde conceptuele en mechanistische modellen bieden handvatten voor het opzetten van effectieve monitoringsstrategieën en het beoordelen van de cumulatieve impact van menselijke activiteiten. Deze inzichten zijn bijzonder relevant in het licht van de lopende energie-, voedsel- en natuurtransities op de Noordzee. Voor het slagen van deze transities is wetenschappelijk onderbouwd beheer van de Noordzee noodzakelijk, gebaseerd op gerichte metingen, langdurige monitoring en numerieke modellering. Ons onderzoek levert essentiële kennis voor programma's zoals Wozep en MONS, en draagt bij aan het behoud van dit vitale mariene ecosysteem via geïnformeerde, toekomstgerichte besluitvorming.

1

INTRODUCTION

1

1.1. THE NORTH SEA - ONE OF THE WORLDS BUSIEST SEAS

Throughout its history, the Netherlands has always had a love-hate relationship with its seaward neighbour: the North Sea. The relatively short period of the Netherlands as an influential geopolitical power in the 17th century arose mainly because of its naval strength and control over North Sea waters. On the other hand, the North Sea also proved to be perilous: some of the greatest natural disasters in Dutch history were times when water from the North Sea flooded the low-lying lands.

During the past century, our relationship with the North Sea gradually changed. Through continued efforts, the flooding threat decreased. First, by the construction of the Delta Works, which was followed by widespread nourishing of the sandy coast. While the threat diminished, the economic importance of the North Sea began to grow.

During the 20th century, human activities on the North Sea intensified. Sand is mined from designated areas in increasing volumes, both to nourish the sandy coast and to raise land (Stolk and Dijkshoorn 2009). Bottom-trawled fishing evolved from a small-scale to an industrial fleet, regularly sweeping the seabed (Callaway *et al.* 2007, Rijnsdorp *et al.* 2008). In this same period, some of the worlds largest ports (e.g., Rotterdam, Hamburg, Antwerp) developed in the countries surrounding the North Sea. Designated shipping lanes across the North Sea provide access to these port areas and are among the world's busiest shipping routes (Robbins *et al.* 2022). Furthermore, maintenance dredging is required in port basins to maintain a navigable depth, most of which is then spread out at sea (Fettweis *et al.* 2012, Hendriks and Schuurman 2017). The last major development of the 20th century occurred after large oil and gas resources were discovered in the North Sea subsurface in the 1960s. In the following decades, this developed into a sizeable industry, extracting oil and gas from the subsurface through offshore platforms (Sanchez *et al.* 2023). An overview of several activities taking place in the Dutch Coastal Zone (DCZ), the 70-km wide area directly adjacent to the Dutch coast, is shown in Figure 1.1 (Visser *et al.* 1991).

Figure 1.1 also shows the latest major development on the North Sea: offshore wind. To decrease fossil fuel dependency, wind turbines are constructed in offshore wind farms (Breton and Moe 2009) (Figure 1.1), along with auxiliary infrastructure such as cables and landfalls (de Groot 1982, Rouse *et al.* 2017). Although the intensity of some other activities may decrease, the large-scale development of offshore wind will likely lead to a further intensification of human activities on the North Sea (Degraer *et al.* 2019, Emeis *et al.* 2015). The large ambitions for offshore wind (Gușatu *et al.* 2021, Steins *et al.* 2021) may well lead to a 'race for space' in the coming decades.

However, a purely economic or technical perspective disregards a crucial aspect of the North Sea: its role as a nature reserve and habitat for a wide variety of marine species (OSPAR 2023). The species living in the North Sea can only be sustained by a healthy ecosystem, and therefore preserving this ecosystem is of vital importance. To achieve a healthy North Sea, a proper balance between economic and ecological interests is essential (Degraer *et al.* 2019). For this, we need to understand how human activities affect the North Sea ecosystem and quantify their ecological impact (Piet *et al.* 2019).

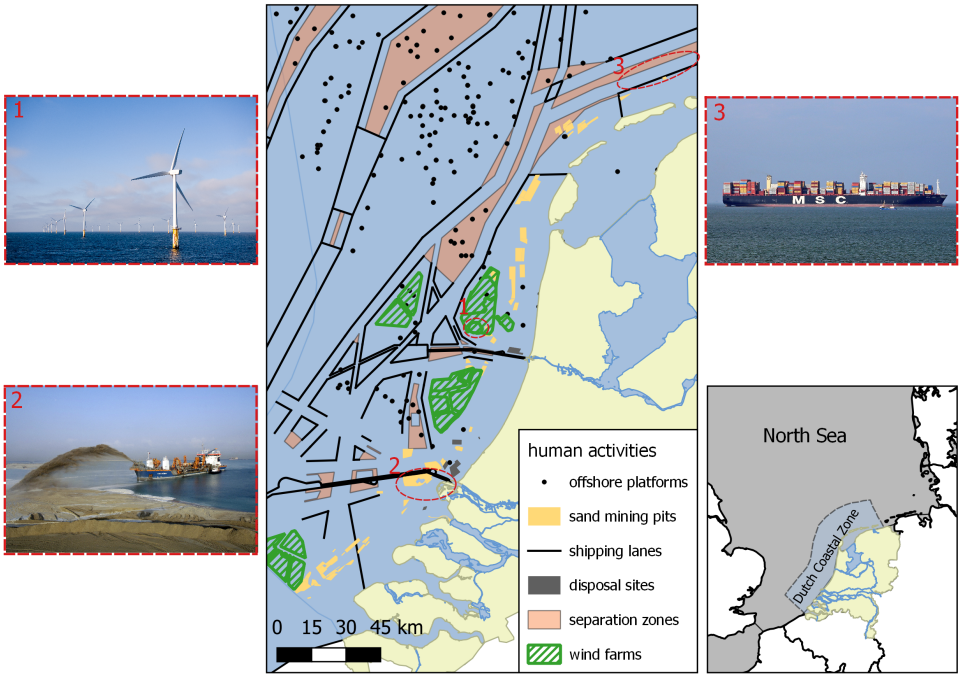

Figure 1.1.: Overview of Dutch Coastal Zone (DCZ), with examples of human activities taking place. These activities include the (1) construction and operation of offshore wind farms, (2) sand mining, (3) shipping, dredged sediment disposal and oil and gas extraction. *Images taken from: beeldbank.rws.nl.*

1.2. THE NORTH SEA ECOSYSTEM - AND HOW HUMAN ACTIVITIES AFFECT IT

The North Sea ecosystem consists of two main subsystems: the seabed and the overlying water column, i.e., the benthic and pelagic environment. Together, they form a coupled system with many interconnected processes (e.g. Kirby *et al.* 2007, Provoost *et al.* 2013). For example, bottom-dwelling organisms feed on nutrients and plankton from the water column (Aldridge *et al.* 2007), while biogenic reefs on the seafloor may provide shelter and sources of food for fish and other pelagic species (van der Reijden *et al.* 2019).

Human activities affect both environments. The effect on the benthic environment is most apparent in the near-field of these activities (de Wit *et al.* 2014). For example, both sand mining and bottom trawling eliminate the benthic community in a certain area (de Jong 2016, Witbaard and Craeymeersch 2023), but outside of their footprint the direct effects are relatively limited.

Effects on the pelagic environment are often indirect, but may eventually lead to a larger ecosystem impact. One of the most important effects associated with human activities is the increase in turbidity in the water column. In the North Sea, this turbidity has increased steadily in the 20th century (Capuzzo *et al.* 2015), originating from the ad-

ditional *fine sediment* in suspension due to human activities. Due to increased turbidity, light penetration is hampered, which already occurs when suspended sediment concentrations increase by as little as 100 mg/l (van Duin *et al.* 2001) This eventually leads to a decrease in phytoplankton growth rates. As phytoplankton forms the base of the marine food web, this may affect a wide variety of marine species (Capuzzo *et al.* 2018).

A relatively recent example of this is provided by the Environmental Impact Assessment (EIA) for Maasvlakte II, the most recent seaward extension of the Port of Rotterdam. This study revealed how far-field environmental impact depended heavily on the additional fine sediment released due to large-scale sand mining (van Prooijen *et al.* 2007, van Kessel *et al.* 2011).

A key process determining the extent and magnitude of these far-field effects is the exchange of fine sediment with the mostly sandy seabed (van Kessel *et al.* 2011). As most of the North Sea is relatively shallow, with water depths of 30 metres or less, fine sediment is regularly exchanged between the water column and the seabed (Laane *et al.* 1999, van Kessel *et al.* 2011). Similarly to the ecosystem, the coupling between the water column and the seabed is crucial.

However, these fine sediment fluxes into and from the seabed are also the major unknowns in understanding fine sediment dynamics (e.g. Sanford 2008, Winterwerp *et al.* 2021). This limits the ability to correctly predict environmental impact. So, to better quantify far-field effects of human activities, we must obtain a better understanding of how fine sediment is exchanged with a sandy seabed.

1.3. FINE SEDIMENT IN A SANDY SEABED

In most parts of the southern North Sea, the seabed mainly consists of **sand** with a small fraction of **fines** in it (Eisma *et al.* 1987, Huthnance 1991, Irion and Zollmer 1999). These two sediment types behave fundamentally different. Sand has a grain size between 63 and 2000 μm and is non-cohesive. While suspended, sand particles have a constant in-situ density and settle relatively fast compared to fines, with a settling velocity in the order of 10^{-2} m/s (Ferguson and Church 2004). Fines, on the other hand, have a grain size smaller than 63 μm and are cohesive (Winterwerp and van Kesteren 2004). They form aggregates (i.e. flocs) with other small suspended particles. Hence, their in-situ density varies in time and is lower than that of sand. As a result, fines settle slowly once suspended, in the order of 10^{-3} to 10^{-4} m/s (van Kessel *et al.* 2011).

A combination of waves and currents, i.e., hydrodynamic forcing, can reshape the seabed and erode sediment from it (e.g., Soulsby 1997). The eroded sediment is then transported and deposits at another location. Eventually, the shape and composition of the seabed result from the balance between erosion and deposition (e.g., Reineck and Singh 1980).

Additionally, the combination of hydrodynamic forcing and seabed composition determines how much and what kind of sediment is brought into suspension (Winterwerp *et al.* 2021). Because of their difference in size, fines are generally more easily eroded than sand. When fines are readily available on the seabed, tidal currents in the North Sea are generally strong enough to resuspend them every tidal cycle (van Kessel *et al.* 2012, van der Hout *et al.* 2017). However, when they are buried within a sandy seabed,

their availability depends on the erodibility of the sandy seabed (van Kessel *et al.* 2011). So, to understand and quantify the fluxes of fine sediment into and from the seabed, we must also understand the dynamics of the sandy seabed itself.

These fluxes of fines into and from the sandy seabed are referred to as **burial** (into the seabed) and **remobilisation** (out of the seabed). The subsequent stages of burial and remobilisation are called **fine sediment exchange**. The sequence of these fluxes over time is indicated in Figure 1.2. We start from an initial situation (I) with a limited amount of fines in the water column, and a predominantly sandy seabed with a small fraction of fines. The fines present in the seabed can only be brought into suspension when they are remobilized from the seabed. This happens mainly during storms (II), when both sand and fines are eroded from the seabed and suspended due to a combination of waves and currents. As a result, suspended sediment concentrations increase strongly. When a storm wanes, fines will settle and deposit on top of the sand (III), because of the difference in settling velocity between the two sediment types. If fines would remain on top of the sandy seabed, this would have two consequences: (1) suspended sediment concentrations would remain high after storms as fines would be resuspended every tidal cycle and (2) the fines fraction in the seabed would eventually go to zero. Neither is the case. Hence, there must be a process which buries the fines in the seabed, resulting in a return to initial conditions (IV).

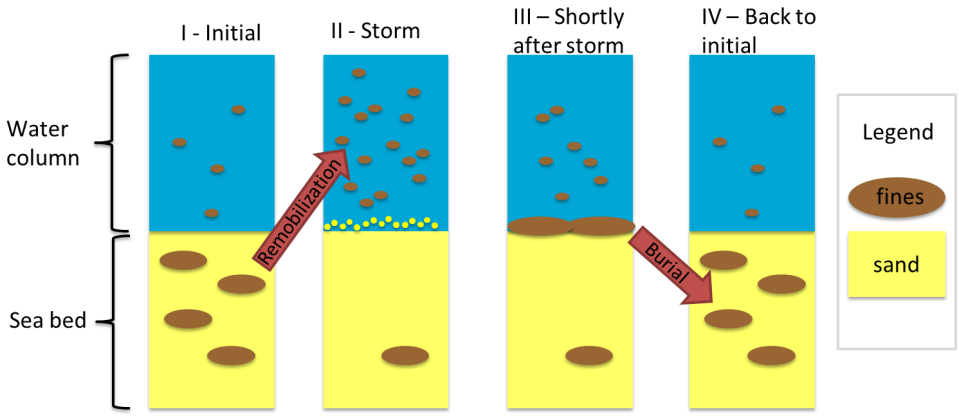

Figure 1.2.: Conceptual sketch of fine sediment exchange with a sandy seabed. (i) Shows the initial situation, where a small amount of fines is buried within the seabed. (II) During a storm, these buried fines are remobilized due to erosion of the sandy seabed. (III) Shortly after a storm, both the sand and and fines will deposit. Due to the difference in settling velocity, the fines will deposit on top of the sandy seabed. (IV) To return to the initial situation, the fines should be buried within the seabed again.

For this fine sediment exchange to occur, there must be a supply of fines. While this may seem trivial, it is a fundamental boundary condition: without a supply, neither burial nor remobilisation is possible.

In the southern North Sea, this supply can originate locally through seabed erosion or be transported in suspension from more distant sources (Eisma 1981, van Alphen 1990). The subtle balance between supply and the fraction that remains locally determines the spatial **distribution** of fines in the upper decimetres of the seabed (Winterwerp *et al.* 2021). This distribution, and its evolution over time, reflects the interplay between supply, burial, and remobilisation. Quantifying it is the first step in this thesis.

Beyond its intrinsic value, understanding the spatial distribution of fines also helps identify where burial and remobilisation are likely to occur and under what environmental conditions. This is essential for improving our understanding of these processes, which are not yet fully understood.

Dankers (2005) proposed several burial processes based on an extensive literature review, but these have yet to be validated with field data. For remobilisation, a process-based description is still lacking. Nonetheless, previous studies suggest that remobilisation occurs primarily during energetic conditions, such as storms, as the sandy substrate needs to be eroded (Kleinhans *et al.* 2005, van der Hout *et al.* 2017, Flores *et al.* 2017).

Accordingly, this thesis is structured around three main topics: (1) the **distribution** of fines in the seabed of the southern North Sea, (2) **burial** of fines, and (3) **remobilisation** of fines. These topics are addressed in this order throughout the thesis.

1.4. RESEARCH OBJECTIVE

The goal of this dissertation is to establish how the seabed - water column exchange of fine sediment affects the distribution of fines in the southern North Sea. Additionally, we aim to generalise these findings and apply them to other shallow coastal shelf seas. To achieve these goals, we formulate three main research questions. These are supported by a set of underlying supporting questions.

1. Where are fines found in the seabed of the southern North Sea?
    a) Which conditions determine the large-scale distribution of fines?
    b) How is this large-scale distribution affected by human interventions?
2. How and when are fines temporarily buried in the seabed?
    a) Which physical process governs the burial of fines?
    b) On which length- and timescales does the burial process operate?
    c) How can the burial of fines in the seabed be parameterised for use in numerical models?
3. Under what conditions are fines remobilised from the seabed and for how long do they remain in the water column thereafter?
    a) When are fines remobilised from the bed?
    b) How long do these fines remain in the water column after being remobilised?
    c) How can remobilisation from the seabed be parameterized for use in numerical models?

1.5. RESEARCH SETUP AND OUTLINE

In this research, we will mainly work with in-situ datasets. Apart from being one of the world's busiest seas, the North Sea is also one of the worlds most extensively monitored seas (see, e.g., Stephens and Diesing 2015). We analyse existing data sets which were initially collected as monitoring data, but provide a wealth of information on fine sediment dynamics (Borst *et al.* 2013, Witbaard *et al.* 2013). We supplement these with dedicated measurements carried out on the North Sea during two research cruises in 2017 (see also Damveld *et al.* 2018, Cheng 2021).

To properly analyse the in-situ data, we developed conceptual thinking models. These were developed in conjunction with the analysis of the data and provide a means to interpret the different data sources. Furthermore, they enable us to understand how the system functions on a variety of temporal and spatial scales.

These data analyses and conceptual models provide a basis for translating the studied processes into numerical model formulations, as such models are the main tool used for environmental impact assessments. Devising these model formulations is outside the scope of this dissertation, but we clearly have them in mind.

The research questions presented in Section 1.4 are addressed in chapters 2, 3 and 4, by applying different methods:

In Chapter 2, we present the large-scale distribution of fines in the DCZ from a multi-year sediment sample dataset. Here, we develop a conceptual model to interpret observed patterns. This conceptual model unites large-scale fine sediment transport along the Dutch coast with local deposition and accumulation.

In Chapter 3, small-scale processes that lead to the burial of fines in the seabed are studied. We present a mechanistic description of the burial of fines into a sandy seabed. This is compared to newly collected data from the southern North Sea, specifically focusing on interpreting small-scale sedimentary structures, and the interaction of small-scale bedforms with fine sediment exchange.

In Chapter 4, we investigate the remobilisation of fines from the seabed during storms by analysing a high-frequency dataset collected in the DCZ during a period of 2 years. This analysis sheds new light on the timing of fines remobilisation relative to storms and how long they remain in the water column after they have been remobilised.

The conclusions of this work and implications for system understanding, modelling, and marine governance are presented in the Synthesis (Chapter 5).

2

THE DISTRIBUTION OF FINES IN THE SEABED OF THE SOUTHERN NORTH SEA

This chapter has been published as: **Hendriks, H.C.M.**, van Prooijen, B.C., Aarninkhof, S.G.J., Winterwerp, J.C. (2020). *How human activities affect the fine sediment distribution in the Dutch Coastal Zone seabed.* Geomorphology, 367, 107314.

2.1. INTRODUCTION

The seabed of the southern North Sea has a significant ecological and economic value. It accommodates a substantial amount of living and non-living resources and fulfils vital ecosystem services, by providing habitat for a wide range of benthic organisms (Aldridge *et al.* 2007, Stephens and Diesing 2015). Over the past years, human activities affecting the seabed have increased (Degraer *et al.* 2019, Emeis *et al.* 2015). These activities include sand mining, operation of offshore platforms (Stolk and Dijkshoorn 2009), beam trawling (Rijnsdorp *et al.* 2008), accommodation for pipelines and cables buried in the sea bed (de Groot 1982, Rouse *et al.* 2017), and the construction and operation of offshore wind farms (Breton and Moe 2009). These human activities lead to increasing pressure on the southern North Sea ecosystem (Burdon *et al.* 2018, Piet *et al.* 2019). To make sure these human activities are carried out in a sustainable way, a balance between economic and ecological interests must be maintained. An important parameter affecting the local ecosystem is the amount of fines in the water column and seabed, which are related. This requires knowledge about the dynamics and composition of the seabed sediment (Degraer *et al.* 2019, Reed *et al.* 2012).

In a large part of the southern North Sea, the seabed mainly consists of sand (Eisma *et al.* 1987, Huthnance 1991, Irion and Zollmer 1999), containing a relatively small fraction of fines, i.e., sediment with a grain size smaller than 63 μm. However, many studies have shown that small fractions of fines can readily exert a profound influence on the behaviour of the seabed and the benthic ecosystem (e.g., Degraer *et al.* 2008,Heip *et al.* 1992, van Ledden *et al.* 2004). Benthic communities are richer when the seabed contains fines compared to purely sandy substrates (van Hoey *et al.* 2004), because nutrients adhere to fines (van Raaphorst and Malschaert 1996). On the other hand, fines may have a detrimental effect on the pelagic ecosystem when remobilized from the seabed. Once fines are suspended, they can abrade fish gills, leading to gill damage in several fish species (Au *et al.* 2004, Sutherland and Meyer 2007). Furthermore, suspended fines increase the turbidity of the water, thereby attenuating the light climate and thus the growth rate of phytoplankton (e.g., Anthony *et al.* 2004, van Duin *et al.* 2001). Favourable or not, fines influence the ecological functioning of shallow coastal seas.

Stephens and Diesing (2015) and Bockelmann *et al.* (2018) were the first to quantify the spatial distribution of fines for the entire North Sea, based on a large number of seabed samples. They quantified the seabed sediment composition (e.g. mass percentages of fines, sand and gravel) of the entire North Sea by using a geostatistical approach. Because of their large spatial extent, the resolution of these maps is relatively low (Bockelmann *et al.* 2018, Stephens and Diesing 2015). Furthermore, these studies did not explicitly include the effect of human activities on seabed sediment composition. This makes them less applicable to coastal areas, where environmental gradients are large and human activities are ubiquitous. To understand how fines are distributed in the seabed of coastal areas, the processes which play a role on smaller spatial scales have to be understood, including the role of human activities.

In this chapter, we analyse the fine sediment distribution in the seabed of the Dutch Coastal Zone (DCZ), a coastal area characterized by strong environmental gradients and a variety of human interventions. The aim of this chapter is to identify the processes and conditions which determine the distribution of fines in the surficial seabed of the

DCZ, and assess the response of the system to human interventions. We present a new, extensive sediment dataset, collected by the Port of Rotterdam authority in the DCZ from 2006 to 2014 (Borst *et al.* 2013). These data are used to map the distribution of fines in the seabed of the DCZ at unique spatiotemporal scales. To interpret these distributions, we develop and apply a conceptual framework, utilizing hydrodynamic model data and bathymetric data of the DCZ. This framework is used to evaluate the effects of human interventions on the distribution of fines in the DCZ. Additionally, we discuss other areas where the framework could be applied.

This chapter is structured as follows. In Section 2.2.1 we present our study area and discuss the sediment dataset, bathymetric and hydrodynamic data. Next, we present the results of our analyses on the sediment dataset and introduce our conceptual framework. We then apply this to the study area, evaluating the effect of large-scale human interventions, and also discuss how the framework could be used in other areas.

2.2. MATERIALS AND METHODS

2.2.1. STUDY AREA

The study area is depicted in Figure 2.1a and covers part of the Dutch coastal zone (DCZ) (Fettweis and Van den Eynde 2003, Visser *et al.* 1991), which is situated in the southern North Sea (Figure 2.1a). The DCZ is a shallow coastal shelf sea with maximum water depths up to 30 meters and tidal currents with maximum speeds ranging between 0.7 and 1.1 m/s (de Kok 1996, van der Giessen *et al.* 1990). The progressive tidal wave propagates through the North Sea in a counter-clockwise direction (Kelvin wave). It has an amplitude of 1-2 m along the Dutch coast (van der Hout *et al.* 2015, Visser *et al.* 1991), with tidal currents oriented mainly parallel to the shore. Furthermore, the outflow of the River Rhine induces a Region of Freshwater Influence (ROFI), which extends for over 100 km along the coast with an average width of less than 20 km (Pietrzak *et al.* 2011). This ROFI determines the vertical current structure and resulting suspended matter distribution (de Boer *et al.* 2009, Pietrzak *et al.* 2011, Simpson *et al.* 1993, Souza and Simpson 1996).

Apart from these physical traits, this area is known for a multitude of human activities taking place. Figure 2.1b shows a selection. From multiple offshore platforms, gas and oil is extracted and several major shipping lanes cross the DCZ, where opposing traffic lanes are separated by separation zones. More recently, wind farms have been constructed and are planned. Closer to the shore, sand mining areas and disposal sites are found. At these disposal sites, sediment dredged from harbours is deposited, containing large amounts of fines. Sand from the mining areas serves multiple purposes: it is used for coastal protection, construction and land reclamations.

A major land reclamation realized in the past decade was Maasvlakte 2 (MV2). MV2 is the recent extension of the Port of Rotterdam constructed mainly in 2009 and 2010. This required a total volume of 220 million m^3 of sand, which was mined from the MV2 sand mining pit, located approximately 10 kilometres west of the River Rhine outflow. During 2009 and 2010, a total volume of 170 million m^3 was mined (Borst and van Tongeren 2012)). After 2010, sand mining for MV2 continued for several years, but at substantially

smaller rates (de Jong 2016).

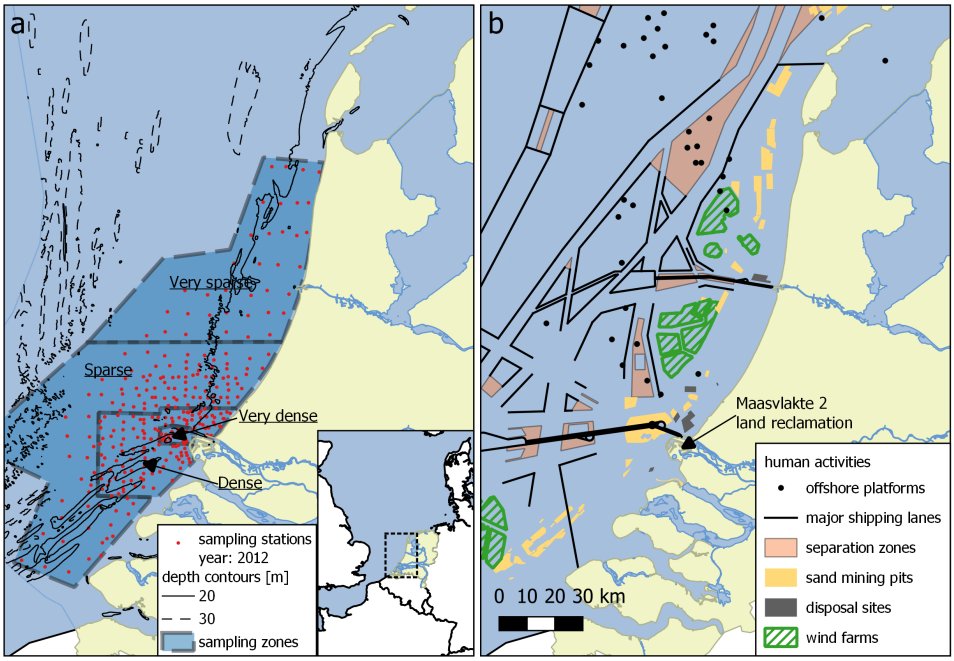

Figure 2.1.: (a) Overview of the study area. Sampling stations visited in 2012 are indicated with dots. Sampling density zones are delineated with thick dashed lines. Sampling density ranges from very dense near the MV2 sandpit to very sparse in the north. The 20 m and 30 m depth contours are indicated by solid and dashed lines, respectively. (b) Map indicating human activities in the Dutch coastal zone (Rijkswaterstaat 2019)

.

2.2.2. SEDIMENT SAMPLES DATASET

We present a new dataset consisting of more than 1700 bed samples. This dataset is established from an extensive monitoring programme carried out between 2006 and 2014 by the Port of Rotterdam authority (Borst *et al.* 2013, Borst and Vellinga 2012)). The aim of this programme was to monitor the far-field and near-field effects of sand mining for MV2 on the benthic ecosystem. Within this programme, bed samples were collected at pre-defined sampling stations from 2006 until 2014 on a yearly basis, except in 2007. However, the exact sampling locations varied a bit from year to year around the pre-defined stations. In every sampling year, samples were collected in the period of April to June, which is the post-storm season.

In 2009, 2013 and 2014, only near-field effects of the sand mining were monitored. To establish these near-field effects, 100 to 120 seabed samples were collected within a

densely sampled 15 kilometre radius around the MV2 sand mining pit. In 2006, 2008, 2010, 2011 and 2012, up to 300 stations were visited to monitor far-field effects of the sand mining. In these years, the sampling domain covered the majority of the study area shown in Figure 2.1a. The far-field sampling domain includes the near-field domain, but with a lower sampling density. Still, most dense sampling was done around the MV2 sand mining pit. To the north and south, sampling density decreased. Figure 2.1a shows the spatial sampling density in 2012, while Table 2.1 lists the number of stations visited each year, classifying the sampling years according to sampling domain and MV2 chronology.

Table 2.1.: Number of sediment sampling stations per year.

Year	**Number of sampling stations**	**sampling domain**	**MV2 chronology**
2006	256	far-field	pre-MV2
2008	300	far-field	pre-MV2
2009	100	near-field	MV2 construction
2010	300	far-field	MV2 construction
2011	296	far-field	post-MV2
2012	300	far-field	post-MV2
2013	118	near-field	post-MV2
2014	120	near-field	post-MV2

A standard protocol was followed to collect sediment samples. A large seabed sample, with a maximum height of 25 cm and 30 cm diameter, was taken with a boxcorer. Three Perspex tubes (length: 15 cm, diameter: 10 mm) were inserted into the boxcorer sample, before the overlying water was siphoned off, not disturbing the sediment interface. These tubes were carefully removed from the mother sample, removing the excess sediment around. Each tube was then split into two parts: an upper part (0-5 cm from the surface) and a lower part (5-10 cm). The lower parts of each tube were combined and stored in one 20 ml vial, i.e., the lower subsample. The same procedure was followed for the upper parts, i.e., the upper subsample. The vials were labelled and stored in a freezer at -20° C. After all stations were visited, the vials were taken to the laboratory ensuring the sediment remained frozen.

The grain size distribution of the samples was determined in the laboratory. First, the subsamples were freeze-dried and passed over a 1 mm sieve. Then, the sieved material was homogenized in local tap water and part of it inserted into a Malvern Mastersizer 2000. The Malvern Mastersizer determines the grain size distribution of a sediment sample by laser diffraction and returns the volume percentage of different size classes. The volume percentage of particles smaller than 63 μm is returned as a separate size class. We refer to this size class as fines, and do not distinguish between the clay and silt fractions.

We assume the volumetric fines percentage measured with the Malvern Mastersizer is close to the gravimetric fines percentage. This is valid if the density of the sediment does not vary considerably, i.e., when the amount of organic matter in the sediment samples

is limited (Callesen *et al.* 2018, Yang *et al.* 2015). Based on Loss on Ignition (LOI) data of the sediment samples this is an appropriate assumption, as LOI was smaller than 2% for more than 95% of the samples.

As the grain size distribution of the upper and lower subsamples taken from the box-core is statistically dependant, they are not treated as separate samples. We define the average grain size distribution as the average of the two subsamples. This reflects the grain size distribution of the surficial seabed, i.e. the top 10 cm, for a visited sampling station per sampling year. Furthermore, to account for measuring accuracy, a sample is classified as containing fines if its fines percentage is at least 0.1%. If the fines percentage is smaller, it is classified as a sample with no fines.

To characterize the sediment composition for each station, we aggregated the particle size distribution of the samples collected during the various sampling years. However, sampling at a particular station was not carried out at exactly the same location over the years, while also the sampling density and domain varied. Therefore we introduce a spatial clustering procedure to assess which data are attributed to which station.

The spatial clustering consists of three subsequent steps. First, a circular buffer is defined around each sampling point in QGIS. As the sampling density varied across the study area, the radius of this buffer depends on the sampling point location. Four main sampling density zones were defined: very sparse, sparse, dense and very dense (Figure 2.1a). The corresponding buffer radiuses for each zone are listed in Table 2.2. An example is shown in Figure 2.2 for an arbitrary sampling station in the sparse sampling zone.

Second, sediment composition data are aggregated to form a data cluster if their buffers overlap. When a buffer overlaps any other buffer, its data is added to the cluster. For the sampling station in Figure 2.2, the data cluster represents the samples from 2006, 2008, 2010, 2011 and 2012. Third, data clusters were designed such that they do not contain multiple samples from one year, except for the very dense sampling zone (Figure 2.1a). In this zone, clusters may contain multiple samples taken during one year.

After aggregating the data, the mean and standard deviation were calculated for the fines percentage per cluster. Furthermore, we established the fraction of samples in a cluster which contain fines. This fraction is an estimate for the probability of fines being present in a sample for any cluster.

Table 2.2.: Sampling density zones in sampling domain with corresponding buffer radius

Zone	**Buffer radius [m]**
Very sparse	1000
Sparse	500
Dense	250
Very dense	125

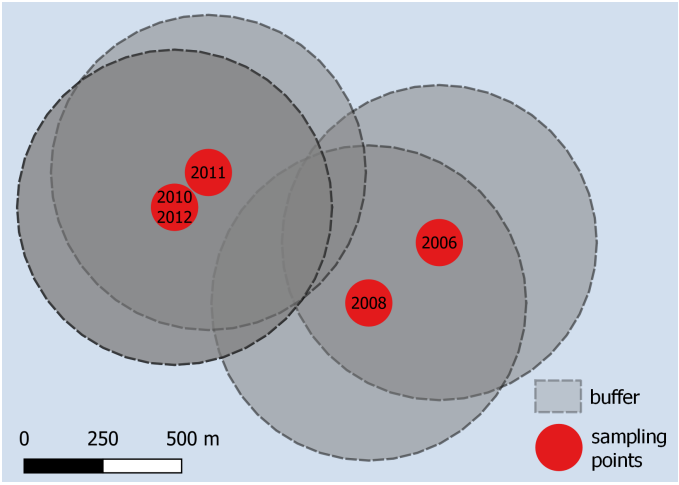

Figure 2.2.: Example of clustering data from various years in the sparse sampling zone. Labels of the sampling points indicate the various sampling years.

2.2.3. BATHYMETRIC AND HYDRODYNAMIC DATA

We use bathymetric data collected by the Netherlands Hydrographic Office and *Rijkswaterstaat*, already interpolated to an equidistant grid with 25x25 m^2 resolution (Damen *et al.* 2018, NLHO and Deltares 2019). Bathymetric data collected during multiple years was merged onto a single grid, as the area of interest was only partially surveyed during subsequent years. For the pre-MV2 bathymetry, we use data collected from 1994 until 2008, and for the post-MV2 bathymetry, data collected from 1994 until 2015. If areas were surveyed multiple times, the bathymetry was based on the latest survey. Missing values on the merged grid were filled by linearly interpolating from surrounding grid points within a 500 m radius, using inverse distance weighting.

Flow velocities and salinity for the study area are extracted from a validated three-dimensional hydrodynamic model, with 10 equidistant vertical layers (Arcadis 2014, Arcadis and Deltares 2019). The southern and northern boundaries of this model are located at 51.1°N and 52.8°N, respectively. Its eastern boundary lies along the Dutch shoreline and its western boundary runs parallel to the shoreline, 50 km offshore. The resolution of the curvilinear model grid is most coarse at the western boundary with cell sizes of 2500x2500 m^2. It refines in shoreward direction and is highest in the dense and very dense sampling zones (Figure 2.1a). In the area of interest, cell sizes range from 250x350 m^2 to 500x700 m^2, where the along-shore length of the grid cell is smallest. Note that the computational grid is therefore much coarser than the bathymetric grid, the relevance of which is discussed in Section 2.4.

With this model, Arcadis (2014) carried out hindcast simulations for the years 2006 to 2014. For each model year, Arcadis (2014) updated the model with the latest bathymetric data. Water levels and salinity at the seaward boundaries of the model were taken from the southern North Sea (ZUNO) model (Gautier and Caires 2015). River discharges at

the landward boundary were based on output from a calibrated 1D model of the fresh water distribution in the Rhine-Meuse delta (SOBEK) and measurements. The model has been validated for water level, temperature and salinity. For these three quantities, model performance was assessed as:

- Water level: BIAS = 5 cm, $RMSE_0$ = 8 cm
- Temperature: BIAS = -0,5° C, $RMSE_0$ = 0,5° C
- Salinity: BIAS = 0.5 PSU, $RMSE_0$ = 1.5 PSU

More information on the model setup and validation can be found in Alkyon (2010) and Arcadis (2014). The model output was resampled to a 500x500 m^2 grid using inverse distance weighting for all sampling areas shown in Figure 2.1a. We define two representative years for pre-MV2 and post-MV2 hydrodynamic conditions: 2008 (pre-MV2) and 2012 (post-MV2).

In our analyses, we relate the distribution of fines to current- as well as wave-induced bed shear stresses. Current-only bed shear stresses ($\tau_{b,c}$) are calculated based on the flow velocities computed by the Arcadis (2014) model, following Soulsby (1997):

$$\tau_{b,c} = \rho C_D U_b^2 \tag{2.1}$$

Here, ρ denotes the density of seawater (1030 kg/m^3), U_b is the magnitude of the flow velocity at the lowest model level and C_D is the drag coefficient. Thus, computed bed shear stresses are positive scalar values. The value of C_D is determined by the bed roughness length z_0 and the height above the bed z, according to:

$$C_D = \frac{\kappa^2}{\ln(\frac{z}{z_0})^2} \tag{2.2}$$

Here, $z_0 = \frac{d_{50}}{12}$, and d_{50} is the median sand grain size, for which we take d_{50}=250 μm.

Wave-induced bed shear stresses were taken from the MoS^2 model (Cronin and Blaas, 2013).

2.3. RESULTS

2.3.1. MAPPING THE DISTRIBUTION OF FINES IN THE DUTCH COASTAL ZONE

An overview of the monitoring programme results is presented here. We focus on the percentages of fines found in the surficial seabed layer (i.e., 0-10 cm from the seabed surface). First, the results of all years (2006-2014) are discussed, a total of 1790 bed samples. The aggregated data are discussed later. The distribution over the years is indicated in Table 2.3. The mass percentage of fines in a sample is denoted as φ_{fines} and we compute a conditional mean percentage, $\langle\varphi_{fines}\rangle$, and a conditional standard deviation φ_{fines}'.

The percentage of samples containing fines in the far-field domain ranged between 17% and 33% (Table 2.3). The mean fines percentage increased from 3.7% in 2006 to

Table 2.3.: Number of samples collected per year, with descriptive statistics for samples containing fines.

year	total number of samples	number of samples containing fines (percentage of total)	$\langle \varphi_{fines} \rangle$ [%]	φ_{fines}' [%]
Far-field sampling years				
2006	256	63 (25%)	3.7	5.6
2008	300	51 (17%)	5.3	6.0
2010	300	99 (33%)	5.9	7.3
2011	296	84 (28%)	5.1	6.7
2012	300	100 (33%)	9.2	12.1
Near-field sampling years				
2009	100	43 (43%)	5.7	4.5
2013	118	59 (50%)	8.7	10.4
2014	120	96 (80%)	9.7	9.8

about 5-6% in the period 2008-2011 and then further to 9.2% in 2012, with a considerably higher standard deviation in 2012.

The percentage of near-field samples containing fines was larger than in the far-field domain (Table 2.3), with percentages varying between 43% and 80%. In this area, $\langle \varphi_{fines} \rangle$ was generally higher than in the far-field. Even though local temporal differences exist in fines percentage, the difference between the far-field and near-field sampling years is primarily attributed to the difference in sampling density and domain.

The spatial distribution of fines in the surficial seabed of the DCZ, aggregated from all sampling years, is presented in Figure 2.3a. It shows four classes of average fines percentage per sampling station. The location of these stations reflects the sampling coordinates of 2012. Only stations with clusters containing at least three samples are displayed (Section 2.2.2). The classes for fines percentages are conform van Alphen (1987a), to allow for comparison.

The highest percentages of fines are found directly north and south of the River Rhine outflow. In these areas, mean fines percentages may range up to 25%. To the north, most fines are found on the lower shoreface, in a narrow alongshore strip 2 to 3 km wide. This strip extends to the northern boundary of the study domain. To the south, fines are mainly found in the troughs of tidal ridges and in the former tidal channels in front of now-closed estuaries. Both the average fines percentages and fraction of samples containing fines decrease with increasing distance offshore. This fraction is small or equal to zero for the majority of stations beyond 20 km offshore (Figure 2.3b).

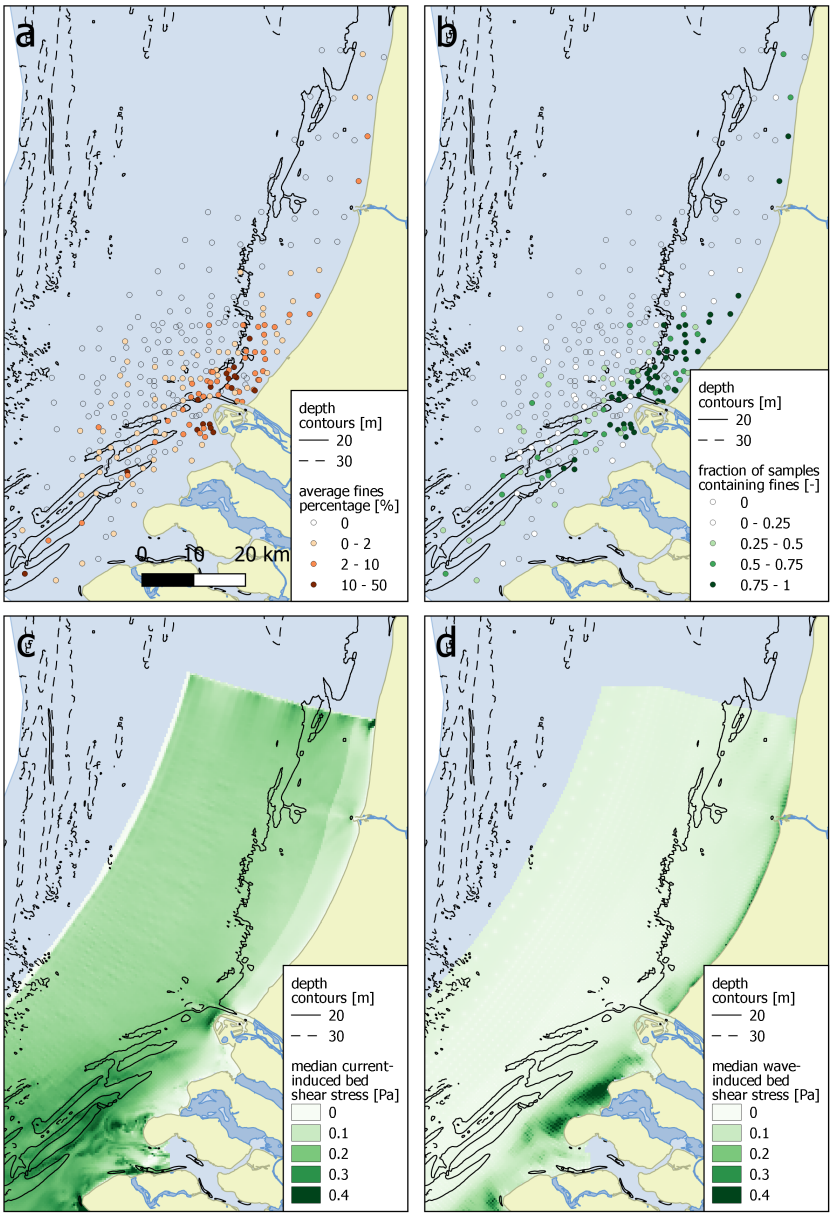

Figure 2.3.: a: overview map of average percentages of fines in the DCZ. b: fraction of samples containing fines for each sampling station. c and d: median bed shear stress due to tidal currents and waves computed for 2012, respectively.

2.3.2. COMPARISON WITH HISTORICAL DATA AND SPATIAL DISTRIBUTION

The percentage of fines in the surficial seabed of the DCZ has been mapped before by Eisma (1968) and van Alphen (1987a). Although the sediment collection method, determination of the grain size distribution, and definition of surficial seabed, i.e. ranging from top 5 cm (Eisma 1968) to top 5-15 cm (van Alphen 1987a), differ from the present study, a qualitative comparison is possible. Figure 2.3 shows that the results of Eisma (1968) and van Alphen (1987a) are globally similar to the current results. This is consistent with the fact that no long-term trends in the alongshore flux of fines in the DCZ have been reported (Cronin and Blaas 2015, Eisma 1981, Salden 1998, van Alphen 1990).

Eisma (1968) characterizes the shoreface between Rotterdam and Den Helder as "an area with fine grained deposits about parallel to the coast at roughly 5-15 m depth" (left panel Figure 2.4). This area is also reflected by our data in the right panel of Figure 2.4. Though Eisma's definition of fines is slightly different (i.e. <50 μm), the agreement between the two datasets is promising. Moreover, this implies that for our analyses, their interpretation and application of our concept elsewhere, the precise definition of fines does not seem crucial.

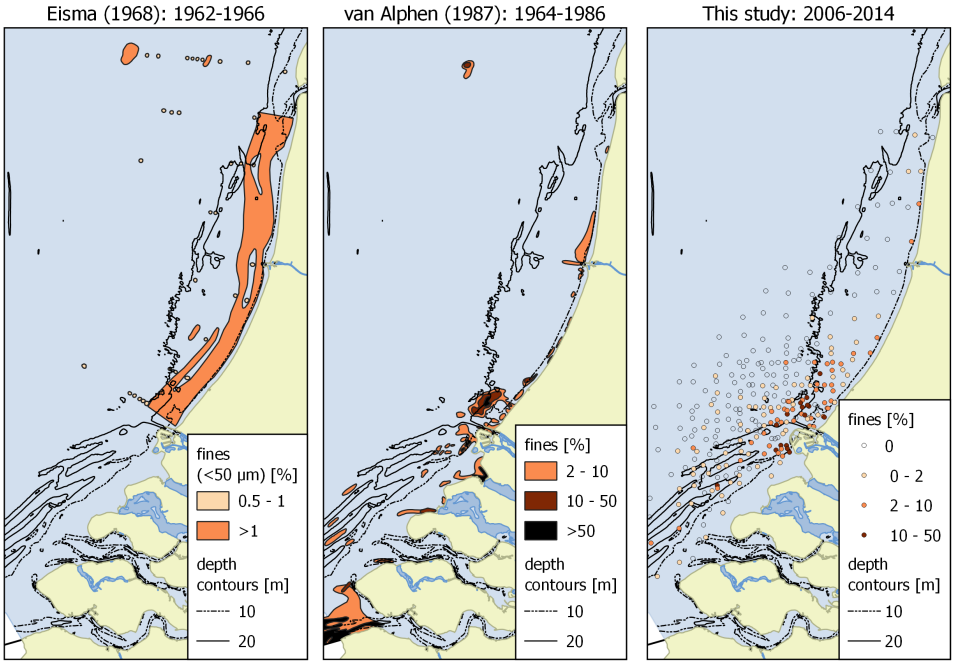

Figure 2.4.: Comparison of results from this study with historical data of Eisma (1968) and van Alphen (1987a). The period during which samples were collected in each study is mentioned above the corresponding panel.

Later, van Alphen (1987a) presented a more detailed analysis of the fines distribution in the DCZ, based on data collected between 1964 and 1987 (middle panel Figure 2.4).

van Alphen (1987a) notes that fines are found in several areas: in the former tidal channels of the Southern Delta, around *Loswal Noord* (close to Hook of Holland), the site where sediment dredged from the Port of Rotterdam was disposed until 1996, and in a narrow 1-2 kilometre wide strip along the coast. In this strip, fines are mainly found in troughs between the breaker bars and around the 10 meter depth contour. The fines distribution map by van Alphen (1987a) resembles that of the current study. However, spatial patterns around the River Rhine outflow have changed. Furthermore, in the current study some fines are also found further offshore. In all three studies, the alongshore occurrence of fines coincide with a zone where computed current-only bed shear stresses are low (Figure 2.3c). This is caused by a decrease in tidal velocities at smaller water depths. On the other hand, wave-induced shear stresses become larger at smaller water depth, as these stresses scale inversely quadratic with water depth (Figure 2.3d). Thus, fines in the DCZ are mainly found where tidal velocities are small and wave stresses are larger than in the majority of the DCZ. At water depths beyond 10 m, our simulations show that, averaged over a year, the role of waves reduces compared to the flow-induced bed shear stresses (detailed results not presented).

To examine the cross-shore variability in fines percentage, we plot all samples containing fines as a function of distance perpendicular from the shore. Figure 2.5a shows that the majority of samples with fines is found within 20 km from the shore, with fines percentages generally higher than 1% and up to 60%. Further offshore, the fines percentages decrease, ranging between 0.5 and 2%.

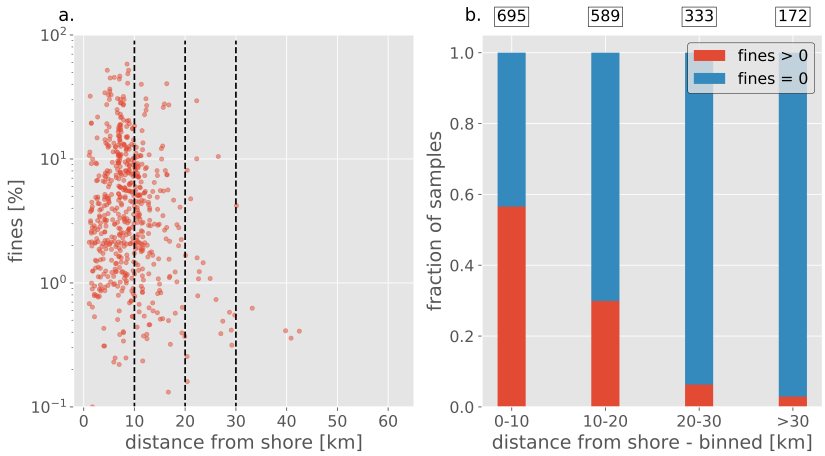

Figure 2.5.: a: Fines percentage as a function of distance from shore. b: samples binned according to distance from shore, categorized in whether they contain fines or not. The number of samples in a particular bin are indicated above the bars.

In Figure 2.5b, all samples are grouped into four bins, based on their distance from the

shore. Beyond 20 km offshore, less than 5% of the samples contain fines. This is consistent with van Alphen (1987a), who concluded that fines are virtually absent beyond 20 km offshore. Closer to the shore, fines were found in 30% of all samples in the 10-20 km bin and in 57% of all samples taken within 10 km from the shore. However, within this last area the spatial and temporal variability in the measured fines percentage is significant.

2.3.3. TEMPORAL AND SPATIAL VARIABILITY IN ROTTERDAM AREA

To investigate the variability in fines percentages within the nearshore zone (< 10 km offshore), we zoom in on the area around the River Rhine outflow. Since the River Rhine outflow is also the entrance to the port of Rotterdam, we will refer to this area as the Rotterdam area. As the construction of MV2 was the major human activity in this area during the 2006-2014 period, sampling years were classified relative to the construction of MV2. Hence, the sampling years 2006 and 2008 are pre-MV2 and the sampling years 2011-2014 are post-MV2 (Table 2.1).

After applying the spatial clustering as described in Section 2.2.2, we established the pre-MV2 and post-MV2 fines percentage. Since the pre-MV2 and post-MV2 sampling layout differ to some extent, the difference in fines percentage per station was calculated by comparing points within 1000 m distance (Figure 2.6). This provided enough distance between sampling stations, but also allowed to compare enough stations. The average pre-MV2 fines percentage per station was subtracted from the post-MV2 fines percentage, i.e., a positive value in the right panel of Figure 2.6 indicates an increase in fines for the post-MV2 period.

In the left and middle panel of Figure 2.11, only stations with clusters containing at least two samples are displayed. We have also indicated where human activities take place.

For the pre-MV2 years (left panel Figure 2.6), we observe the highest fines percentages around the disposal sites *Verdiepte Loswal*(1) and *Noordwest*(2), and to the northeast of these sites. Fines are also found within several kilometres from the shore, mainly in the vicinity of the River Rhine outflow. However, large spatial gradients in fines percentages are observed everywhere. Sampling stations without fines are adjacent to stations where fines percentages are between 2-10% or even exceed 10%.

Overall, fines percentages are higher for the post-MV2 years than for the pre-MV2 years (middle and right panel Figure 2.6). The areas northeast of the disposal sites remain characterised by high percentages of fines. Furthermore, fines percentages increase by more than 10% in the area directly south of the MV2 reclamation (indicated with the cross-hatched area). Considerable spatial gradients persist in this area.

High fines percentages, of up to 30%, are observed in and around the sand mining pit approximately 10 km offshore from the MV2 reclamation. Though this area was not sampled in the pre-MV2 period, historical data does not show these high fines percentages in this area, and are not expected on the basis of our analysis below. Therefore, these high fines percentages likely are a recent development.

In the most southern part of the sampling domain, there are several stations with persistent high percentages of fines. These stations are located either in the troughs of tidal

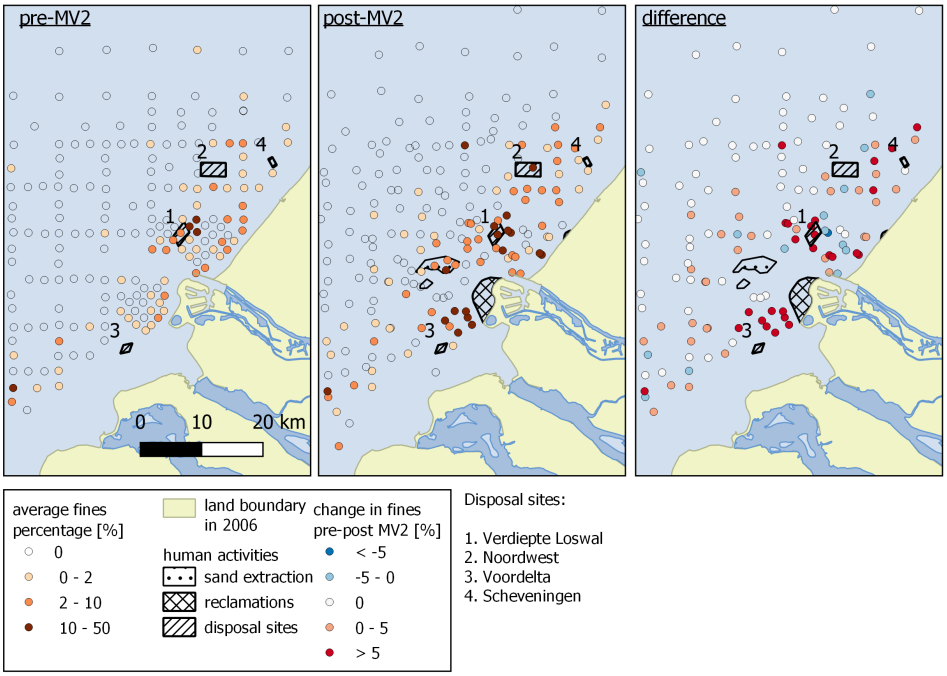

Figure 2.6.: Pre-MV2 and post-MV2 fines percentages around Port of Rotterdam, as well as the difference between the stations.

ridges, or in former tidal channels where fines have accumulated after closure of the estuaries. In the following section, we will use a conceptual framework to interpret the observed trends.

2.4. INTERPRETATION

2.4.1. CONCEPTUAL FRAMEWORK

To interpret the presented spatial distribution of fines, we propose a conceptual framework. This can be used to analyse the natural distribution of fines in a coastal zone and the effects of human interventions thereupon. It consists of three components:

- Source of fines
- Transport pathways of fines
- Accumulation potential for fines

These components are schematically drawn in Figure 2.7. The presence or absence of fines in the seabed depends on all three factors. (1) Multiple local sources of fines exist within a coastal zone. From these sources, fine sediment can follow different transport pathways. (2) The exact pathways are not meaningful, as these are erratic owing to

the erratic driving forces. Therefore, we construct envelopes around a large number of potential pathways, representing mean dispersion patterns. (3) If conditions for accumulation are favourable in an area, fines can deposit and accumulate in and on the bed. Such areas are referred to as potential accumulation areas.

For fines to be present in the seabed, all conditions have to be met. For example, an area can be very calm fulfilling the local conditions of an accumulation area, but if there is no pathway from a source to that area, no fines will accumulate (Figure 2.7). Oppositely, there can be a large supply of fines, but local accumulation potential determines whether this yields a temporary (Figure 2.7 – II) or a permanent deposit of fines (Figure 2.7 – IV). Furthermore, permanent deposits can interrupt the transport pathway of fines.

The natural spatial distribution of fines only depends on the undisturbed interplay between these three components. Human activities can modify the sources, transport pathways and/or accumulation potential.

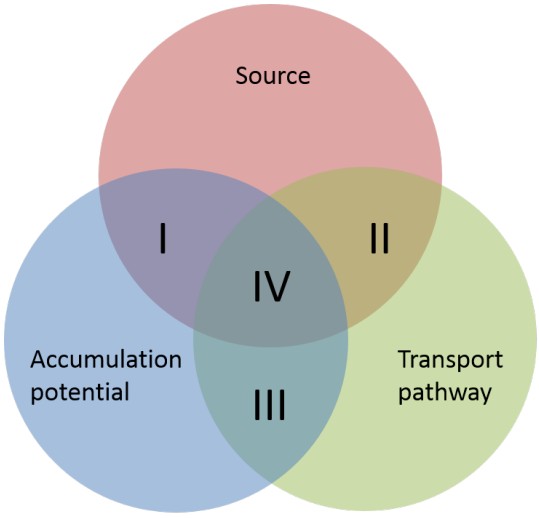

Figure 2.7.: Conceptual framework for the accumulation of fines in a sandy seabed, consisting of three components and their potential overlap.

The three components indicated in Figure 2.7 are elaborated upon below. Sources of fines can have a natural or anthropogenic origin. Natural sources of fines are erosion of geological layers (Adriaens *et al.* 2018), coastal (cliff) erosion (Eisma 1981), riverine input

(Salomons and Eysink 1981) and input from other seas or oceans (McManus and Prandle 1997). Furthermore, fines which were buried within the seabed during calm conditions can be remobilized during storms (van Kessel *et al.* 2011). Hence, on an annual timescale parts of the seabed may alternately be an accumulation zone and a source.

Anthropogenic sources of fines include disposal of sediment from maintenance dredging (Fettweis *et al.* 2009) and sand mining overflow (Nichols *et al.* 1990, Spearman *et al.* 2011). These sources are represented by a mass flux (ϕ_{fines}):

$$\phi_{fines} = \frac{m_{fines}}{T} \tag{2.3}$$

Here, T denotes a timescale and m_{fines} denotes the dry mass of fines.

Sediment transport pathways in shallow coastal areas are the consequence of a myriad of combinations of barotropic and baroclinic processes governed by tide, wind, waves, and density-driven flows (Otto *et al.* 1990). To exactly define these pathways, one would either need a high-resolution sediment dataset (McLaren and Powys 1991) or a complex numerical model (Kim and Lim 2009). Instead of using the exact pathways, we propose to use the envelope of the pathways. These envelopes are similar to the Depth of Transport concept introduced by Valiente *et al.* (2019).

The accumulation potential is defined as a parameter reflecting the interaction between the local bathymetry (i.e. the local geomorphological features, such as bedforms) and the prevailing hydrodynamic conditions. It is defined as a binary parameter, which is either high or low. If the accumulation potential is low, fines may be transported into an area, but it is unlikely that they can accumulate on/in the bed.If the accumulation potential is high, sediment deposits on the bed and remains there (Figure 2.7).

As hydrodynamic conditions in a coastal zone are determined by tidal currents and waves, they are strongly time-dependent. To make the accumulation potential independent of time, we define a representative parameter for the prevailing hydrodynamic conditions. Van Kessel *et al.* (2011) hypothesize that fines are remobilized from the seabed during storms. Afterwards, during calm conditions, these fines will deposit and are buried in the seabed again. However, these can only accumulate if conditions are calm enough. Hence, in our analyses of post-storm season data, it is not the energetic conditions which determine the accumulation potential, but rather whether the calm conditions are calm enough.

If the wave height over water depth ratio is relatively small, calm conditions are best represented by the magnitude of the tidal current. We assume this is valid for the majority of the DCZ. Calm conditions can then be quantified by selecting an appropriate percentile of the yearly current-only bed shear stress. We use the 90^{th} percentile of the current-only bed shear stress, as it provides a proxy for the maximum tide-induced bed shear stresses during a spring-neap cycle, and denote it with $\tilde{\tau}_{b,c}$. The current-only bed shear stress has been defined in Section 2.2.3.

The interaction between bathymetry and hydrodynamics manifests itself on a variety of scales. The larger, regional scale is characterized by geomorphological features such as tidal ridges, sand waves, navigation channels and large sand mining pits, while the smallest scale is determined by the dimensions of ripples. This smallest scale cannot be resolved in any field dataset or hydrodynamic model output. However, the scale-

dependency of this interaction is crucial for the local behaviour of fines, and should be explicitly included in the assessment of the accumulation potential.

For the (small-scale) bathymetric contribution to the accumulation potential, we use the *DEV* parameter proposed by De Reu *et al.* 2013. *DEV* expresses the bathymetric level of a central point (z_b) relative to the bathymetry in its direct vicinity. *DEV* is based on the Bathymetric Position Index (*BPI*) (Iampietro *et al.* 2005, Verfaillie *et al.* 2006, Wilson *et al.* 2007). *BPI* measures the difference between the elevation of a point (z_b) and the average elevation ($\overline{z}$) in a circle with radius (R) around it (Wilson and Gallant 2000):

$$BPI = z_b - \overline{z} \tag{2.4}$$

$$\overline{z} = \frac{1}{n_R} \sum_{i \in R} z_i \tag{2.5}$$

n_R indicates the number of observations within the circle. *DEV* is a modification of *BPI*, and uses the standard deviation (σ_z) of the bathymetry within radius R to normalize the *BPI*:

$$DEV_R = \frac{z_b - \overline{z}}{\sigma_z} \tag{2.6}$$

$$\sigma_z = \sqrt{\frac{1}{n_R - 1} \sum_{i=1} \left(z_i - \overline{z}\right)^2} \tag{2.7}$$

The DEV_R parameter depends directly on the selected spatial scale, as both σ_z and $\overline{z}$ depend on the radius R. Hence, from a proper choice of R, bathymetry-induced sub grid effects in e.g. bed shear stresses can be captured. A positive DEV_R value means the bed level of that point is relatively high with respect to its surroundings. It therefore experiences larger bed shear stresses than its surroundings. A negative value means a relatively low bed level, with relatively low bed shear stresses.

The bathymetric and hydrodynamic contributions to the accumulation potential are classified through low or high accumulation potential areas, as sketched in Figure 2.8. For a bed shear stress lower than a critical value ($\tilde{\tau}_{\min}$), accumulation of fines is always expected. With increasing current-only bed shear stress, the relative elevation of an area becomes important. Above a certain bed shear stress ($\tilde{\tau}_{\max}$), accumulation is no longer possible as currents are too strong.

2.4.2. APPLICATION OF FRAMEWORK TO ROTTERDAM AREA

In this section, we apply the framework to the area around the River Rhine outflow, to study how human activities in this area have influenced the spatial distribution of fines in the seabed (Figure 2.6). We specifically focus on the impact of the construction of MV2. We consider all three components of the framework and determine whether and how these have changed in the 2006-2014 period.

We start by defining (1) the sources of fines in the DCZ, including the fines that enter the study area from outside the domain. This links to (2) the transport pathway

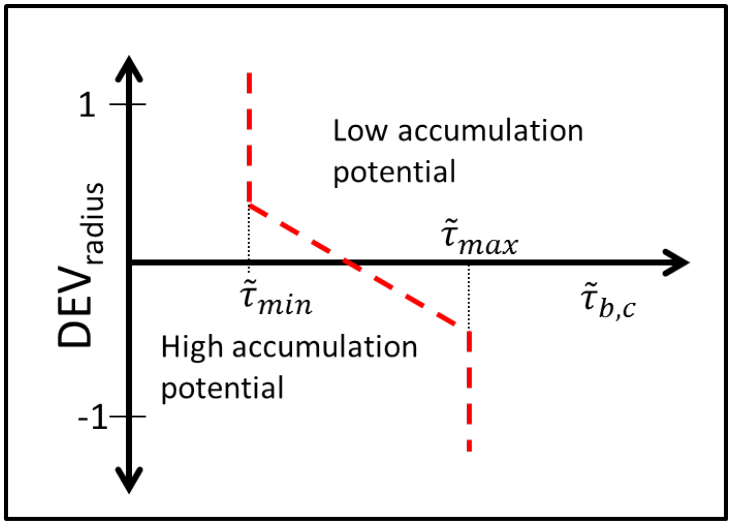

Figure 2.8.: Parameter space for classification of accumulation potential based on DEV_R and $\tilde{\tau}_{b,c}$

.

envelopes. Finally, (3) the accumulation potential in the area is determined. Both the pre-MV2 and post-MV2 period are considered.

The main natural sources of fines in and around the DCZ are erosion of fines from geological layers in the Belgian Coastal Zone (e.g. Adriaens *et al.* 2018), fines entering the North Sea from the Atlantic Ocean (Eisma 1981), McManus and Prandle 1997) and a small contribution from the Rhine, Meuse and Scheldt (Laane *et al.* 1999, Salomons and Eysink 1981). Hence, the major sources of fines are not located in the DCZ, but south of it. These fines are transported alongshore in a residual north-easterly direction, with the yearly transport flux estimated at 22 ± 10 MT/year (van der Hout *et al.* 2015).

The transport of fines along the Dutch coast is predominantly determined by tidal currents and their modification by the Rhine ROFI. The freshwater discharge leads to a salinity difference in cross-shore direction, e.g. Souza and Simpson (1996), Pietrzak *et al.* 2011, inducing a net shoreward near-bed transport of fines. This net transport results from cross-shore density gradients and tidal straining(de Boer *et al.* 2009, Rijnsburger *et al.* 2016, van der Hout *et al.* 2015). Storms may occasionally transport fines in offshore direction, but this sediment is returned onshore by the previously described processes (Flores *et al.* 2017).

Once the fines enter the DCZ, about 10% deposits in the estuaries in the southwestern delta. The northward flux at the Rotterdam area is still in the order of 20 ± 10 MT/year, (Eisma 1981). A considerable amount of fines deposits and accumulates in the entrance channels and harbor basins of the Port of Rotterdam. These are dredged regularly and disposed on the disposal sites *Verdiepte Loswal* and *Loswal Noordwest* (Figure 2.6). From there, the alongshore transport mostly continues in northeasterly direction. From 2000 to 2016, an average of 0.6 and 2.2 MT fines were disposed yearly at *Loswal Noordwest*

and *Verdiepte Loswal*, respectively (Hendriks and Schuurman 2017). Though no new fines are introduced into the DCZ, we include these sites in our analyses as they are the main disposal sites in the DCZ and can buffer fines permanently or temporarily.

A major anthropogenic source of fines originates from the overflow during sand mining, thus located at the MV2 sand mining pit. In 2009 and 2010, approximately 2 MT fines were yearly released this way (van Kessel *et al.* 2011). As this is the only major additional source of fines in the DCZ during the construction of MV2, we investigate whether it has contributed to the post-MV2 distribution of fines. The magnitude of this source strongly decreased after 2010, as extracted sand volumes strongly decreased in subsequent years.

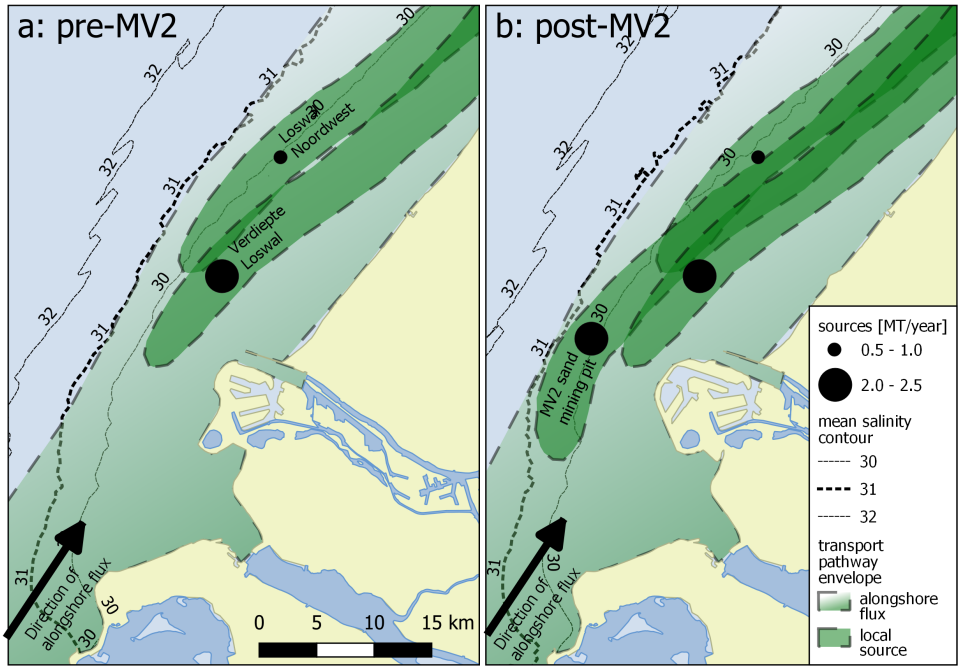

Figure 2.9.: Sources of fines in the Rotterdam area with their associated transport pathway envelopes. Mean salinity contours are computed for the representative years 2008 (pre-MV2) and 2012 (post-MV2).

In Figure 2.9a and Figure 2.9b, we illustrate the location of these sources and their assumed transport pathway envelopes, for the pre-MV2 and the post-MV2 situation, respectively. Though the MV2 sand mining is a temporary source, it is included in Figure 2.9b as it may have affected post-MV2 fines percentages. For the yearly natural transport flux, we only draw its envelope, as its major sources lie outside the Rotterdam area. The arrow indicates the residual transport direction.

Several assumptions have been made to establish the envelope of the sediment transport pathways for the anthropogenic sources. Assuming that the majority of fine sedi-

ment transport in the DCZ takes place within the Rhine ROFI, the offshore boundary for the transport pathways is determined by the offshore limit of the ROFI. This is assumed to be at the 31 PSU mean surface salinity contour, which was assessed from the hydrodynamic model output. On the nearshore side the transport envelopes are – ultimately – bounded by the land boundary. Within this area, the transport pathway envelope is expected to develop along the mean salinity contours. The alongshore (north-south) boundaries are determined by the north-easterly residual current along the Dutch coast, with a magnitude of 0.10-0.15 m/s (Simpson 1997, van der Giessen *et al.* 1990). As tidal currents are the main alongshore transporting agent, the southern boundary is set at one tidal excursion south of a local source (approximately 10 kilometres). To the north, the envelope extends in north-easterly direction with time.

No significant difference was found between the computed mean salinity contours for the pre-MV2 and post-MV2 periods (Figure 2.9). No substantial differences between the pathway envelope of the alongshore flux between the pre-MV2 and post-MV2 period are therefore expected. The magnitude of the natural alongshore flux is not substantially affected by the construction of MV2, nor have flow patterns on the scale of the DCZ changed considerably (Cronin and Blaas 2015). Therefore, the magnitude of the alongshore flux entering the study domain is not substantially affected by the construction of MV2.

The transport pathway envelopes for the anthropogenic sources (i.e., the disposal sites and the sand mining pit) overlap substantially. Fines from the MV2 sand mining pit which are transported northward, either end up in the pathway envelope of *Loswal Noordwest* or of the *Verdiepte Loswal*. It is therefore difficult to discriminate between the effects of different human interventions in the DCZ, as fines from different sources can be transported to the same location. However, in combination with the local accumulation potential, the envelopes may give a good impression on where to expect an increase or decrease of fines percentages in the seabed.

The next step is to quantify the conceptual accumulation potential diagram (Figure 2.8) for the Rotterdam area. The relationship between DEV and $\tilde{\tau}_{b,c}$ can be quantified by applying a logistic regression to a selection of the sediment dataset. This regression predicts a binary response, i.e. the presence or absence of fines in a sediment sample (cf. Section 2.3.1), to a set of explanatory variables. We only discriminate between presence or absence of fines, as their amount is strongly determined by the non-uniform supply of fines (Figure 2.11). All samples taken in the post-MV2 period within 20 kilometres from the shore are included in this regression, as few fines are encountered beyond (Figure 2.5).

DEV_R and $\tilde{\tau}_{b,c}$ are used as the explanatory variables in this regression. They are calculated for every selected sample, using the high-resolution bathymetric and hydrodynamic model data (Section 2.2.3). The DEV_R value of each sampling point is assessed for a radius R of 1000 m, i.e., DEV_{1000}. Radiuses of 250, 500 and 1500 m were also tested. However, the 1000 m radius was used in the analysis below as it can represent the larger geomorphological features in the area (i.e. bedforms, navigation channels and sand mining pits), while still contrasting the bathymetric differences adequately. $\tilde{\tau}_{b,c}$ has been calculated for the representative post-MV2 year 2012. Furthermore, the logistic regression is applied between a $\tilde{\tau}_{\min}$ of 0.15 Pa and a $\tilde{\tau}_{\max}$ of 0.60 Pa. The results of this regres-

sion are shown in Table 2.4.

Table 2.4.: Logistic regression results. This regression method optimizes the log-likelihood of the presence of fines using the two explanatory variables. The p-value of the Log Likelihood Ratio (LLR) shows that this approach is statistically significant.

Log likelihood:	-363.8	# **Obs:**	569	
LL-Null:	-394.4	**Df Residuals:**	566	
LLR p-value:	5.06E-14	**Df Model:**	2	
	coefficient	**standard error**	**z**	**P>|z|**
intercept	1.026	0.097	10.54	0.000
$\tilde{\tau}_{\mathbf{b,c}}$	-2.606	0.231	-11.29	0.000
$\boldsymbol{DEV_{1000}}$	-0.696	0.035	-19.99	0.000

From the coefficients for the intercept, DEV_{1000} and $\tilde{\tau}_{b,c}$, we can infer the relationship: $DEV_{1000} + 3.74\tilde{\tau}_{b,c} = 1.48$. Combining this relation with the chosen values for $\tilde{\tau}_{\min}$ and $\tilde{\tau}_{\max}$ yields the dashed lines in Figure 2.10, distinguishing between the classes introduced in Figure 2.4.

Figure 2.10 shows that the bed shear stress itself is not discriminative for predicting the presence of fines in the range between 0.15 and 0.6 Pa. DEV_{1000} greatly improves the predicted accumulation potential. This likely implies that the presence of fines is strongly influenced by sub-grid effects, i.e. morphological features smaller than the model resolution of 500x500 m^2. Thus, the power of the DEV parameter lies in resolving these sub-grid effects, quantifying local bed features on a 25x25 m^2 resolution.

The accumulation potential classification of Figure 2.10 is applicable for supply-limited systems. In such systems, seabed topography and bed shear stresses mainly determine the distribution of fines. However, the DCZ cannot be regarded entirely as a supply-limited system. There are also areas where there is either no supply of fines, or where this supply is abundant. When there is no supply, the majority of sampling points will be randomly distributed in the 0% category. When supply is abundant, sub-grid hydrodynamic conditions are not discriminative, as eroded fines are replaced continuously (Figure 2.7– II). Then, sampling data will be randomly distributed in the more than 10% fines class.

The accumulation potential in the study domain is visualised in Figure 2.11, by combining the hydrodynamic and bathymetric data with the accumulation potential classification. These maps show alternating areas with high and low accumulation potential, both for the pre- and post-MV2 period. The average fines percentages for both periods (Figure 2.6) are also plotted in these maps.

Figure 2.11 shows that the accumulation potential parameter provides a good explanation of the variability in fines percentages measured in the Rotterdam area. Stations where no fines are found, are generally located in low accumulation potential areas. Stations containing fines are generally located in high accumulation potential areas. The

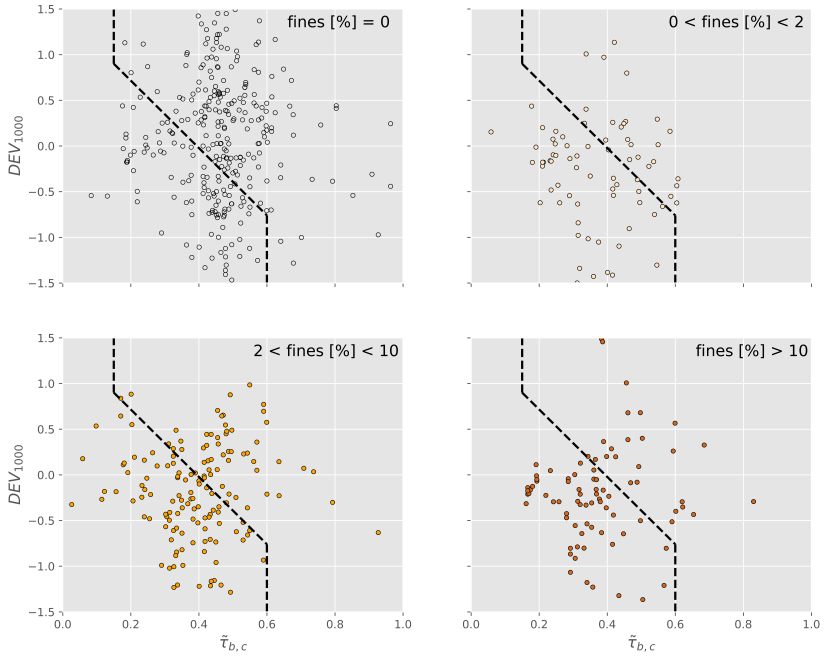

Figure 2.10.: Accumulation potential parameter space, where the dashed line discriminates between high and low accumulation potential.

accumulation potential classification predicts these sites correctly for 65% of the data. Below, we discuss the areas indicated and numbered in Figure 2.11.

First we combine our analysis of accumulation potential with the transport pathway envelopes of the major anthropogenic sources, indicated with a light grey hatch in Figure 2.11a and b. Where the *Verdiepte Loswal* (1) envelope overlaps areas with high accumulation potential, high fines percentages are found for both the pre-MV2 and post-MV2 period. This also holds for *Loswal Noordwest* (2), although fines percentages are lower. Where the transport pathway envelope of the MV2 sand mining pit (4) overlaps with the envelopes of the two disposal sites, a relatively large increase in fines percentage over the pre-MV2 to post-MV2 period (right panel Figure 2.6 and Figure 2.11b) is observed. The increase must be the result of the MV2 sand mining activities, as the amount of fines disposed at *Verdiepte Loswal* and *Loswal Noordwest* did not change substantially in the 2006-2014 period.

At *Loswal Noord* (3) the fines percentages are mostly zero for both periods. This can be explained by the disposal strategy: fines were disposed here until 1996, but later only sand. As a result, *Loswal Noord* (3) lies relatively high and the accumulation potential is

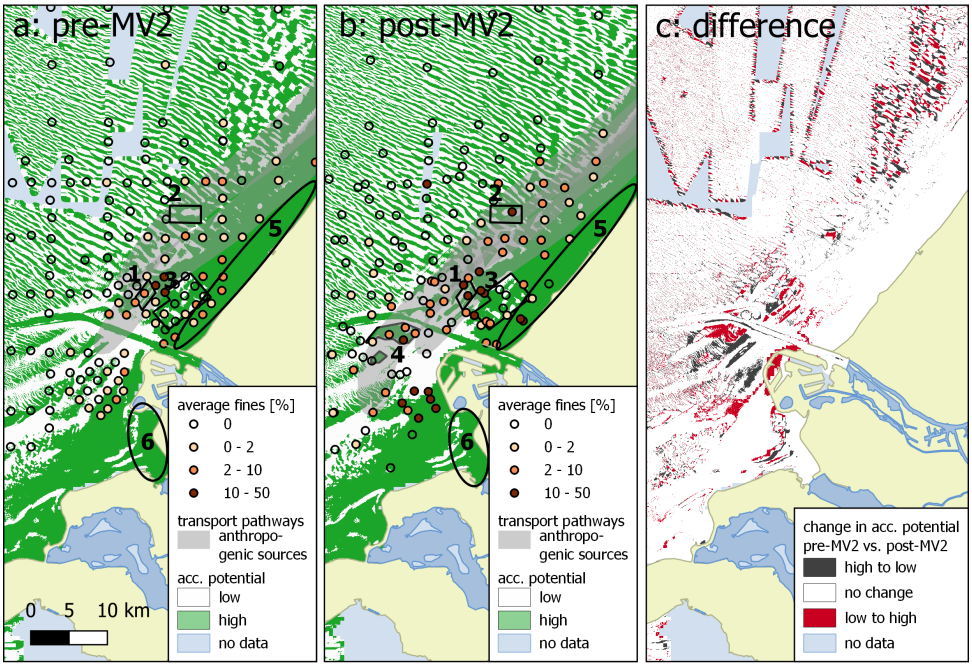

Figure 2.11.: Accumulation potential map in the Rotterdam area for the pre-MV2 (a) and post-MV2 (b) period. The accumulation potential is either high (green) or low (white), based on the accumulation potential classification. The difference map (c) shows changes in accumulation potential from pre-MV2 to post-MV2 period. We discuss the numbered sites with black contour lines below.

therefore low.

In the post-MV2 period (Figure 2.11b), the MV2 sand mining pit (4) forms a major accumulation zone. The high accumulation potential in this pit is mainly due to its 20 m larger depth (Figure 2.12a), though the 90th percentile of the bed shear stress is also smaller than during the pre-MV2 period (Figure 2.12b). This shows how sand mining influences the distribution of fines in two ways. Sand mining itself acts as a source of fines due to overflow from the hopper. During post-dredging conditions, the resulting pit becomes a sink for fines.

Directly south of MV2, accumulation potential increased, because of a local decrease in bed shear stress. This is caused by a change in the tidal flow pattern, as MV2 protrudes further into the North Sea, deflecting the tidal flow. This leads to a decrease in tidal current magnitude directly to the north and south of MV2, but also to tidal flow contraction directly west of MV2, where the tidal current magnitude increased (Figure 2.12b). Indeed, the data show an increase in fines percentage over the pre- to post-MV2 period directly south and north of MV2 (Figure 2.6 and Figure 2.11).

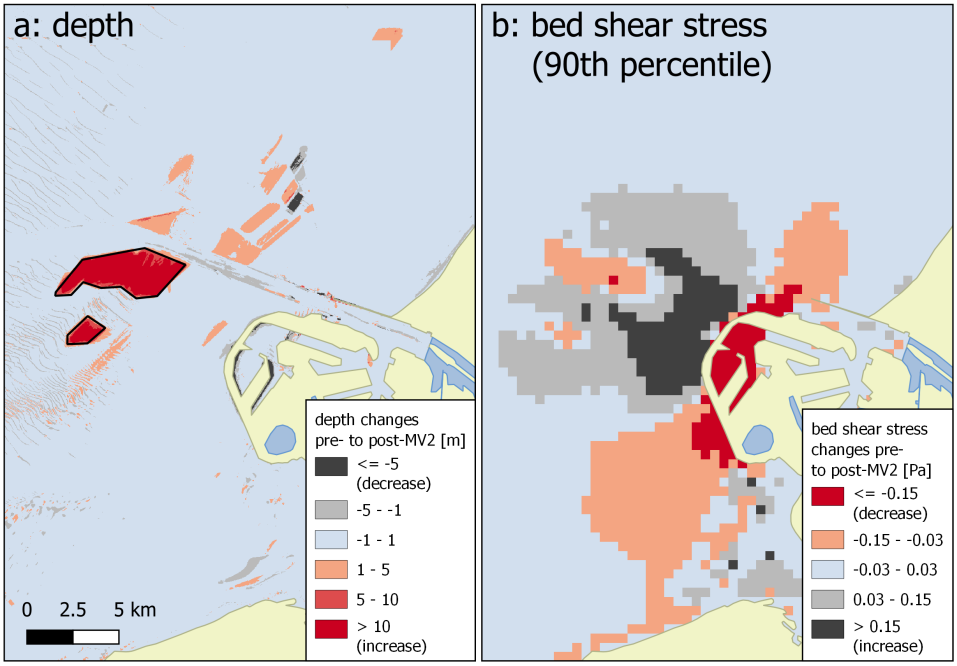

Figure 2.12.: Changes in depth (a) and computed bed shear stress (b) between the pre-MV2 and post-MV2 period. The MV2 sand mining pit is indicated with the thick black line in the left panel.

Beyond 15-20 km offshore, the spatial distribution of accumulation potential is mainly determined by large-scale bedforms, leading to alternating accumulation potential patterns. A substantial part of the offshore area is thus classified as a potential accumulation zone. Nevertheless, fines are virtually absent here (Section 2.3.2). This is explained by a lacking supply of fines, reflecting either the absence of sources or because transport pathways remain closer to shore.

Another zone with high fines percentages, earlier addressed by both Eisma (1968) and van Alphen (1987a), is found within 2-3 kilometres from the shore along the Holland coast (area 5 in Figure 2.11). In this area, computed tide-induced bed shear stresses are so low, that it is classified as a potential accumulation zone (Figure 2.11), in spite of local high DEV-values. At low $\tilde{\tau}_{b,c}$, data will mostly fall in the high accumulation potential range (see Figure 2.8 and Figure 2.10).

2.5. DISCUSSION

2.5.1. ACCUMULATION POTENTIAL AND THE EFFECT OF HUMAN INTERVENTIONS

The proposed conceptual framework can be used to assess the effect of different human interventions on the spatial distribution of fines in the seabed. These interventions likely

affect the local accumulation potential, which can be illustrated by the MV2 sand mining pit and MV2 reclamation. Due to the reclamation,both the area directly south of MV2 (Figure 2.11), and the MV2 sand mining pit became accumulation zones.

These interventions affected local accumulation potential in different ways, as visualized in the accumulation potential diagrams of Figure 2.13. DEV_{1000} values decreased strongly in the sand mining pit because of its 20 m larger depth, accompanied by a small decrease in bed shear stress. Thus, the accumulation potential in the sand mining pit increased (Figure 2.13a). South of MV2, DEV_{1000} values remain more or less constant, implying small bathymetrical changes. While pre-MV2 data indicate accumulation potential was already high in parts of the area, accumulation conditions became even more favourable because of the decreased bed shear stress in the post-MV2 period (Figure 2.13b).

Earlier human interventions in the DCZ have also led to a local increase in accumulation potential. Closure of estuaries in the southwestern delta led to a strong decrease in tidal currents, resulting in accumulation of fines in the former tidal channels (van Alphen 1987a). Such an area where bed shear stresses became very low, lies directly west of the *Haringvliet* mouth, area (6) in Figure 2.11. Due to the closure of the *Haringvliet* estuary and the construction of Maasvlakte 1, a sheltered area was created (Elias *et al.* 2017). Although our sediment dataset does not provide information, multiple studies have shown that accumulation of fines in this area is significant (Elias *et al.* 2017, Piekhaar and Kort 1983, van Alphen 1987a, van Heteren 2002). The computed accumulation potential is indeed high both in the *Haringvliet* mouth and in the former tidal channels of the southwestern delta (Figure 2.11). This confirms that our conceptual framework is capable of predicting the effect of closing tidal inlets on the distribution of fines in the seabed, and is consistent with previous studies.

The accumulation potential concept can also be used to quantify sub-grid effects in assessing the fines percentage in the seabed from numerical model simulations. The computational grid size in numerical models always exceeds the spatial dimensions of (small) bed forms. We have shown that small-scale elevation differences of the seabed strongly influence the presence of fines in the bed, and therefore explain the large spatial variability in observed fines percentage. Hence, if bathymetric data is available at scales smaller than the computational grid size, the accumulation potential can be used to obtain a first order estimate of the variability of fines percentage over the computational cells. This may be relevant, for instance, for analyses of the ecological functioning of the system.

2.5.2. VARIATIONS IN HYDRODYNAMIC FORCING AND RESPONSE OF THE SEABED

The spatial distribution of fines in the seabed results from the hydrodynamic forcing and the response of the seabed thereupon. The forcing is driven by tidal currents and waves. The seabed response consists of two major parts. Fines which previously accumulated are remobilized by wave action during storms and then transported by tidal currents. Afterwards, during calm conditions, these fines will deposit and are buried in the seabed again. Multiple timescales are associated with the forcing and seabed response, which

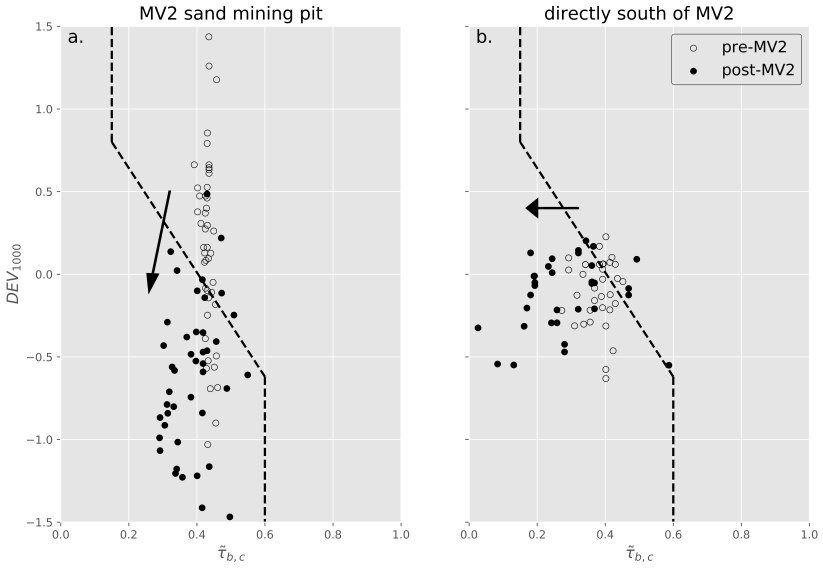

Figure 2.13.: Pre-MV2 vs. Post-MV2 accumulation potential, in MV2 sand mining pit (a) and south of MV2 (b). The MV2 sand mining pit data are based on the sampling stations visited in 2014. The locations of the data points south of MV2 area are based on the points in the post-MV2 period, i.e. from 2011 onwards. At these locations, DEV_{1000} and $\tilde{\tau}_{b,c}$ values for both the pre-MV2 and post-MV2 periods were computed.

are crucial to our analysis.

Logically, the fines percentage in the seabed decreases during storms because of remobilization. During subsequent calm conditions, fines percentages may increase again due to deposition and burial. Since storms occur frequently in the DCZ during winter, a seasonal variability in fines percentage is likely. Therefore, sampling was carried out after winter (storm season) to allow for a proper assessment of anthropogenic effects, undisturbed by seasonal variations (Section 2.2.2).

The accumulation of fines during calm conditions depends on the available time for deposition and burial, which should be sufficiently long. Hence, it depends on the ratio between the timescale for deposition and burial, and the timescale of hydrodynamic forcing variations. This ratio should be reflected by the hydrodynamic contribution to the accumulation potential. The first timescale is subject of ongoing research, but is likely in the order of several days to a week. The second depends on the dominant contribution to the hydrodynamic forcing, as currents and waves vary on different timescales themselves.

Tidal currents vary on diurnal and fortnightly scales, while waves occur more erratic.

If the wave height over water depth ratio is small apart from storms, calm conditions are governed by the magnitude of the tidal current. Prolonged calm conditions then relate to the maximum currents that occur during a spring-neap cycle, i.e. the fortnightly timescale. Therefore, we have schematised the hydrodynamic contribution to the accumulation potential through the 90^{th} percentile of the current-only bed shear stress, as it is representative for these maximum currents.

This approach is valid for the majority of the sampling locations, as they lie at water depths larger than 10 meters. At such water depths in the DCZ, the seabed is only subject to large wave-induced shear stress during storms. However, with decreasing water depth, waves become more important and will also define calm conditions. Therefore, the accumulation potential is not accurately predicted in the shallow nearshore, i.e. the breaker zone and around (e.g. parts of area 5 in Figure 2.11). The differences between observed fines percentage and its prediction by the accumulation potential are thus partly explained by how calm conditions are schematised.

2.5.3. APPLICATION OF CONCEPTUAL FRAMEWORK TO OTHER COASTAL SHELF SEAS

The conceptual framework was developed for the southern North Sea, but its concept is generic and it can be used to analyse the dynamics of fines in other coastal shelf seas, provided they have a sandy substrate. The framework allows to study the effect of human activities on these dynamics in a structured way. This enables engineers to effectively assess and thus mitigate the impact of these activities. Here, we provide several examples of how the conceptual framework could be utilized.

In the Seine estuary, France, material dredged from harbours is disposed at sites off the coast of Le Havre. Marmin *et al.* (2014) demonstrated that relocating this disposal site for, mostly fine, sediment is constrained by both economic and natural restrictions. Apart from the local effects on biota at the dumping site, the far-field effects need to be studied as well. Marmin *et al.* (2014) mention "these effects depend on a variety of environmental conditions (Essink 1999), but differ greatly from one site to the other, thus general conclusions are difficult to draw". By estimating the transport pathways from a site and determining accumulation potential in the area, the influence of this newly introduced source can be assessed more specifically. Furthermore, the conceptual framework can be used to assess the differences between a concentrated disposal strategy at one location versus smaller disposal locations across a larger area.

Human interventions in the shelf seas surrounding Australia are subject to strict regulations, as they pose a threat to the present coral reefs (Erftemeijer *et al.* 2012). In terms of the conceptual framework, accumulation potential is high between and on the coral reefs (Fisher *et al.* 2015, Jones *et al.* 2015). Thus, to avoid smothering of the coral reefs, the transport pathway envelope from disposal/dredging sites has to be established. This can form the basis for revised project design or the implementation of mitigating measures.

The North Sea is one of the world's most actively studied shelf seas. However, in many shelf seas the seabed has only been sparsely sampled, such as the Andaman Sea. For example, Kamp-Nielsen *et al.* (2002) and Feldens *et al.* (2012) observed patches of fine

sediment off the coast of Thailand from local high-resolution surveys. The presence of these patches depended on small-scale topography, with sharp boundaries between a patch and the sandy environment. Combining hydrodynamic model results with bathymetric data provides a valuable first estimate of where to expect fines. This can then be incorporated in the design of seabed sampling campaigns. The framework can be utilized to trace back the fine sediment to its respective sources, once the pathways are established.

2.6. CONCLUSIONS

In this chapter, we studied the processes and conditions which determine the distribution of fines in the surficial seabed of the Dutch coastal zone (DCZ). A new dataset was analysed to determine this spatial distribution and then compared with previous datasets. The large extent and high spatiotemporal resolution of the new dataset enables to study fine sediment dynamics in the North Sea at scales smaller than before.

At mega-scale, the spatial distribution of fines in the DCZ is generally in agreement with previous work by Eisma (1968) and van Alphen (1987a). Virtually no fines are found beyond 20 km offshore. Further nearshore, variability in fines percentage is found on both smaller (tens of metres) and medium (kilometres) scales. Locally, fines percentages exceed 10-20%. Highest percentages are found within 2 to 3 km from the shore, north and south of the River Rhine outflow, and in the former tidal channels in front of closed estuaries. Large-scale human interventions invoked local changes of the fines percentage in the seabed in the order of 10% and above.

To analyse the large-scale distribution of fines in the seabed and enable quantitative prediction of the effect of large-scale human interventions, a conceptual framework was developed. This framework consists of three components: (1) sources of fines; (2) transport pathways from these sources; and (3) accumulation potential. It was shown that the large-scale distribution of fines in the DCZ is mainly determined by the first two components, whereas accumulation potential mainly influences the local distribution. Differences in fines distribution in response to the construction of MV2, a seaward extension of the Port of Rotterdam, were caused by an additional source of fines released from overflowing during sand mining, and by local changes in accumulation potential – most notably in the deep mining pit and the sheltered zone south of MV2.

The new framework enables the assessment of individual human interventions in terms of source, pathway and/or accumulation effects. It further allows for the assessment of cumulative effects due to multiple interventions (and their interactions) in one area. Such analyses can establish a sound basis for Environmental Impact Assessments and may form a starting point for successive analyses on ecological effects. In this way, the framework developed here can help engineers and policy makers to assess how human interventions affect the ecosystems like the North Sea and to limit or mitigate their environmental impact.

3

THE BURIAL OF FINES IN A SANDY SEABED

This chapter has been published as: **Hendriks, E.**, van Prooijen, B.C., Cheng, C.H., Aarninkhof, S.G.J., Winterwerp, J.C., Soetaert, K.E. (2022). *An explanatory model for the burial of fines in the sandy seabed of the southern North Sea.* Marine Geology, 454, 106953.

3.1. INTRODUCTION

Shallow seas are increasingly exposed to human interferences (Degraer *et al.* 2019), like beam trawl fishing (Rijnsdorp *et al.* 2008), dredging for land reclamation (Stolk and Dijkshoorn 2009) and construction of offshore wind farms (Breton and Moe 2009). These interferences lead to a modification of the suspended sediment concentration (SSC) (Piet *et al.* 2019, Capuzzo *et al.* 2015). Most suspended sediment consists of fine sediment (i.e., fines, sediment smaller than 63 μm), which plays a major role in the ecological functioning of shallow coastal seas. When suspended in the water column, fine sediment leads to an increase in turbidity (Fettweis *et al.* 2019), thereby impeding sunlight penetration into the water column (Kirk 1994). This may lead to a decrease in phytoplankton growth rate (e.g., Anthony *et al.* 2004, van Duin *et al.* 2001) and thus a decline in ecosystem health, as phytoplankton form the base of the marine food pyramid. We focus on the southern North Sea, where ecosystem functioning is strongly influenced by fine sediment dynamics (van der Molen *et al.* 2017), even though its seabed is predominantly sandy.

In the southern North Sea, SSC varies strongly in both time and space. On short temporal scales, it depends on the occurrence of storms (Stanev *et al.* 2009, van der Hout *et al.* 2017). During storms, a simultaneous increase in SSC occurs in the entire southern North Sea within days of the storm onset (Fettweis *et al.* 2012, Pietrzak *et al.* 2011, Suijlen and Duin 2001). Subsequently, SSC steadily decreases, while still varying on tidal timescales (Flores *et al.* 2017, van der Hout *et al.* 2017). Within a week, SSC in the entire area has again decreased to pre-storm values (Fettweis *et al.* 2010, Suijlen and Duin 2001, Kleinhans *et al.* 2005). Spatially, mean SSC mainly depends on cross-shore distance (de Boer *et al.* 2009). Concentrations are generally high within 2-3 kilometres from the shore, strongly decreasing in an offshore direction (Fettweis and Van den Eynde 2003, van Alphen 1990, van der Hout *et al.* 2015).

Both the temporal and spatial variations indicate that SSC magnitude strongly depends on the exchange of fines with the sandy seabed (van Kessel *et al.* 2011, van Prooijen *et al.* 2007). The simultaneous increase of SSC during storms over a large domain can only be explained from local sources of fines throughout the system. Advection, dispersing sediment from one or a few isolated sources, is too slow of a process to explain the quasi-instantaneous increase of SSC over this large domain. Likely, these local sources consist of fines which are remobilised from the seabed by waves (Fettweis *et al.* 2010, Flores *et al.* 2017).

The system-wide decrease in SSC within a week after a storm suggests local sinks of fines within the system, forming the SSC source for the next storm. During calm conditions, fines settle out of suspension and deposit. Due to their small settling velocity, they deposit on top of the sandy seabed. As tidal currents resuspend fines into the water column when they are readily available on the seabed (Terwindt and Breusers 1972, van Maren *et al.* 2020, Widdows *et al.* 2007), a decrease in SSC implies that they are no longer available, but are buried within the seabed. Thus, burial in the seabed provides local sinks for fines. This short-term water-bed exchange leads to considerable short-term variations in fines percentage in the southern North Sea bed (Hendriks *et al.* 2020, Witbaard *et al.* 2016). However, it does not affect the fines percentage in the upper strata of the North Sea bed on decadal time scales (Eisma 1968, van Alphen 1987a,Hendriks *et al.* 2020).

Despite its importance for fine sediment dynamics, the burial of fines into a sandy seabed is currently not well understood. A mechanistic description is lacking for this process, thus only heuristic burial parameterisations are used in the literature (Sanford 2008, van Kessel *et al.* 2011, van der Molen *et al.* 2009). This limits the modelling of fine sediment dynamics in shallow coastal seas (van Maren *et al.* 2020). To improve this, a conceptual description for the burial of fines is required.

Previous research suggests three possible processes which may bury fines into the seabed, but for none of these a mechanistic description is available. These processes are: (1) pore water flow induced by pressure gradients over bedforms, (2) bioturbation and (3) bedform migration (Dankers 2005, Eisma 1968, Graf and Rosenberg 1997, Huettel *et al.* 1996, Huettel and Rusch 2000, Jennes and Duineveld 1985, Le Hir *et al.* 2007, Martinius and van den Berg 2011). Pore water flow rates are generally small, and only make a considerable contribution in coarse sediment where pressure gradients are large (Harrison *et al.* 1983, van der Loeff 1981, Webb and Theodor 1968). Hence, it is expected that they hardly bury fines in the southern North Sea bed, with median grain sizes (d_{50}) of 200-350 μm, even over long timescales (Kleinhans *et al.* 2005). Bioturbation is an effective mixing mechanism (Graf and Rosenberg 1997, Kleinhans *et al.* 2005, Kristensen *et al.* 2012, Le Hir *et al.* 2007, Volkenborn *et al.* 2007, Witbaard *et al.* 2016), but is only able to accumulate fines over longer timescales, on the order of weeks to months, or even years (Kleinhans *et al.* 2005, Lecroart *et al.* 2007, Middelburg *et al.* 1997). As there are no indications of increased biogenic activity after storms, bioturbation will not lead to sufficient burial of fines in the days after a storm. This leaves bedform migration as the only likely mechanism for the considered area.

The objective of this chapter is to develop a conceptual mechanistic model explaining the burial of fines into a sandy seabed induced by the formation and migration of bedforms. This model is inspired by in-situ observations in the North Sea, and its development was an iterative process in concert with analysing the data. To properly assess the data, one needs to be informed by the conceptual model. Therefore, we start by introducing this model in Section 3.2, which provides a phenomenological description of the burial process. It has been deduced from an analysis of the relevant bedforms in the North Sea, and sedimentological theory on flaser bedding (Reineck and Singh 1980). Subsequently, the data collected in the North Sea are presented (Section 3.3). Using these data, we verify and discuss the proposed burial model (Section 3.4). Finally, we discuss the implications of our findings and present our conclusions (Section 3.5 and 3.6). This chapter only discusses the ingress of fines into a sandy seabed, not the remobilisation of fines from that seabed during a storm.

3.2. BEDFORMS AND THEIR ROLE IN FINE SEDIMENT BURIAL

3.2.1. BEDFORMS IN THE SOUTHERN NORTH SEA

A wide variety of bedforms is found on the southern North Sea bed (Passchier and Kleinhans 2005), formed by the interaction between hydrodynamic forcing and the seabed (Damen *et al.* 2018, Hulscher and van den Brink 2001). Both the hydrodynamic forcing and seabed characteristics vary in space and time and, as do the resulting bedforms. Their length varies from multiple kilometres (i.e., mega-scale) to decimetres (i.e., small-

scale) (Figure 3.1). Smaller bedforms may develop atop larger ones, hence the seabed topography may ultimately become quite complex (Kleinhans 2005).

Bedforms can be formed by tidal currents and waves, or a combination of both. This affects their length, shape, and associated time scale. Mega- and large-scale bedforms (wave lengths larger than tens of metres) are predominantly current-induced and tend to be asymmetric (van Gerwen *et al.* 2018), while small-scale bedforms (wave lengths smaller than several metres) can be formed by either tidal currents, waves or a combination thereof (Brakenhoff *et al.* 2020). Once formed, bedforms are not static but tend to migrate, and then change both in form and size. Migration rates are inversely related to bedform size (Baas *et al.* 2000). While mega-scale bedforms only migrate on decadal timescales, small-scale bedforms can migrate multiple times their own length within hours to days (Lichtman *et al.* 2018).

From this wide range of bedforms, we propose that only small- and meso-scale bedforms are relevant for the burial of fines. As burial predominantly takes place within the week after a storm, the relevant bedforms should be mobile enough to migrate or change shape over the course of a few days. Seaward from the surf zone, bedforms longer than several decametres can partially transform (Houthuys *et al.* 1994), but do not migrate nor transform entirely on these short timescales. Hence, we will not consider these in our analysis. We thus only consider the small- and meso-scale bedforms, known as ripples and megaripples (Figure 3.1 – lower 2 panels). At this length scale, bedform size and shape vary strongly with time, due to wave and tidal flow (e.g. Amos *et al.* 1996, Li and Amos 1999. Resulting (mega-) ripples and their characteristics are summarised in Table 3.1. On the lower shoreface of the southern North Sea, ripple height is a few centimetres during calm, tide-dominated, periods (Meirelles *et al.* 2016, Schrijvershof *et al.* 2019, van der Werf *et al.* 2022, Wengrove *et al.* 2017). When the wave- and current intensity increase, so do ripple length and height. Above a certain threshold, ripples transform to megaripples (Soulsby *et al.* 2012. For current-induced bedforms, this transformation occurs around a Shields value of 0.1 (Marten 2010), while for wave-induced bedforms, this transformation occurs gradually as their length and height depend on the orbital excursion (Table 3.1). The height of storm-induced megaripples and ripples on the lower shoreface varies from 0.05 cm to 0.2 m (Wengrove *et al.* 2018, Wengrove *et al.* 2019). However, bedforms need time to adjust to the governing hydrodynamic conditions. Hence, the transformation from current-induced to storm-induced bedforms is gradual (Soulsby *et al.* 2012, Traykovski 2007). Likewise, the transition back to current-induced ripples is also gradual, and generally takes place within hours to several days (Wengrove *et al.* 2018).

3.2.2. FINES BURIAL BY A MIGRATING RIPPLE

We argue that small, current-induced ripples are the principal bedform type burying fines into a sandy seabed. This burial process is sketched in Figure 3.2, showing a ripple cross-section. It presumes that ripples migrate in a single direction, with intermittent periods of slack water, and are two-dimensional. These presumptions aim to make the process description more straightforward. The first presumption is based on the fact that tidal currents along the Dutch shore are flood-dominated (Grasmeijer *et al.* 2022). As

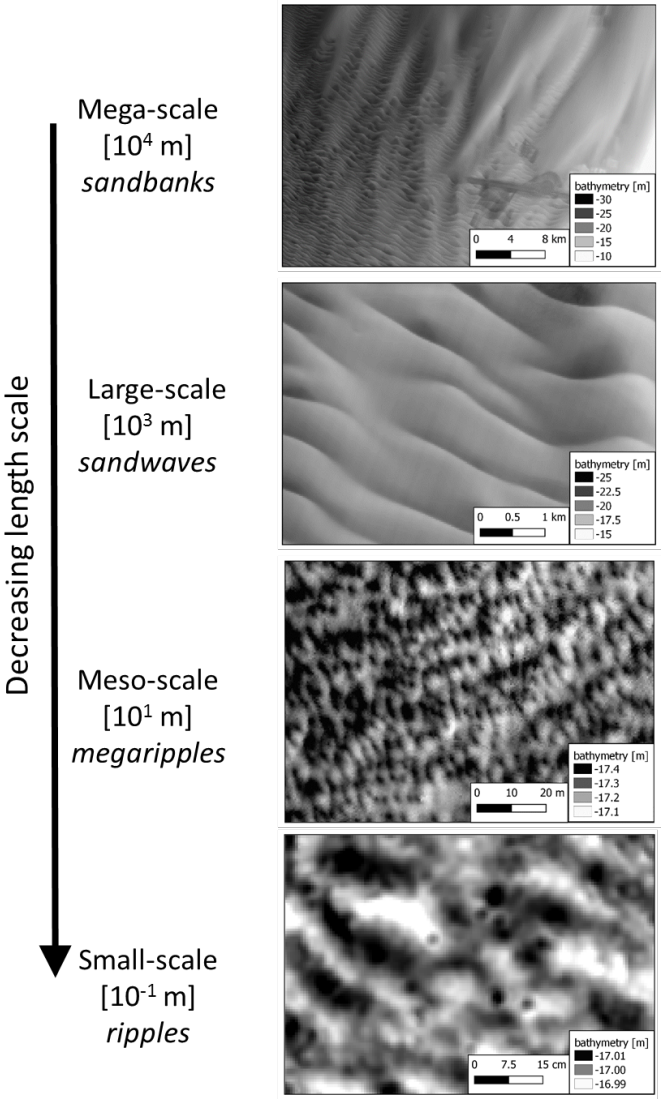

Figure 3.1.: Bedforms on different length scales along the Dutch coast. Length scales vary from 10 4 metres (top panel) to 10 -1 metres (bottom panel). Upper two panels from NLHO data (Arcadis and Deltares 2019). Lower two panels using data from the Coastal Genesis 2.0 dataset (van der Werf *et al.* 2022). Top left corner of each map in ETRS89 UTM31N coordinates: I. (563971, 5837427), II. (580136, 5805159), III. (656068, 5927954), IV. (584832, 5793243).

current-induced ripple migration rates scale non-linearly with flow velocity (Table 3.1), this asymmetry leads to a dominant migration direction. This is consistent with the find-

Table 3.1.: Ripple and megaripple characteristics based on dominant hydrodynamic forcing. Ripple properties : η_{eq} – equilibrium ripple height, λ_{eq} – equilibrium ripple length, v_{mig} – migration rate. Parameters : $D*$ – dimensionless grain size (e.g., van Rijn 2007), d_{50} – median grain size, d_0 – near-bed orbital excursion, θ – Shields parameter, u_c – current-induced velocity and u_w – wave-induced velocity. The typical values are for fine sand, and for wave-induced bedforms only apply to orbital (mega-) ripples.

Type -> Property	**Current-induced ripples**	**Wave-induced ripples**	**Combined wave-current**
η_{eq} [m]	$\eta_{eq} = d_{50}202D_*^{-0.554}$ (Soulsby *et al.* 2012)	$\eta_{eq} = 0.1d_0$ (Wiberg and Harris 1994)	$\eta_{eq} = \alpha 0.1d_0$, where $\alpha = f\,(D_*, u_c, u_w)$ (Tanaka and Dang 1996)
λ_{eq} [m]	$\lambda_{eq} = d_{50}(500 + 1881D_*^{-1.5}$ (Soulsby *et al.* 2012)	$\lambda_{eq} = 0.62d_0$ (Wiberg and Harris 1994)	$\lambda_{eq} = \alpha 0.62d_0$, where $\alpha = f\,(D_*, u_c, u_w)$ (Tanaka and Dang 1996)
Steepness (η_{eq}/λ_{eq}) [-]	0.06-0.1	approx. 0.16	0.1-0.15
Shape [-]	asymmetric	symmetric	asymmetric
v_{mig} [m/s]	$v_{mig} = 0.1154\theta^{3.03}$, for $d_{50} = 238\ \mu$m (Baas *et al.* 2000)	depends on wave skewness (Traykovski 2007)	depends on wave skewness and θ (Amos *et al.* 1999)

ings of van van der Werf *et al.* (2022), who showed that the critical Shields parameter is only occasionally exceeded on the Dutch lower shoreface by ebb currents alone. In reality, ripples will likely be three-dimensional and can also migrate in opposing directions. Though this may affect burial rates (quantitative) it will not affect the relevant processes (qualitative). Below, we elaborate on the different steps in the burial process.

Due to tidal currents, asymmetric current ripples of 2-3 cm high are formed in fine sand with a steepness of 0.06-0.1 (Figure 3.2a) (Soulsby *et al.* 2012, van der Werf *et al.* 2022). Due to this asymmetry, flow separation occurs from the ripple crest (flow separation area indicated by the dash-dotted lines in Figure 3.2). Hence, a wake forms at the steep lee side of the ripple. In this wake, the bed shear stress is (at least) 20% lower than on the crest (Fernandez *et al.* 2006, McLean *et al.* 1994). These ripples will migrate along the bed if the tidal currents are strong enough to exceed the critical Shields parameter.

During slack water, current velocities decrease and ripple migration ceases. Consequently, fines settle out of suspension and deposit on the seabed (Figure 3.2b). The amount of deposited fines depends on the slack water duration, concentration of suspended fine sediment and characteristic settling velocity (Winterwerp 2007). The largest net deposition is expected to occur on the lee side and in the ripple trough (Reineck and Wunderlich 1968). As the in-situ density of suspended fines is relatively low (i.e. water

content is high), a relatively thick, but soft layer of fines is expected to build up in the trough (Terwindt and Breusers 1972). The critical shear stress for resuspending these freshly deposited fines is generally low, on the order of 0.1 Pa (van Kessel *et al.* 2011, van Maren *et al.* 2020, Widdows *et al.* 2007).This is lower than the critical shear stress for fine sand, which is approximately 0.2 Pa (van Rijn 2007).

When the tidal current increases again, so does the bed shear stress. Fines on the lee side of the ripple are (partially) eroded because of their low critical shear stress. However, in the wake of the bedform and the induced return flow, part of the fines remains within the trough, also at larger flow velocities. When the bed shear stress exceeds the critical shear stress for sand, sand grains on the stoss side will be transported as bedload (Figure 3.2c). As the bed shear stress is not uniformly distributed over the ripple, sand transport on the stoss side starts shortly after fines start to be eroded on the lee side. Once the sand grains are transported over the ripple crest, they deposit atop the fines still present in the trough. As more sand grains are transported, the ripple migrates.

After a short period of time, the ripple has migrated by distance x_{mig} and has buried some fines (Figure 3.2d). Due to the load imposed by the overlying sand, the layer of fines consolidates. As a result, its density increases while the layer thickness decreases. These fines are buried in the upper seabed strata as individual lenses, and likely not mixed with the sandy substrate. This yields a flaser bedding, as described in sedimentology (Martin 2000, Reineck and Singh 1980, Reineck and Wunderlich 1968, Terwindt and Breusers 1972).

This process is relatively fast, as current-induced ripples can migrate several times their own length within a tidal cycle (Lichtman *et al.* 2018). Because of the non-uniformity of bed shear stress over the ripple, this process explains why not all fines are eroded before they are covered by sand. However, the explanation provided here is not yet complete, for two main reasons. Firstly, due to the limited height of these ripples, fines would only be buried in the top centimetre of the seabed. Measurements indicate that fines are present not only in the top 1cm, but are also found 10-15 cm below the seabed surface (Hendriks *et al.* 2020, Passchier and Kleinhans 2005). Secondly, when the ripples migrate further than indicated in Figure 3.2d, the fines which were previously buried at their lee side become exposed again at the stoss side within a short time. If the increase in critical shear stress of buried fines is limited, this would imply that only a little net burial would take place. Hence, an additional process must occur. In the next section, we hypothesise how the interaction between bedforms of different length scales leads to a net burial of fines.

3.2.3. HYPOTHESIS: BURIAL DUE TO INTERACTION OF SCALES

Interaction between bedforms of different length scales enables deeper burial of fines which therefore remain within the seabed for longer periods (i.e., between storms). As Figure 3.1 shows, a multitude of different bedforms can occur on the North Sea bed, which can co-exist in both space and time. Bedforms of different scales, from mega- to small-scale, interact with one another. Our hypothesis elaborates on the interaction between bedforms of small- and meso-scale, i.e. ripples and megaripples (two lower panels Figure 3.1).

This interaction is sketched in Figure 3.3, which proposes four distinct phases in the

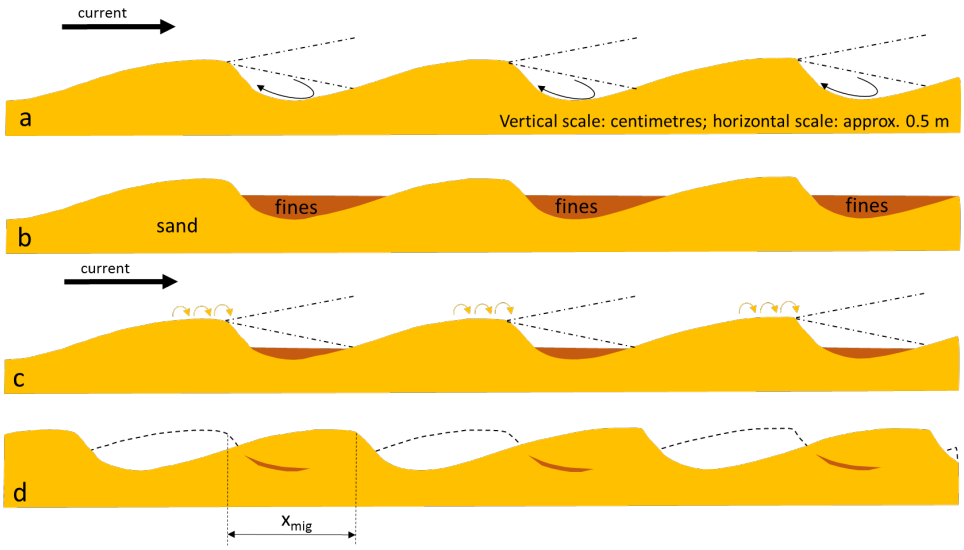

Figure 3.2.: Sketch of different steps for burial of fines by migrating small-scale bedforms. (a) Current-induced ripples migrating from left to right due to tidal current. Flow separation, indicated by the dash dotted lines, leads to a wake on the lee side of ripples. (b) During slack water, fines settle out of suspension, forming soft layers on the seabed. Largest net deposition is expected in the ripple troughs. (c) When tidal currents increase again, part of the previously deposited fines are eroded. Sand grains transported over the ripple crest deposit on the fines accumulated in the ripple troughs. (d) The ripples have migrated by distance x_{mig}, burying fines into the seabed. Fines are present as thin lenses.

burial process. Together, these form a dynamic cycle. For each phase, we discern between the behaviour of the sandy seabed and the presence of fines. The latter can either be suspended in the water column, deposited on, or buried within the seabed.

We start with phase 1, which occurs in a relatively calm period, dominated by tidal currents. Only small current-induced ripples are formed on the seabed. Hence, the height of the active ripple layer is limited to 2-3 cm Most fines were buried in the seabed during previous cycles, deeper than this active layer. SSC is low and at slack tide, thin layers of fines deposit on the seabed, preferentially in the ripple troughs. The small-scale ripples migrate (similar to Figure 3.2), but the exchange of fines is limited.

Phase 2 represents a storm build-up phase. Wave energy increases and wave-induced bedforms are formed on the seabed. These gradually develop into megaripples. During this phase, bedform height increases and fines are remobilised from the seabed. Since bed shear stresses are high, fines are not likely to deposit on the seabed. Thus, burial will be absent or limited. Combined, this leads to a net flux of fines into the water column and therefore an increase in SSC.

Phase 3 represents the storm peak, with maximal wave energy. The developed megaripples have reached their maximum height. We assume that these bedforms do not migrate substantially, owing to the symmetry of the waves. Most fines buried during the previous cycles have now been remobilised, leading to high SSC in the water column. As bed shear stresses are high, deposition of fines on the seabed is unlikely.

Phase 4 represents the post-storm phase, when wave energy is low again and tidal currents are dominant. Current-induced ripples form, superimposed on the megaripples. These ripples will migrate, leading to a net sand transport towards the megaripple troughs for two reasons. First, bed shear stresses on the stoss and crest of the megaripples are higher than on the lee side and troughs. Second, the bed elevation gradients lead to net sand transports (van Rijn 1984, Walstra *et al.* 2007). As a result, the storm-induced megaripples gradually flatten out and the smaller ripples become dominant again.

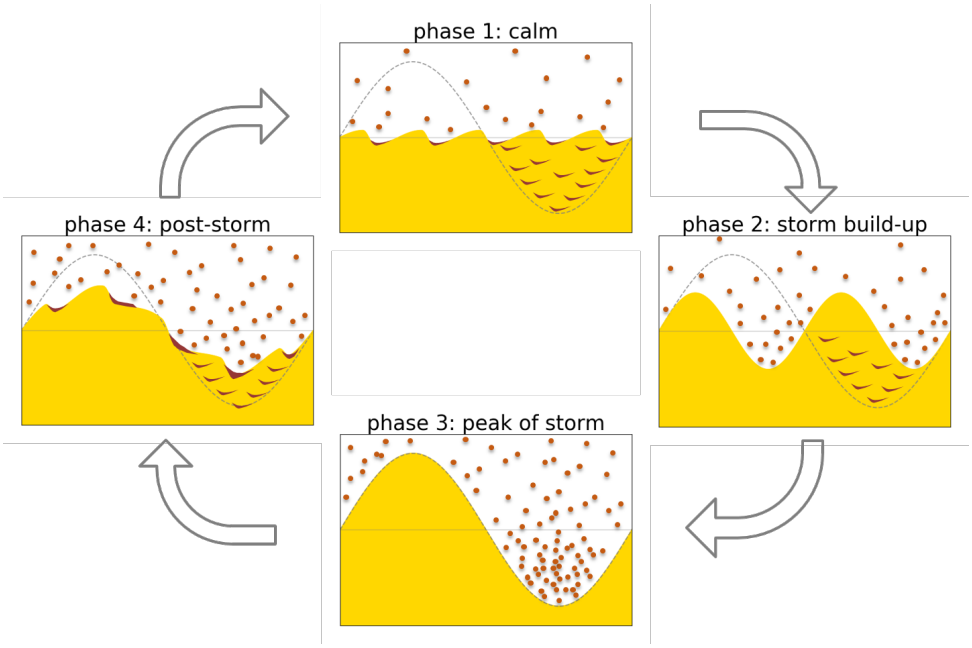

Figure 3.3.: Schematic of burial of fines in a sandy seabed due to reconfiguration and migration of larger and smaller bedforms. Yellow polygon indicates the sandy seabed. Brown lenses indicate fines in and on the seabed, while brown dots indicate suspended fines. Dashed grey line indicates maximum ripple dimensions formed during phase 3.

Fines are buried into the seabed during phase 4, because of the migrating small-scale ripples. Similar to Figure 3.2, fines deposit in the troughs of the small-scale ripples during slack tide. Since SSC is still high due to the preceding storm, deposition rates will be high and a relatively thick layer of fines is formed. Subsequently, the fines are buried when the ripples migrate. Because of the asymmetry in sand transport, the ripples migrating towards the trough of the former megaripple will be covered by subsequent mi-

grating ripples. In this way, fines end up at different depths in the bed and become unavailable for resuspension by the tidal currents.

This process generates distinct signatures of where and how fines are found in the seabed. Burial depth is contingent on bedform height, thus the maximum depth at which fines are buried depends on the height of bedforms created during storms. When fines have been buried in the seabed, they are present as distinct lenses. Furthermore, fines predominantly end up in the former troughs of megaripples and not in their crests. This implies that fines percentages vary substantially on megaripple length scales, from zero at the former megaripple crest to a high fines content in the former trough in the form of (multiple) lenses.

3.3. MATERIALS AND METHODS

3.3.1. STUDY SITE AND MEASUREMENT PERIOD

The conceptual model was developed and tested with data collected in the southern North Sea. As the seabed and water column form a coupled system, simultaneous measurements of both elements are required. Seabed samples were taken along a cross-shore transect offshore of Egmond aan Zee, the Netherlands (Figure 3.4a) in 2017. This transect starts at 1 km offshore (52.6371 °N, 4.6054 °E) and extends to 10 km offshore 52.6389 °N, 4.4722 °E). It is located approximately 80 km north of the River Rhine outflow, thus in the far-field region of the Rhine Region of Freshwater Influence (ROFI). Therefore, the water column at Egmond aan Zee periodically experiences weak stratification (Rijnsburger *et al.* 2016). It lies 20km north of the port of IJmuiden, where no significant volume of freshwater is discharged into the North Sea. However, approximately 1 MT of dredged fine sediment is disposed of directly north of the harbour entrance channel annually (Winterwerp 2001. This disposal site lies 15 km south of the studied transect, and fines deposited there will eventually reach the Egmond aan Zee transect as the residual transport direction of fines along the Dutch coast is in north-easterly direction (de Boer *et al.* 2009).

The seabed along this transect is mostly sandy, with a d_{50} of 200-250 μm and a fines percentage of up to 10% (Witbaard *et al.* 2016). A net shoreward transport of fine sediment exists during calm periods (van der Hout *et al.* 2015), inducing elevated levels of turbidity between 1–3 km from the shore (van (van Alphen 1990, van der Hout *et al.* 2015). Morphologically, the area is characterised by the presence of several shoreface-connected ridges (van de Meene and van Rijn 2000a). The bed level along the transect varies from -10 m to -20 m (Figure 3.4b), situating it entirely on the lower shoreface (Anthony and Aagaard 2020, Grasmeijer *et al.* 2022). All bed levels are referenced to the Dutch Ordnance level (NAP, *Nieuw Amsterdams Peil*).

The first sampling campaign took place from 9 to 11 June 2017 and the second from 19 to 26 October 2017. In the remainder of the text, we refer to them as the 'June' and 'October' campaigns, respectively. These campaigns were performed using the RV Pelagia of the Royal Netherlands Institute for Sea Research (NIOZ). During both campaigns, multiple measurements were done along this transect, comprising seabed sampling and measurements from instrumented landers. The applied techniques and data postpro-

cessing are discussed in Section 3.3.2 and Section 3.3.2.

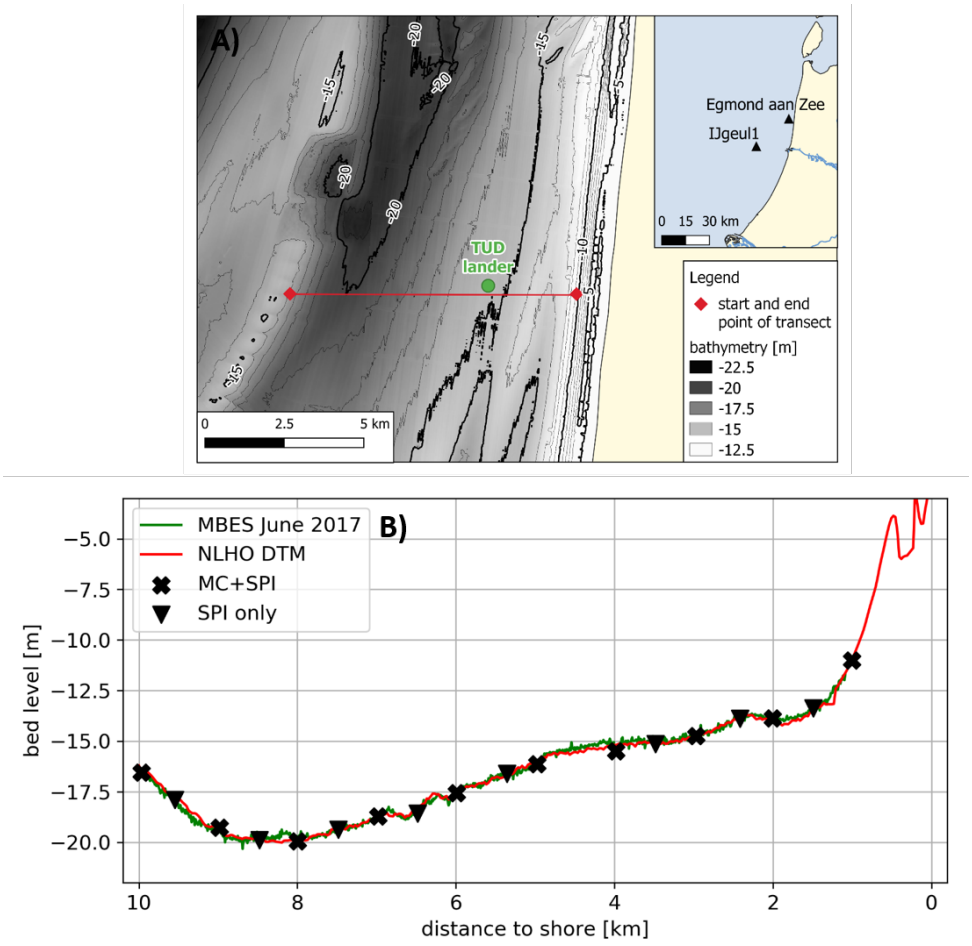

Figure 3.4.: (A) Egmond aan Zee cross-shore transect. Bathymetry based on NLHO Digital Terrain Model (DTM), based on bathymetric surveys from 2009, 2012 and 2014 (Arcadis and Deltares 2019). The inset indicates the location of the study site along the Holland coast and the location of the wave buoy IJgeul 1. (B) Bed level along the transect as determined from the NLHO DTM and multibeam echosounding during the campaigns, also indicating the seabed sampling stations for both Multicorer (MC) and Sediment Profiling Imagery (SPI).

3.3.2. SEABED SAMPLING

The seabed was sampled at predefined stations along the transect (Figure 3.4b) using two methods. The first method was the Multicorer (MC), which simultaneously collects up to 8 bed sediment samples at a station. The MC was deployed at 1000-m intervals in both campaigns. The second method, Sediment Profiling Imagery (SPI), was used to take images of the upper seabed layer. The SPI stations were evenly spaced at 500-m intervals in June and October (Figure 3.4b). However, in the latter campaign, we adjusted the spacing of the stations in the most offshore 5 km part of the transect to a 1000 m interval, as preliminary results from the June campaign showed more fines within the inner 5 km. This allowed us to sample the stations within 5 km twice. As the vessel was not equipped with Dynamic Positioning, seabed samples from the same station were not collected exactly at the same position in June and October but 10 to 30 metres apart.

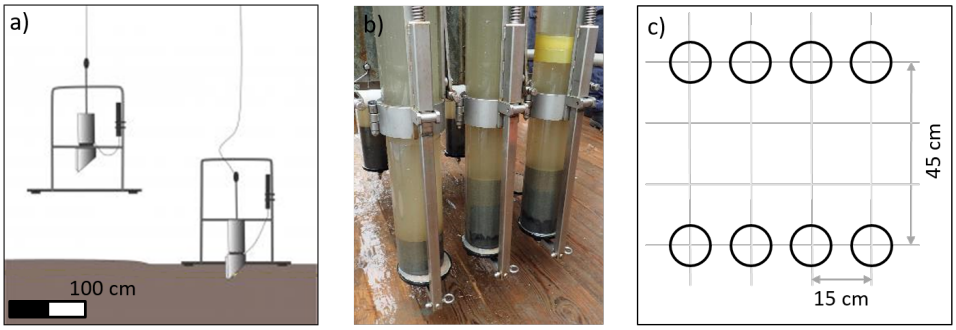

Figure 3.5.: (a) SPI deployment sketch (VLIZ 2022), (b) Photo of Multi Corer (MC) with collected sediment samples, (c) MC array with indication of dimensions.

A standard protocol was followed to collect sediment samples with the MC. The device is equipped with eight 10-cm diameter cores (see Figure 3.5b for image of MC frame). These are arranged in a fixed layout of two rows (Figure 3.5c), which are 45 cm apart. Within a row, the centres of adjacent cores are 15 cm apart.

At least six sediment cores were required per station. Three of these were used to determine the grain size distribution, while the other three were used to determine substrate permeability (Cheng *et al.* 2020). In this chapter, we only discuss the grain size distribution results. Cores with more than 10 cm of sediment were processed. If not enough cores of sufficient length could be collected within a single MC deployment, sampling was repeated until at least six sediment cores of sufficient length were collected. Additional sampling locations were located within 20 m from the initial location and taken within 30 minutes after the first deployment. The total number of MC deployments per station is listed in Table 3.2.

Once the sediment cores were retrieved from the MC, the overlying water was siphoned off carefully, without disturbing the sediment interface. The main cores were then subsampled using smaller acrylic tubes (length 15 cm, diameter 3.5 cm). These sub-cores were sliced at 1cm intervals for the upper 5 cm and at 2-cm intervals for the lower part.

Table 3.2.: Number of MC deployments per sampling station, for the June and October campaigns

km offshore	**10**	**9**	**8**	**7**	**6**	**5**	**4**	**3**	**2**	**1**
MC deployments - June	1	1	1	1	1	4	1	3	4	1
MC deployments - October	1	1	2	2	1	6	3	3	1	1

Sediment slices were stored in a freezer at -20° C in labelled vials. After the campaign, these vials were transported to the NIOZ laboratory ensuring the sediment remained frozen. There, the subsamples were first freeze-dried for 48 hours, followed by sieving over a 1 mm mesh. During sieving, the material was thoroughly homogenised and wetted in tap water. A small subsample was analysed with a Malvern Mastersizer 2000 particle sizer. This instrument determines the grain size distribution by laser diffraction (McCave *et al.* 1986), yielding the volume percentage of different size classes. The size class of particles smaller than 63 μm is referred to as fines. We do not distinguish between the clay and silt fractions. Similar to Callesen *et al.* (2018) and Hendriks *et al.* (2020), we assume that volume percentages are representative for mass percentages.

The SPI system consists of a camera held within a frame, initially developed by Rhoads and Germano (1982) (Germano *et al.* 2011). Figure 3.5a shows how the SPI system is deployed. Ten seconds after each landing on the seabed, the first photo is taken. A duplicate photo is taken ten seconds later. After collecting two photos, the SPI frame is hoisted up several metres and lowered again at several decametres from the first sampling point. Here, another two photos are collected before it is brought back up to the ship deck.

The SPI photos provide a profile of up to the top 30 cm of the seabed. For sandier beds, the depth to which the camera prism penetrates the bed reduces to 5-10 cm and sometimes even less. If the penetration depth of the SPI camera is limited, the SPI image provides a pseudo-3D image of the seabed-water interface, showing parts of the seabed surface located away from the SPI prism (Figure 3.6). Furthermore, the impact of the frame when landing on the seabed likely redistributes part of the fines on the seabed.

SPI images were post-processed following a standard procedure, illustrated in Figure 3.6. The original images (Figure 3.6-1) were cropped to 60% of their original height, and the RGB colours were converted to greyscale. The histogram of these greyscale images was then normalised based on the greyscale intensity limits of the substrate. A grid was laid over the images to measure lengths and heights. These normalised greyscale images (Figure 3.6-2) were then converted back to a coloured image (Figure 3.6-3) by applying the *'seismic'* false colour map in *matplotlib* (Hunter 2007). Normalisation and colouring of images made it easier to discern between fines and sand. In the coloured images, patches of fines show up as red, textureless patches (Figure 3.6-3). The sandy substrate, on the other hand, is mainly light to dark blue. Each coloured image was then assessed using the criteria in Table 3.3, similar to Karakassis *et al.* (2002) and Romero-Ramirez *et al.* (2013), which enabled a quantitative assessment of the SPI images.

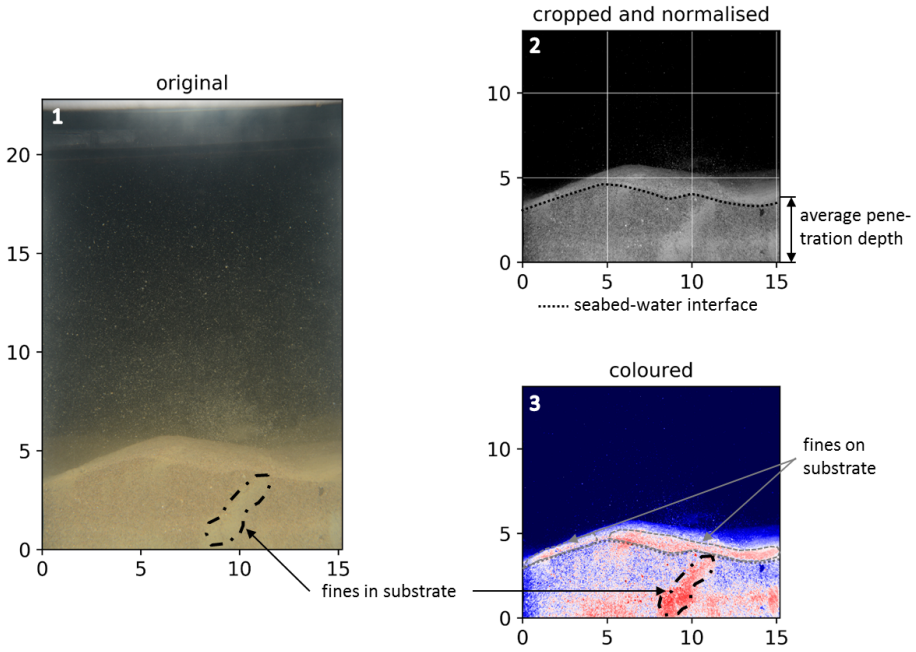

Figure 3.6.: SPI image processing. Original image (1) is cropped and normalised (2). Then coloured (3) using the 'seismic' colour map, after which the fines in and on the substrate can be distinguished better. Assessment criteria are shown for each image. Original image taken in June 2017, at 2.5 km offshore.

Table 3.3.: SPI image assessment criteria

Criterion	Classification	Attribute
Penetration depth	N/A	Depth in cm
Fines on substrate	Yes / no	Thickness of deposited layer
Fines in substrate	Yes / no	Patchy/well-mixed

3.3.3. INSTRUMENTED LANDERS

DEPLOYMENT AND CONFIGURATION

At the beginning of both campaigns, multiple instrumented landers were deployed on the seabed to measure a variety of physical parameters. In this chapter, we focus on the data collected with the *TUD lander* at 4 km offshore (June: 52.6400 °N, 4.5644 °E; October 52.6401 °N, 4.5651 °E). At this location, the bed level is -15 m NAP. A suite of instruments mounted on the lander measured flow velocity, turbidity and small-scale bathymetry (Table 3.4). Flow velocity and turbidity were measured at multiple heights in the water column.

In June, the landers were retrieved from the seabed at the end of the campaign. In

October, the landers were retrieved one day before the end of the sampling campaign because of workability conditions.

Table 3.4.: Instruments mounted on the TUD lander. Instruments measured at different heights, indicated in metres above bed (mab). This table only lists the instruments of which the data was used in this chapter.

Instrument name	**Measurement volume at (in metres above bed - mab)**	**Parameter**	**Period**
Nortek Vector ADV	0.15, 0.3 mab	Velocity in single point	June & October
Campbell OBS 3	0.15, 0.3, 0.45, 0.6 mab	Turbidity	June & October
Marine Electronics Ripple Profiling Sonar	1.0 mab (sonar head)	Small-scale bathymetry	October

POSTPROCESSING LANDER DATA

The two Acoustic Doppler Velocimeters (ADVs) both measured at a 16 Hz frequency. The ADV installed closest to the bed (measurement volume at 0.15 mab) operated in bursts of 10 minutes, measuring for 9 minutes and 50 seconds with a 10 second interval before starting a new burst, while the ADV at 0.30 mab operated in continuous mode.

Velocity timeseries were first corrected for pitch and roll of the lander, followed by a transformation from a local XYZ coordinate system to global ENU (East-North-Up) coordinates. The data were then filtered using a correlation and signal-to-noise (SNR) ratio mask (Elgar *et al.* 2005). Data points for which the beam correlation for all three ADV beams was below 80% and with an SNR smaller than 15 were removed from the data. If more than 30% of the samples within a moving 5-minute window had to be filtered out, the entire 5-minute window was removed. After filtering the data, the velocity time series were despiked (Goring and Nikora 2002). Velocities were then rotated 6° in clockwise direction to obtain along-shore and cross-shore velocity components. Subsequently, the sign of the cross-shore velocity component was then reversed, so that it is defined as positive in the offshore direction.

The local bed elevation is determined from the ADV positioned at 0.15 mab, which recorded the distance to the seabed at the beginning of each 10-minute burst. This data was filtered in two steps. First, values equal to zero were removed from the data. Second, a moving average with a time window of two hours was implemented. Values with an absolute difference larger than 4 cm from this mean were removed. Local bed elevation was then computed by subtracting the distance to the bed at the start of the deployment from the filtered signal.

Turbidity readings from the optical backscatter sensors (OBS) were calibrated for SSC using sediment-laden water samples collected at the Egmond aan Zee site. These samples were collected at the end of each campaign, stored in four 10-L buckets and transported to the TUDelft laboratory There, all OBS's were calibrated following the procedure by (Colosimo *et al.* 2020). Concentrations were generally smaller than 1 g/l, hence a linear regression was sufficient to convert turbidity to SSC.

The ripple profiling sonar was used to obtain a small-scale 2D bathymetric map in the vicinity of the lander. The raw ping data from the sonar was converted to bed levels

using the Bearing Direction Indicator method (Wengrove *et al.* 2017). These bed levels were then corrected for pitch and roll and interpolated to a regular grid with a 0.5 cm x 0.5 cm resolution. As the sonar head was positioned at 1.0 mab, and collected pings within a 150° arc, the maximum radius of the small-scale bathymetry was 3.8 m. Since the sonar steps through the swath at 0.9° increments, the resolution at the edges of the swath area is quite coarse. Hence, only the gridded data within a 2x2 m^2 area around the lander was used. A low-pass filter was then applied to remove the small-scale spikes deviating more than 10 cm from their direct surroundings. Missing values were interpolated using a linear interpolation from the nearest 5 cm in both directions. Finally, bedform heights and lengths were then computed using the 2D-spectral method of Wengrove et al. (2018).

3.4. RESULTS

3.4.1. HYDRO- AND MORPHODYNAMIC CONDITIONS

In June, the campaign took place several days after a fierce summer storm. During this storm, maximum significant wave heights of up to 4.5 m were measured at the nearby *IJGeul 1* wave buoy (Figure 3.7c – grey hatch indicates campaign duration). During the storm, wave direction was west to southwest. Hydrodynamic conditions were calm during the campaign (Figure 3.7b). Near-bed flow velocities (at 0.15 mab) show a semi-diurnal flood-dominant tide (Figure 3.7a), with maximum along-shore velocities of 0.5 m/s and maximum cross-shore velocities of 0.15 m/s. Near-bed SSC shows a decreasing trend with peaks of up to 0.2 g/l on 09-06, and generally less than 0.1 g/l on the subsequent days (Figure 3.7d). Note that the SSC signal at 0.15 mab overlaps with the 0.3 mab SSC signal in Figure 3.7d. The SSC peaks seem uncorrelated with the tidal velocity, though some peaks occur during the peak ebb phase (dashed lines in Figure 3.7a, d). Moreover, the local bed elevation (Figure 3.7e) appears fairly constant throughout the measurement period, showing oscillations of 1-2 cm only during the peak flood phase.

In contrast, the campaign in October took place during a storm, with maximum wave heights of approximately 3 m at the *IJGeul 1* buoy (Figure 3.8c). Wave directions gradually varied over the course of the storm from southwest to northwest. While the velocity still has a semi-diurnal character, it is modulated by waves from 20 until 23 October (Figure 3.8a, b). This leads to higher onshore velocities during the flood phase, together with a higher along-shore velocity. Ebb velocities decrease during the storm. Near-bed SSC increases from less than 0.05 g/l on 19-10 up to 0.7 g/l on 22-10 (Figure 3.8d). Small-scale bathymetry suggests that the steep increase in SSC takes place shortly after the storm peak, roughly 2 days after the onset of the storm (Figure 3.8e, f). The delay in SSC increase after storm onset is similar to the observations by van der Hout *et al.* (2017) at 1 km offshore from Egmond aan Zee. The subsequent SSC peaks mostly occur during the ebb phase, similar to the June measurement (dashed lines in Figure 3.8a, d). These do not coincide with the peaks in local bed shear stress. A possible explanation could be the advection of fines from a nearby sediment patch. The preceding storm remobilised fines, which are not uniformly deposited in space. During the ebb phase, a larger amount of sediment could have been available for resuspension, even by weak tidal currents. There is no clear decrease in maximum SSC until the end of the measurement period.

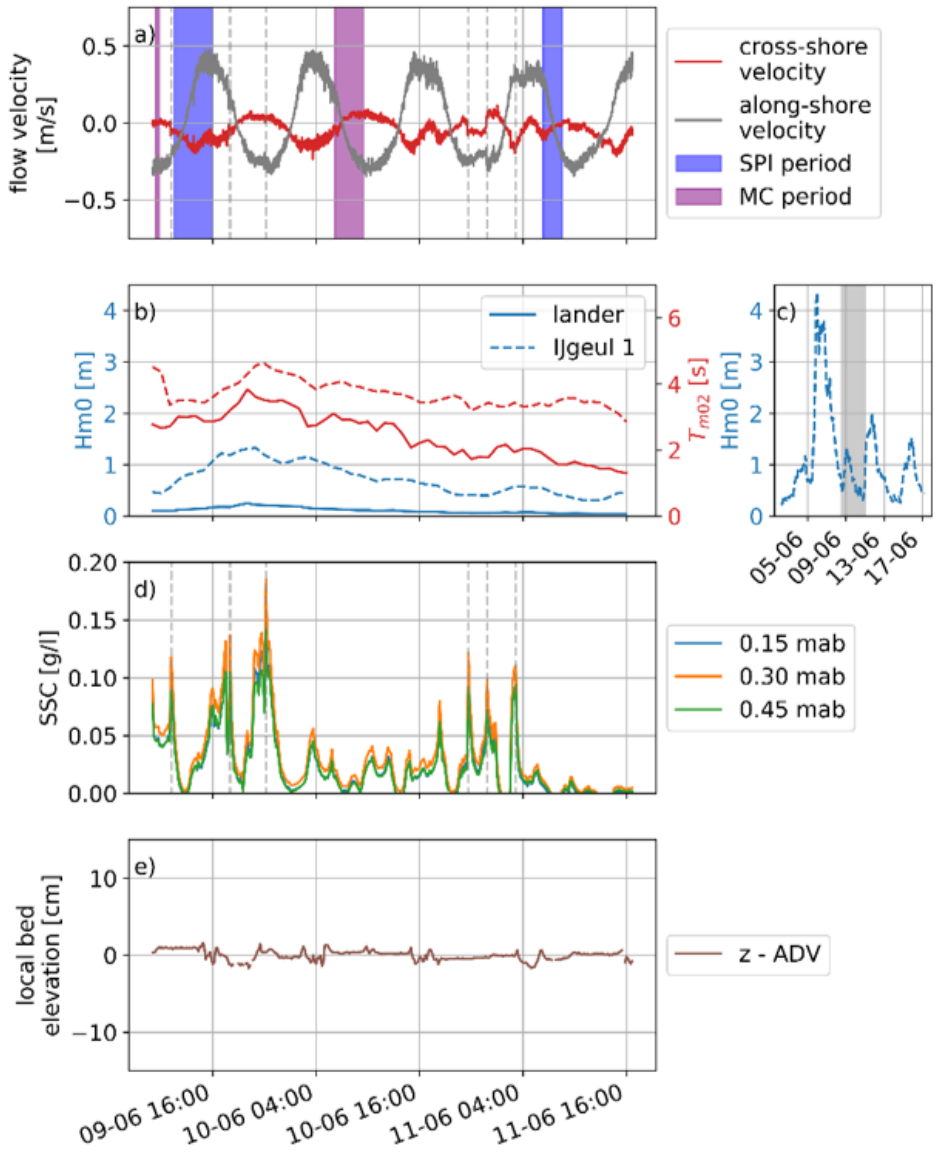

Figure 3.7.: Hydrodynamic conditions in June 2017. (a) ADV flow velocity; (b) wave heights and period during campaign at TUD lander and IJgeul 1 wave buoy; (c) timing of campaign compared to wave height in June at IJgeul 1 wave buoy; (d) SSC; (e) local bed elevation - ADV.

The energetic conditions during the October campaign are confirmed by the local bed elevation as measured by the ADV (Figure 3.8e – brown line). This varies strongly over the course of several hours to days. In the night from 21-10 to 22-10, local bed elevation increases from -3 to +9 cm. However, on 22-10 it decreases from +9 to -1 cm. These single point measurements cannot distinguish between vertical bed level changes in response to erosion/deposition or migration/reconfiguration of bed forms. The results of the ripple profiling sonar (see below) mainly suggest the latter.

Generally, the mean bed elevation measured by the sonar ($\bar{z}$) increased during the measurement period (Figure 3.8e – blue line). It shows similar trends as the bed elevation from the ADV, though the peaks are less pronounced. Before the onset of the storm, the ripple height (η) is generally small, i.e., 3 to 5 cm (Figure 3.8f). During the storm, ripple height gradually increases to a maximum of approximately 0.1 m on 22-10 02:00. The maximum ripple height roughly coincides with the peak in local bed elevation (Figure 3.8e). After reaching a maximum on 22-10, ripple heights first decrease strongly to 2 cm, then increase to 6 cm. In the wake of the storm, ripple heights are similar to pre-storm values, while the mean bed elevation under the sonar is still 5 cm higher (Figure 3.8e).

In total, three sonar images collected before, during and after the storm (Figure 3.8g, h, and i, respectively) to illustrate the seabed state. The blanked out areas in these sonar images represent removed data points; the colour map indicates the bed elevation. Before the storm, ripples are relatively short and are generally oriented from left to right (Figure 3.8g). At the ripple height peak, the domain is almost entirely dominated by a few large storm-induced megaripples (Figure 3.8h). These are longer and higher than the small-scale ripples. Their orientation is not clear since their length scale is similar to the sonar footprint. Some scouring seems to have taken place directly left of the lander legs after the storm. After the storm, small-scale ripples can be observed again (Figure 3.8i). These are oriented left-to-right and are superimposed on the decaying storm-induced bedforms. The contours of the latter are still visible in Figure 3.8i, but much less pronounced than during the storm peak.

3.4.2. TRENDS IN BED SEDIMENT COMPOSITION

Figure 3.7a and Figure 3.8a depict when the seabed was sampled with the SPI and MC, in June and October, respectively. In October, MC samples and the second part of the SPI images were collected after the *TUD lander* had been retrieved. This means no direct sampling conditions are available, but the preceding conditions nevertheless provide a reliable estimate of these conditions (Figure 3.8a).

First, we search for large-scale sediment distribution trends along the transect, comparing the results of both campaigns. In Figure 3.9a, we show the mean fines percentage (p_{fines}) for the three sister samples taken at the ten sampling stations along the transect. These samples are grouped per station and plotted at the corresponding distance to shore. The mean fines percentage of each sample is indicated by the height of the coloured bars. Those collected in June are plotted above the line representing the bed level (indicated with the red line) while those of October are plotted below this line.

In June, more samples contained fines than in October, 60% versus 50%, and p_{fines}

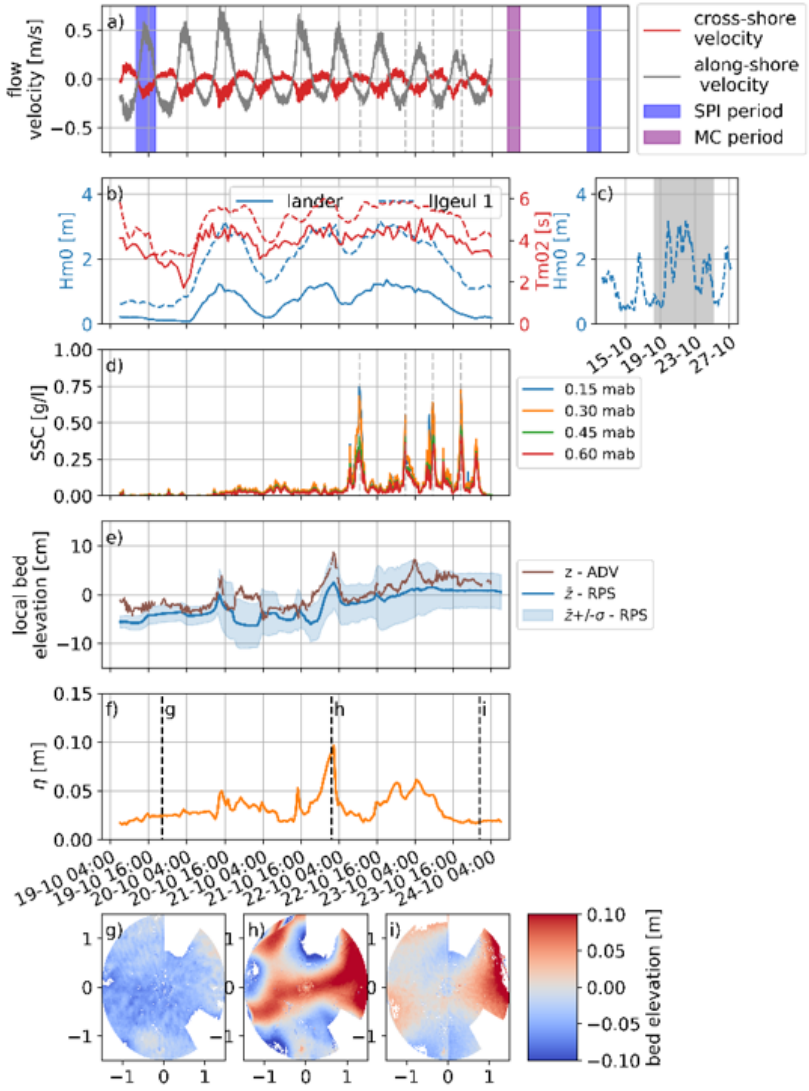

Figure 3.8.: Hydro- and morphodynamic conditions in October 2017. (a) ADV flow velocity; (b) wave heights and period during campaign at TUD lander and IJgeul 1 wave buoy; (c) timing of campaign compared to wave height in October at IJgeul 1 wave buoy; (d) SSC; (e) local bed elevation – ADV, mean bed elevation with standard deviations – ripple profiling sonar; (f) ripple height from elevation spectrum of sonar data; (g, h and i) small-scale bathymetry at three points in time.

was also higher. The conditional mean percentage, i.e. averaging only over the samples which contained fines, decreased from 2.4% in June to 1.0% in October. However, these averages are not representative for the fines distribution along the transect.

In addition, as Figure 3.9a shows, fines percentages vary considerably on multiple spatial scales and over time. In June, the majority of the samples had a mean fines percentage of 0-3%. However, maximum fines percentages per sample of up to 8.5% (2 km offshore), 6.7% (4 km offshore) and 4.8% (6 km offshore) were observed (Figure 3.9a). In October, the mean fines percentage mostly ranged from 0-1.5%. The only exception are the mean fines percentages at 6 km offshore (bed level at -18 m), which ranged from 2.4 to 3.1%.

Moreover, the variation in mean fines percentage is not only observed between different stations, but also between sister samples collected at a given station (Figure 3.9a). For instance, the mean fines percentage between sister samples from June varied from 0 to 6.5% (4 km), from 0.7 to 4.8% (6 km) or from 0.1 to 2.0% (9 km). As these sister samples were collected through a single MC deployment (Table 3.2), this means that fines percentages vary substantially within 0.5 metres.

Similarly in October, the mean fines percentages between sister samples differed from 0.1-1.0% (2km) and 0-0.8% (5km) (Figure 3.9a). Absolute differences are smaller than in June, but relative differences are on the same order of magnitude. As these sister samples were collected through one or multiple MC deployments, the fines percentage at these stations varied either on a spatial scale of metres or decametres.

Figure 3.9b and c present the fines presence of the upper 15 cm of the three sister samples taken at the 10 stations of Figure 3.9a. Here, fines presence is defined as the mean fines percentage per 1-cm or 2-cm slice. This has been categorised according to van Alphen's classification (van Alphen, 1987). The sister samples have been coded using the distance to shore and a letter. For instance, the third sister sample at 7 km offshore is marked '7C' (Figure 3.9b).

Furthermore, Figure 3.9b and c show that vertical variations in fines percentages are at least as pronounced as the horizontal variability. Most of the sediment slices contain no fines ($p_{fines} = 0$), but if they do contain fines, they usually fall within the 2-10% range. Only a few of the slices fall either within the 0-2% or >10% classes. As an example, we analyse the sister samples 4B and 4C, collected in June (Figure 3.9b). In sample 4B, fines are only found at 2-4 cm below the seabed surface and these slices contain 8-9% fines. None of the other slices from this sample contained any fines. In sample 4C, fines are only found at 5-9 cm below the seabed. Here, the slice from 7-9 cm even contained 38% fines, while the slice underneath contained no fines. This heterogeneity is observed in both the June and the October profiles. The only station where the fines percentage over depth was relatively constant, was at 6 km offshore in October.

Above, we focused on specific trends per sampling campaign and general differences between the June and the October campaign. Comparing the results of both campaigns per station is disputable, as the length scale of fine sediment presence is of the same order as the positioning accuracy of the research vessel.

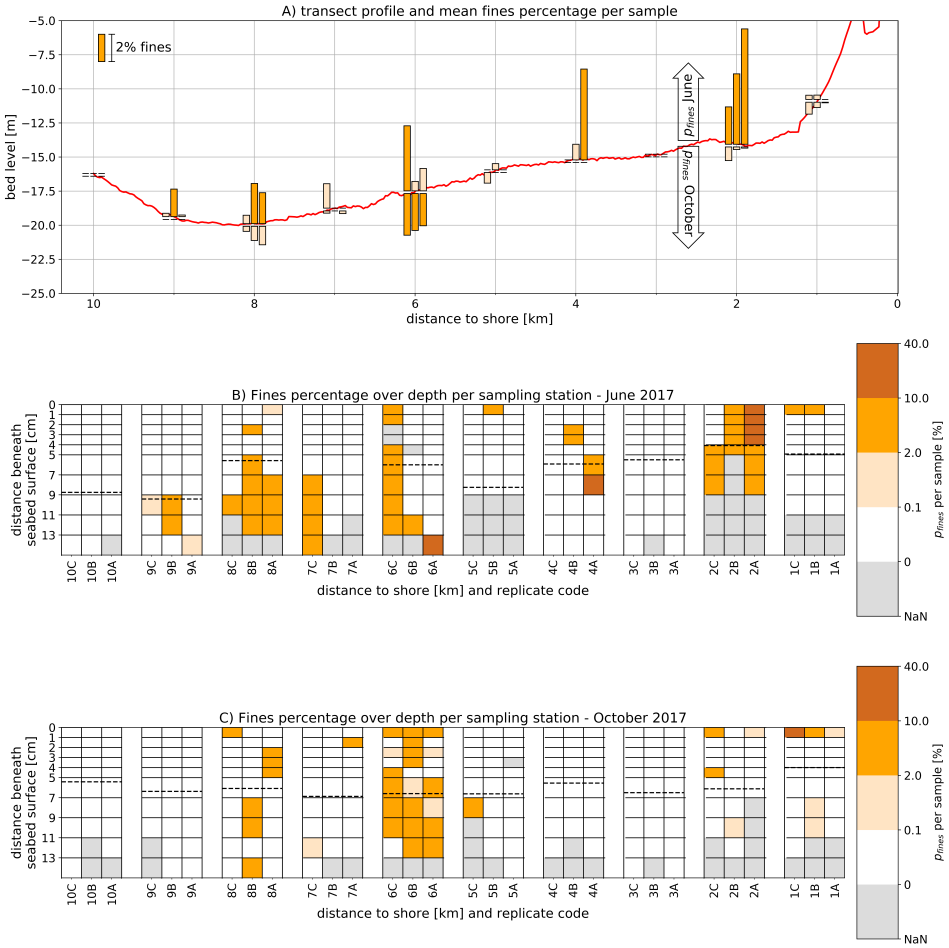

Figure 3.9.: A) Mean fines percentage per sediment sample for both June and October, plotted along transect bed level (from NLHO digital terrain model). Mean percentage indicated by height of bar, 1 m = 1%. (B, C) Fines percentage in sediment slices collected in June and October, respectively. Slice colour indicates fines percentage, as per the classification of van Alphen (1987a) and Hendriks *et al.* (2020). Average penetration depth of the SPI per station is indicated with the dashed line.

3.4.3. SMALL-SCALE SEABED STRUCTURE

The sediment sample data show how the presence of fines varies over multiple length scales, both in the horizontal and vertical directions. The SPI images contain additional information on the small-scale seabed structure. The average penetration depth of the SPI per station, as indicated in Figure 3.9b and c with the dashed lines, was generally

smaller than 10 cm. Within the width of the image, i.e. 15 cm, the presence and layering of sand and fines varies considerably. Examples of small-scale seabed structure are shown in Figure 3.10, which includes SPI images taken in June, at 9.5, 4.0 and 2.0 km offshore.

From 10 to 8 km offshore the substrate is mostly sandy, judging by its texture and uniform sediment colour (Figure 3.10a). Small-scale bedforms are observed in most images, with heights ranging from 1-3 cm. Generally, only very limited fines are present. Closer to shore, the sediment texture becomes less uniform. Patches of several cm wide are visible in the bed, having a texture different than the rest of the bed, indicated in red colour (Figure 3.10b). These are to be interpreted as patches of fines (Section 3.3.2). The water column above the bed is much richer in suspended sediment and the seabed topography is more irregular. At 1.5 and 2 km offshore, the most fines are observed, suspended and both on and in the seabed (Figure 3.10c and Figure 3.11). Figure 3.10c exhibits two bedforms of at least 5 cm length (majority outside the picture), with the trough between them filled up with fines. The thickness of this deposited layer varies strongly over the small scale, from 2 cm to only several mm within a length of 10 cm (Figure 3.10c), following the seabed topography. The maximum observed thickness is 4 cm, at 1.5km offshore (Figure 3.11 – right panel).

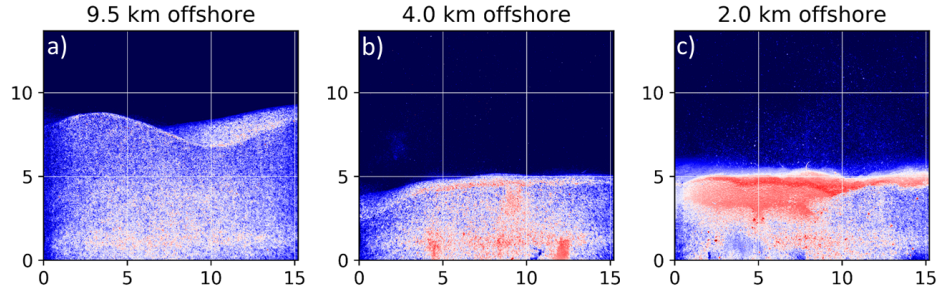

Figure 3.10.: SPI images taken during the June campaign at a) 9.5, b) 4.0 and c) 2.0 kilometres offshore. The grid scale is centimetres. For an explanation of the colours, see Section 3.3.2.

Figure 3.11 shows two SPI images collected in June at 1.5 and 2.5 km offshore, within 30 minutes from each other. Even on the micro-scale of these images, the presence of fines on and in the seabed varies greatly.

In the left panel of Figure 3.11, two patches of fines are buried in the top 2 cm of the seabed by overlying sand. These patches are similar to the lenses drawn in Figure 3.2d, but oriented in the opposite direction. Their shape follows the profile of the asymmetric, current-induced ripples. The depth at which they are buried is larger than the current-induced ripple height, likely immobilising them until the next storm.

In contrast, the right panel of Figure 3.11 shows the fines deposited in the trough of a small-scale bedform – in fact the entire trough is filled in. This small-scale bedform has a

maximum height of approximately 4-5 cm, which is larger than current-induced ripples as the latter have a height of approximately 2 cm. This is possibly a relic bedform from the summer storm which preceded the June sampling campaign.

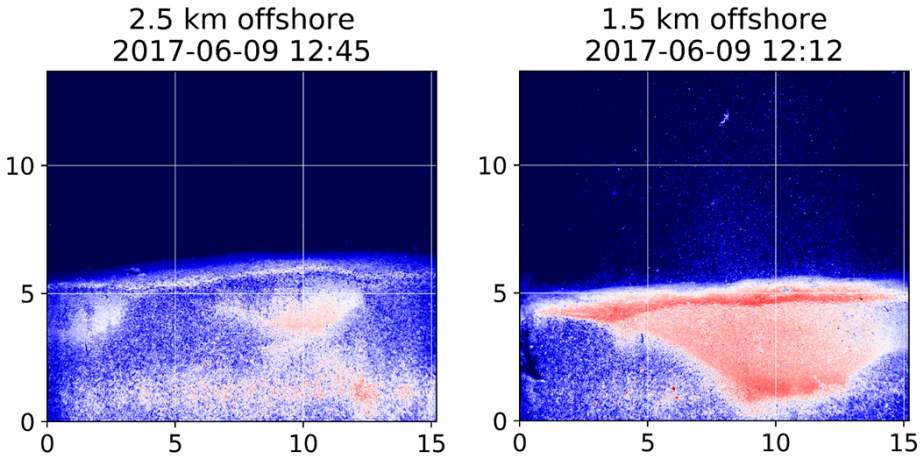

Figure 3.11.: SPI images taken at 2.5 and 1.5 km offshore, which show the interaction between fines and small-scale bedforms. This interaction leads to small-scale variations in the presence or absence of fines.

Figure 3.12 quantifies the number of images where fines were either found on or in the substrate. It is formatted as Figure 3.9a. Each bar along the transect indicates a station where SPI images were taken. As the number of SPI images differed per station, all bars were normalised by the total number of images taken at that station. Hence, all bars have equal length. These bars are coloured partly brown and partly white. The brown colour indicates the fraction of images in which fines were observed, while the white colour indicates the fraction in which they were absent. The bars above the bed level indicate fines on the substrate (such as Figure 3.10c), while the bars below it indicate fines in the substrate (such as Figure 3.10b).

In October (Figure 3.12b), fines were rarely observed on the substrate along the entire transect. The only exception is the station at 1.5 km offshore. Furthermore, very little or no fines were observed within the substrate from 2.5 to 7 km. Closer than 2.5 km offshore and further than 7 km offshore, fines were regularly observed within the substrate.

Qualitatively, the presence of fines as determined from the sediment samples and SPI images agrees well. In 80% of the SPI images where fines are observed, they occur as distinct patches, which is also illustrated by Figure 3.11. This confirms the fines presence observed in the sediment samples (Figure 3.9b and c).

The results from June differ substantially from the October campaign. In June, fines were frequently observed on the substrate up to 5 km offshore (Figure 3.12a), while they

were much less frequently observed further offshore. For fines within the substrate, the same trend generally prevails, with the highest occurrences close to shore. The high fines percentages at 2 km offshore (Figure 3.9a) are also reflected by the SPI images taken at that location.

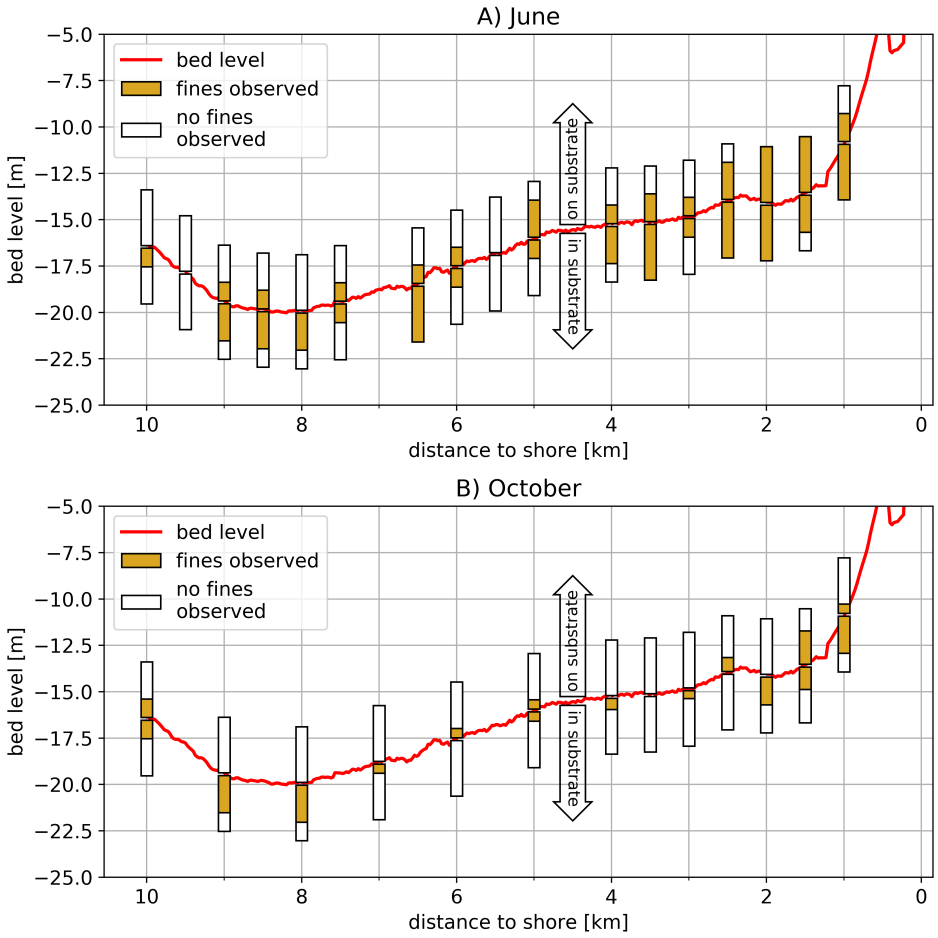

Figure 3.12.: A) fraction of SPI images with fines on and in substrate for June B) fraction of SPI images with fines on and in substrate for October.

3.4.4. SYNTHESIS OF DATA AND CONCEPTUAL MODEL

In this section, the observations from both campaigns are compared to the conceptual model phases. For each sampling period, we determine to which phase of the dynamic cycle (cf. Figure 3.3) the observations correspond and assess if the presence of fines (suspended, on or in the seabed) agrees with our hypotheses.

First, we consider the hydrodynamic conditions preceding and during the sampling period, as the four phases of the dynamic cycle are related to the occurrence of storms and transitions to and from calm conditions. We then establish the presence or absence of fines in the seabed. Next, we discuss the small-scale seabed morphology, i.e., whether the seabed is morphologically active or static during the measurement period. Both campaigns are first discussed separately. Then, both the spatial and temporal patterns are interpreted using the conceptual model.

JUNE CAMPAIGN

In June, sampling took place during a calm period, 3-4 days after a summer storm (Figure 3.7c). Depending on the adjustment period after the storm, this should either be phase 4 (post-storm) or phase 1 (calm period) of the dynamic cycle. We can infer these phases from the bedform characteristics and fine sediment concentrations in both the water column and the seabed.

The small variations in bed elevation (Figure 3.7e) at 4 km offshore suggest that the seabed was mostly morphologically static, and thus in phase 1. This is confirmed by the relatively low SSC at this location (Figure 3.7d). SSC showed a decreasing trend, but were low throughout the observation period. We would thus expect a limited exchange of fines between the seabed and water column as the majority of the fines would already have been buried. This is confirmed by the relatively high fines percentage in the seabed for most of the transect (Figure 3.9a). Furthermore, fines are rarely observed on the substrate from 3 to 10 km offshore (Figure 3.12a).

However, likely not the entire transect was in phase 1. Within 2 kilometres from the shore, the seabed was probably still in phase 4. Here, the majority of SPI images showed fines both on and in the substrate, rather than solely within the substrate (Figure 3.12a). The thick layer of fines on the substrate at 1.5 km offshore (Figure 3.11 – right panel) is characteristic of phase 4. Furthermore, bedforms higher than 2 cm were observed on SPI images at 2 and 1.5 km offshore.

The multiple seabed states are best illustrated by the SPI images shown in Figure 3.11. The thick layer of fines on the substrate at 1.5 km offshore (Figure 3.11 – right panel) is characteristic of phase 4, while the SPI image collected 1 km further offshore clearly showed buried fines (Figure 3.11 – left panel). As these images were collected within 30 minutes of each other, this suggests a variation in burial phase over larger distances (kilometres). Thus, the seabed can be in one phase closer to the shore, while in another phase further offshore.

OCTOBER CAMPAIGN

In October, measurements commenced shortly before a storm, while the seabed sampling took place during the storm peak and shortly post-storm (Figure 3.8a, c). Hence, either phase 3 or phase 4 of the dynamic cycle (Figure 3.3) is expected. The relatively large bedform height (Figure 3.8f) and large variations thereof at 4 km offshore indeed suggest phase 3. Furthermore, the near-bed SSC was high (Figure 3.8d), while the fines percentages in the seabed were low (Figure 3.9a).

Significant reconfiguration and migration of bedforms were recorded at 4 km offshore before seabed sampling took place. However, none of the sediment samples collected at

4 km offshore in October contained fines (Figure 3.9a). This either means that phase 3 of the dynamic cycle was still ongoing when the seabed was sampled, or that conditions in the post-storm period (phase 4) were too energetic for fines to be buried at this location. Possibly, the swift decrease in bedform height shortly after the storm peak (Figure 3.8f) prevented the burial of fines.

Moreover, the limited amount of burial in October is confirmed by sediment samples (Figure 3.9c) and the SPI images (Figure 3.12b). For the majority of the stations, hardly any fines were observed either on or in the substrate. Only the stations at larger water depths (at 6 and 8 km offshore) had considerable amounts of fines in the substrate. Moreover, at 6 km offshore, the SPI images and sediment samples are not entirely consistent as all sister samples at this station contained fines while this was not observed in the SPI images.

INTERPRETATION OF SPATIAL PATTERNS

In June, measurements were collected during phase 1 and 4, while in October measurements were collected during phase 3 and 4 of our conceptual model. The observed presence of fines support the formulated hypothesis. We expected a strong vertical variation in, and patchy occurrences of, fines percentage in the seabed due to the burial process. This is confirmed by the sediment slices (Figure 3.9b and c), which show fines in the seabed in distinct patches. Transitions from layers with fines to pure sand are abrupt, i.e., slices with a fines percentage of 4-5% are often adjacent to purely sandy slices. Fines are found both in isolated lenses and in adjacent slices. The latter are encountered either as larger patches of fines, or as successive layers of fines separated by thin layers of sand. In October, both were observed along the transect. At 8 kilometres offshore, SPI images (not shown here, but available via the data repository) showed larger patches of fines, while at 6 kilometres, images of the sediment cores exhibited successive layers of fines. Only the larger patches of fines may indicate another process than burial by small-scale bedforms. Both the abrupt transitions from fines to sand and successive layers of fines support the hypothesised burial process.

The presence of fines does not only vary vertically within the bed, but also horizontally. This is quantified through the variance in p_{fines} at three spatial scales, i.e. along the transect, per station and per sample (Figure 3.13). For the entire transect, the mean fines percentage per station was used. For the stations, the mean fines percentage per sister sample was used, while per sample, it was the mean fines percentage per slice. The variance is of the same order of magnitude at all scales (Figure 3.13). If fines were present, the variance within this sample sometimes even exceeded the variance along the entire transect, i.e. a larger vertical than horizontal variability.

This quantification agrees with qualitative observations from the SPI. These images (Figure 3.10, Figure 3.11) show how bed structure and the presence of fines vary significantly within 15 centimetres, which is the length of small-scale bedforms, i.e. decimetres. The variance within single stations is attributed to the variability in fines burial on megaripple scale (phase 4 of the dynamic cycle – Figure 3.3), since fines are only buried in the former trough of a megaripple and not under its former crest. Hence, the horizontal variation in fines percentages occurs within a metre (Figure 3.9a), with significant variance.

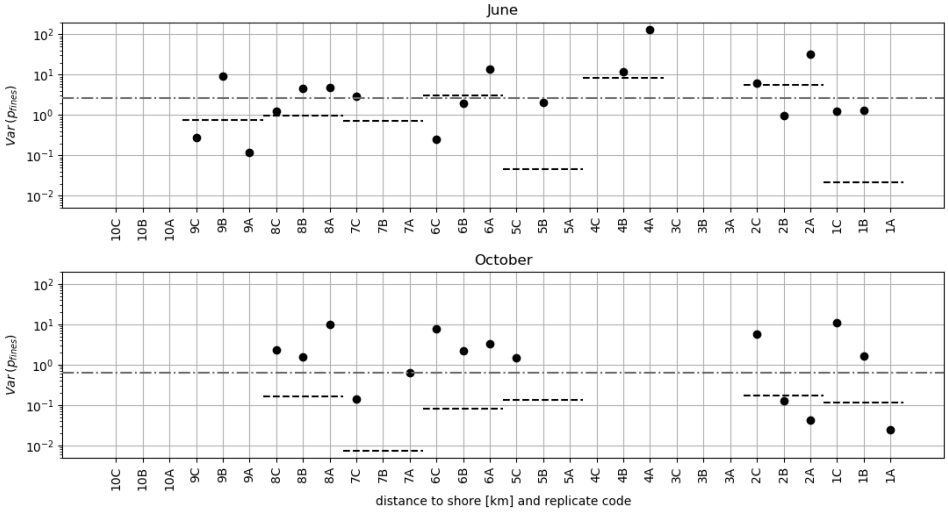

Figure 3.13.: Variance in fines percentage in June and October on three different spatial scales. (1) Grey dash-dot line : variance along the transect. (2) Black dashed lines : variance per station. (3) Black dots : variance per sediment sample.

INTERPRETATION OF TEMPORAL PATTERNS

Another source of variability exists on the meso-scale. The approximate position on the shoreface determines if megaripples will form, owing to the combination of local hydrodynamic conditions and sediment characteristics. However, ripples and megaripples initially develop from small perturbations on the seabed, which are randomly distributed. Hence, the exact megaripple locations will also be randomly distributed. As net burial of fines only occurs in the trough of these megaripples, the presence of fines in the seabed inherits this stochastic behaviour. This may further explain the large variability in fines percentage over both decametres and hectometres. Interpretation of temporal patterns

The observed sediment compositions are two snapshots in time and we cannot determine when the sampled sediment was actually deposited. However, we did observe a considerable change in fines percentages and distribution in the bed between June and October (Figure 3.9a). As there are no indications that large-scale sedimentation or erosion took place between June and October, this implies that the fines present in the seabed in June were no longer there in October. Thus, they were remobilised from the bed between these two campaigns.

However, fines must still have been present in the seabed in the Egmond aan Zee area at the onset of the storm in October. Otherwise, the observed near-bed SSC at 4 km offshore (Figure 3.8d) could not have increased up to 0.7 g/l within 1.5 day after the storm peak. However, if all the fines in the June samples at 4 km offshore would have been remobilised only during this single storm, this would have led to near-bed SSC of more than 3 g/l. Thus, the majority of fines must have been remobilised prior to the October

storm and advected away from the site. Hence, the data suggest that remobilisation of fines during storms can almost completely deplete the upper strata of a sandy seabed of fines. In that case, the SSC at this location is supply-limited through the limited availability of fines in the seabed.

3.5. DISCUSSION

The field data collected in the southern North Sea corroborate the conceptual model with the dynamic burial cycle proposed therein. The presence of fines on and in the seabed varies considerably, both in time and space. In this section, we place our results into a wider perspective and discuss the implications of the hypothesised burial process for understanding fine sediment dynamics in shallow coastal seas.

3.5.1. MEGARIPPLE AND RIPPLE DEVELOPMENT AND IMPLICATIONS FOR BURIAL

We argue that the interaction between wave-induced megaripples and tide-induced current ripples is essential for the burial of fines into a sandy seabed (see Figure 3.3). During tide-dominated conditions, only current-induced ripples are found on the seabed. These bury and release fines during their migration, but are not expected to contribute to net burial after their initial capture, nor are they expected to bury fines at larger depths. Net burial only takes place in the wake of storms, when megaripples formed during the storm gradually adjust, flattening and reforming into current-induced ripples. Hence, in order to understand where and when burial of fines takes place, understanding the formation and subsequent flattening of megaripples is crucial.

When a storm occurs, bedform height and length swiftly adjust to governing conditions. The maximum megaripple length, height, and associated timescale depend on the wave-induced Shields parameter ($\theta_w = \frac{\tau_w}{\rho(s-1)gd_{50}}$) (Soulsby *et al.* 2012, Traykovski 2007), thus on the wave-induced bed shear stress and d_{50}. As this shear stress increases quadratically with decreasing water depth, θ_w strongly varies in both space and time in the southern North Sea (Brakenhoff *et al.* 2020, Wengrove *et al.* 2018). On the ebb-tidal delta of Ameland, for instance, θ_w varies by three orders of magnitude within several kilometres during a one month period, from 10^{-3} to 10^{0} (Brakenhoff *et al.* 2020). Hence, the critical Shields parameter for fine sand ($\theta_{cr} \approx 5*10^{-3}$) is not exceeded in some areas while in others, sheet flow can occur ($\theta_{sh} \approx 10^{0}$). On the lower shoreface of the southern North Sea, where bathymetric gradients are less pronounced than on ebb-tidal deltas, differences in θ_w are still considerable over larger areas, with reported values ranging from $2*10^{-3}$ to 10^{0} (Passchier and Kleinhans 2005, van der Werf *et al.* 2022).

The timescale associated with the flattening of wave-induced megaripples to current-induced ripples (T_r) dictates the period during which deep burial can occur. It depends on the megaripple dimensions formed during storms and the current-induced Shields parameter θ_c. The latter depends on tidal flow velocity and d_{50}. Tidal flow velocities vary over multiple timescales (e.g., diurnal and fortnightly, spring-neap) and in space. Variations in θ_c are generally smaller than θ_w, with values for the lower shoreface of the southern North Sea ranging from $2*10^{-3}$ to $2*10^{-1}$ (Passchier and Kleinhans 2005, van

de Meene and van Rijn 2000b). Moreover, the velocity magnitude decreases in onshore direction (Kleinhans and Grasmeijer 2006).

To illustrate this timescale for deep burial, we sketched how bedform height (η) develops during and after a storm (Figure 3.14a). Before the storm, only tide-induced current ripples with height η_c are found. A storm takes place, and megaripples with height η_{storm} are formed. Three potential pathways are sketched (dashed lines in Figure 3.14a), each having a different ratio between θ_c and the critical Shields parameter θ_{cr}. These are: (I) no change in bedform height as the tidal current is too weak to mobilise sand ($\theta_c < \theta_{cr}$), (II) a strong decrease ($\theta_c \gg \theta_{cr}$) and (III) a gradual decrease ($\theta_c \approx \theta_{cr}$). For each path, the timescale is indicated by $T_{r,n}$.

The first path (I) represents calm post-storm conditions. Hence, fines accumulate in the troughs of the bedforms, atop the seabed. However, no burial takes place as there are no migrating ripples. The associated timescale $T_{r,I}$ is thus (theoretically) infinitely large. Along the second path, megaripples reconfigure swiftly to the post-storm conditions, $T_{r,II}$ is small, leaving little time for deposition of fines in the megaripple troughs. Hence, burial is probably limited. Along the third path, megaripples flatten out gradually, with an associated timescale of several days ($T_{r,III}$). Fines may settle atop the seabed during several successive slack tides and are subsequently buried into the seabed.

These examples imply that if tidal currents are too small or too large, little to no burial takes place. Optimal burial efficiency is likely found somewhere in between at moderate tidal currents. We conceptualised this argument through the relationship between burial and θ_c in Figure 3.14b. This provides a possible way forward for modelling and parameterising the burial of fines in the seabed of coastal shelf seas.

Parameterisations which aggregate the burial process on larger spatial and temporal scales are required, as hydro- and morphodynamic models typically operate on length scales of one to several orders of magnitude larger than the proposed burial process. Hence, these parameterisations should aim at correctly representing large-scale patterns of fines in the seabed, and consider the temporal and spatial variations of wave and current bed shear stress. However, this is beyond the scope of this chapter. For upscaling and validating the conceptual model on a regional level, we advise to study seabed dynamics in detail on other sites in the southern North Sea. Collecting multibeam bathymetry and backscatter with sufficient resolution seems crucial to validate the occurrence of (mega-) ripples (Koop *et al.* 2020). The mobility of small-scale ripples is of interest and may be validated by using instrumented landers.

3.5.2. SPATIAL VARIABILITY IN PRESENCE OF FINES

We have combined the conceptual model and observations to explain why fines presence varies on a small scale, down to metres or decimetres. In this model, seabed structure has been simplified to bi-modal conditions, i.e., indicating the presence or absence of fines. Seabed data have been simplified using similar classifications (Figure 3.9, Figure 3.12). In reality, the surficial seabed and underlying strata are often more complex than a bi-modal classification would suggest. Geological deposits, benthic species, (remnants of) shells can all be found in the upper seabed strata (van der Spek *et al.* 2020). These other elements can be considered passive, not disturbing the burial process, for a

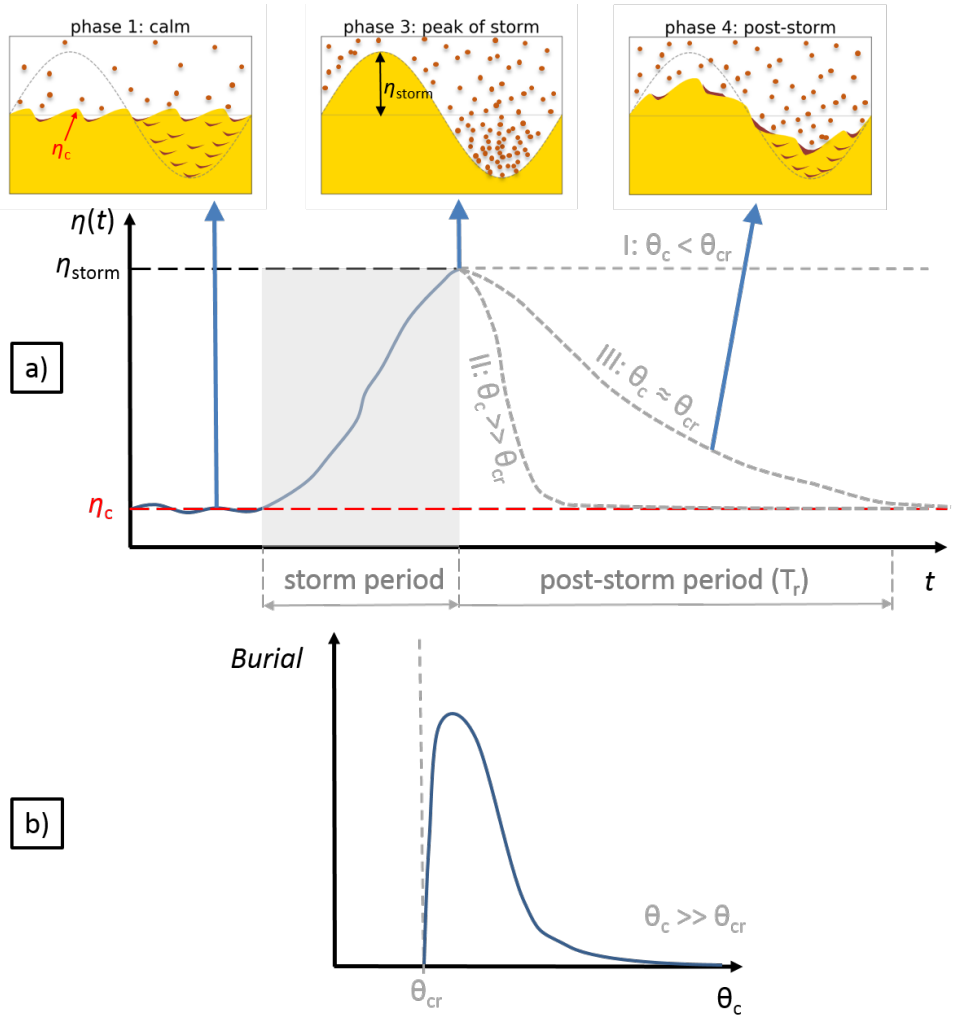

Figure 3.14.: a) Conceptual sketch of bedform height during and after a storm, showing different possible paths determining burial efficiency. b) Hypothetical relationship between burial rate and θ_c.

seabed that is predominantly made up of sand and fines. The formation and migration of bedforms is disturbed if such elements are abundantly present, e.g., as erosion-resistant layers (e.g. peat or stiff clay) (Passchier and Kleinhans 2005) or by abundant presence of shell fragments (Cheng 2021).

For the Egmond aan Zee transect, this bi-modal classification seems justified. The SPI yielded valuable information on seabed structure, which is often lost when sampling it (van Hoey *et al.* 2004). The SPI images show a bed which primarily consists of sand

with distinct patches of fines. Quantification of the seabed structure from the SPI observations was possible as fines were present in patches with a distinct colour and texture compared to other seabed features (Figure 3.12). Further validation of this approach with quantitative methods (e.g. grain size distribution) is recommended.

There is not only a variability in fines presence on the small-scale but also on hectometre-kilometre scale (van Alphen 1987b, Hendriks *et al.* 2020). On these larger scales, the presence of fines in and on the seabed is governed by a combination of three factors: (1) sources of fines, (2) transport pathways and (3) accumulation potential. The latter is determined by a combination of current-induced bed shear stress and seabed topography (Hendriks *et al.* 2020). Whether fines are actually buried in the seabed after deposition depends on the local burial process.

The variability in fines presence on both large and small scale makes it virtually impossible to predict the exact fines percentage in the upper seabed strata at a certain location. Statistical approaches to estimate the probability of encountering fines in the seabed seem more valuable, either by geostatistical approaches (Bockelmann *et al.* 2018, Stephens and Diesing 2015 or physics-based classifications (Hendriks *et al.* 2020).

3.5.3. TEMPORAL VARIABILITY IN PRESENCE OF FINES

When fines are regularly exchanged with the seabed, the water column and seabed must be analysed as a coupled system. Fines presence in the seabed depends on deposition of fines from the water column and subsequent burial. Vice versa, suspended sediment concentrations cannot be understood by only considering processes taking place in the water column.

The presence of fines in the seabed depends on a succession of storms and subsequent calm conditions over the course of months to years. This dependency leads to substantial memory effects, as the individual storms determine how much fines can be buried at which depth. On the short term, the storm's magnitude determines how long the seabed remains affected by that particular storm. Wave-induced megaripples become longer and higher when storms are more intense, leading to a potential deeper burial of fines. Without significant reworking of the sediment by biota, it would require a storm of similar magnitude to remobilise the previously buried fines. The larger a storm, the longer it takes for a similar storm occurs. Hence, some fines are then buried deep for long periods. For weekly to monthly timescales, the burial depths are thus on the order of 10-20 cm, corresponding to megaripple heights formed during a single storm. On longer timescales, on the order of years to decades, burial depths of 30 cm (Laane *et al.* 1999) are probable. On these timescales, the active layer, and thus burial depth, may even be up to 50-60 cm as long-term shoreface erosion and migration or reconfiguration of larger geomorphological features start to play a role (van der Spek *et al.* 2022).

In the water column, SSC magnitude depends on local fine sediment availability (Eleveld *et al.* 2008, Flores *et al.* 2017,Stanev *et al.* 2009, Suijlen and Duin 2001, van der Hout *et al.* 2017). This availability is determined by storms, which remobilise fines that were previously buried within the seabed. Once fines have been remobilised, SSC varies on diurnal and fortnightly timescales (McCandliss *et al.* 2002,Stanev *et al.* 2009, van der Hout *et al.* 2017). Though, their magnitude differs substantially before and after storms. Under similar hydrodynamic forcing, SSC may be up to an order of magnitude higher

after storms than before (Flores *et al.* 2017). How long a storm affects SSC depends on how effectively fines are buried within the seabed after a storm (Figure 3.14). This memory in the system should be considered when interpreting SSC time series, meaning that observed SSC cannot be interpreted as an instantaneous response to prevailing hydrodynamic forcing (Stanev *et al.* 2009, van der Hout *et al.* 2017).

3.6. CONCLUSIONS

In this chapter, we have shown how small-scale bedforms can bury fines in the sandy seabed of the southern North Sea. We developed a mechanistic description of the process, using field data collected in the southern North Sea to develop and test this model.

The burial process consists of four distinct phases forming a dynamic cycle. These phases are related to the occurrence of storms. Fines remobilised during storms will subsequently settle and deposit on top of a sandy seabed. Interactions between bedforms of different scales are then crucial to bury fines in the seabed. Megaripples formed during storms gradually adjust to calmer conditions in the wake of storms. During this adjustment period, fines are buried by current-induced ripples in the troughs of the former megaripples. Thus, fines can be buried in the seabed at depths of up to 10-15 cm. This burial process affects the presence of fines in the bed, both in time and space. The observed temporal variation in fines percentage implies that the seabed is occasionally depleted of fines, resulting in supply-limited conditions. Furthermore, fines percentages in the seabed vary considerably on multiple spatial scales. They both vary on the mega-scale (kilometres) and on the micro-scale (metres-centimetres). Fines are found in distinct patches, both horizontally and vertically. The micro-scale is multiple orders of magnitude smaller than the scale on which hydro-morphological models operate. This means that small-scale variations in monitoring data cannot be reflected in a numerical model outcome. Model parameterisations are needed to aggregate the effects of burial on larger spatial scales.

Moreover, the effectivity and associated timescale for burial depend on the ratio between storm intensity and current magnitude. Theoretically, this leads to an optimum in burial conditions. If tidal currents are too small, sand is not mobilised and no burial takes place. For large tidal currents, the time window for burial is short and likely results in limited burial. Hence, an optimum burial condition is found somewhere in between.

These findings provide a basis for mechanistic model parameterisations of fines burial into a sandy seabed. These are required, since fine sediment dynamics strongly depend on the exchange of fines with the sandy seabed. As suspended fine sediments affect the ecological functioning of shallow coastal seas, a better understanding of these dynamics will prove crucial in conserving these vital ecosystems under increasing anthropogenic pressure.

3.7. DATA STATEMENT

The data that support the findings of this study are openly available in standardised formats through the 4TU.ResearchData repository at https://doi.org/10.4121/c.6001987.

4

REMOBILISATION OF FINES DURING STORMS

4.1. INTRODUCTION

In the two previous chapters, we investigated where fines are found in the seabed of the Dutch Coastal Zone (Chapter 2) and which process is responsible for their burial into the seabed (Chapter 3). The final step is to explore under which conditions the remobilisation of fines from the seabed takes place and how long the fines stay in suspension after they have been remobilised.

During storms, SSC values increase rapidly in the Dutch coastal zone (Eleveld *et al.* 2008, Suijlen and Duin 2001). Depending on the magnitude of the storm, an increase can be found in the entire area from Zeeland to the Wadden Sea. This increase can only be explained by wave-driven remobilisation of local sources of fines distributed throughout the area (van Kessel *et al.* 2011, van Prooijen *et al.* 2007). Advection, which disperses sediment from isolated sources, takes too long to explain the quasi-instantaneous increase of SSC over this large domain. After a storm, SSC steadily decreases, while still varying on tidal timescales (Flores *et al.* 2017). This decrease is governed by the deposition of fine sediment and subsequent deep burial within the seabed. This burial process takes place within several days to a week (Chapter 3). Although previous studies already indicated that storms lead to a strong increase in SSC (Flores *et al.* 2017, van der Hout *et al.* 2017, Kleinhans 2005), it is not fully understood what limits the remobilisation of fines. Although it is likely determined by the properties of the sandy seabed rather than the characteristics of the fines (Le Hir *et al.* 2007, van der Molen *et al.* 2009, van Kessel *et al.* 2011, Winterwerp *et al.* 2021), it is still debated to what extent the seabed is eroded. Existing modelling approaches use the concept of an active layer. The thickness of this layer is either set equal to an instantaneous bedform height (van der Molen *et al.* 2009, Wiberg *et al.* 1994) or assumed constant (van Kessel *et al.* 2011). However, a direct link between the time-dependent seabed development and the remobilisation of fines is lacking.

The objective of this chapter is to better understand and quantify (a) the rate at which and (b) how much fine sediment is remobilised during storms. Therefore, we analyse a 21-month in situ data set collected in the Dutch coastal zone near Egmond aan Zee (Witbaard *et al.* 2013). An iterative cycle is followed by analysing the data, building a conceptual model, and quantifying the fluxes. In this chapter, the result of this process is reported by first describing the conceptualisation of how remobilisation takes place (Section 4.2). The dataset and data analysis methods are described in Section 4.3, while the results are presented in Section 4.4. An interpretation of the results and comparison with literature is provided in Section 4.5, as well as an outlook on how these results can be used to improve existing modelling approaches.

4.2. BEDFORM RELEASE MODEL

Several formulations describe the remobilisation of fines from a sandy seabed (e.g. Le Hir *et al.* 2007, van der Molen *et al.* 2009, van Kessel *et al.* 2011, van Ledden and Winterwerp 2005, Wiberg *et al.* 1994). They all acknowledge that remobilisation rates are determined by hydrodynamic forcing, the properties of the sandy seabed, and the fraction of fines within it. Aggregated parameters, such as the resuspension parameter (van Kessel *et al.* 2011) or a near-bed reference concentration (van der van der Molen *et al.* 2009, are used to compute these rates.

While effective for modelling, these approaches describe only the outcomes of remobilisation, not the underlying mechanisms. This results in a gap between the underlying physical processes and the parameters used to represent them. To address this, we propose a new conceptual formulation that directly relates remobilisation to the formation of storm-induced bedforms. Therefore, we call it the **bedform release model**. This process-based perspective aims to clarify the physical basis of existing formulations and guide the interpretation and calibration of their aggregated parameters.

To take a systematic approach to quantifying remobilisation, we take the buffer model of van Kessel *et al.* 2011 as a starting point. This model is widely used and calibrated for modelling fine sediment dynamics in the Dutch Coastal Zone of the North Sea. A crucial element of this model is its ability to incorporate the stochastic nature of the exchange of fine sediment with the seabed. This stochastic nature is an essential concept for understanding the remobilisation of fines. First, we briefly introduce both the van Kessel *et al.* (2011) buffer model and our bedform release model.

In the buffer model, the seabed is schematised into two layers, a lower buffer layer and a fluff layer on top. A visual representation of this schematization is shown in Figure 4.1a. The fluff layer mainly consists of fines and is easily eroded, while the lower buffer layer is more difficult to erode. Generally, sediment from the fluff layer is resuspended every tidal cycle, while sediment from the buffer layer is only remobilised during high-energy events such as storms or spring tides. As we focus on remobilisation during storms, we will discuss only the properties of the buffer layer, displayed in black (Figure 4.1a). During those storms, the fluff layer is already in suspension.

The buffer layer represents the sandy seabed with a small fraction of fines in it. For a sandy seabed, its thickness is assumed constant and is generally set at a value of 10-30 cm (van Kessel *et al.* 2011). Remobilisation of fines from the buffer layer (E_2 in Figure 4.1a) is described by the multiplication of the fines fraction with the erosion rate (pick-up rate) of the sandy seabed, leading to the first-order erosion formulation:

$$E_2 = E_{buffer} = p_2 M_2 \left(\frac{\tau}{\tau_{cr,2}} - 1 \right)^{1.5} \tag{4.1}$$

where:
M_2 = resuspension parameter for the buffer layer [kg m^{-2} s^{-1}]
τ = bed shear stress [Pa]
$\tau_{cr,2}$ = critical bed shear stress for remobilisation of fines from the buffer layer [Pa]
p_2 = fines fraction in buffer layer [-], defined as:

$$p_2 = \frac{m_2}{(1-n)\,\rho_s d_2} \tag{4.2}$$

where:
m_2 = fines mass in buffer layer [kg]
n = porosity of the sand matrix [-]
ρ_s = density of solids in the seabed [kg/m^3], mainly sand
d_2 = thickness of buffer layer [m]

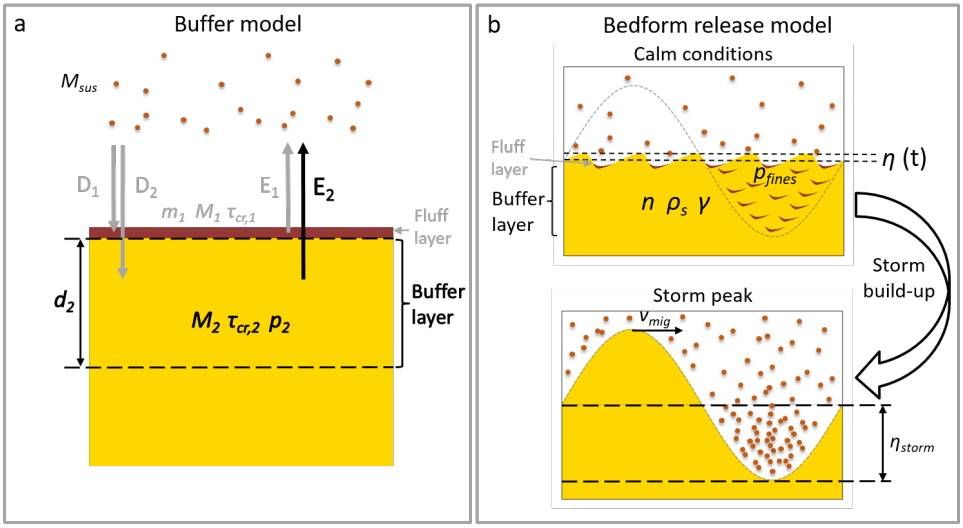

Figure 4.1.: a) Definition of the two-layer buffer model by van Kessel *et al.* (2011), indicating the fluff and buffer layer and their associated parameters. b) Definition of our bedform release model, based on the burial model from Chapter 3. Fines are indicated with the brown colour while sand is shown in yellow. The upper sketch illustrates the upper seabed layer during calm (current-dominated) conditions, while the lower panel illustrates the seabed state during a storm peak.

The buffer model implicitly assumes erosion of the sandy seabed to release fines. We want to make this process explicit and hypothesize that the development of bedforms (megaripples) is responsible for the release of fines; see Figure 4.1b. We hypothesise that fines, buried up to 10-20 cm within the seabed (Figure 4.1b – upper panel), are remobilised during storms due to the formation and migration of megaripples (Figure 4.1b – lower panel). We assume that these processes take place simultaneously and represent both of them by estimating the time-dependent change in ripple height. We then formulate remobilisation (E_{remob}) similar to the buffer model (E_2) by multiplying the fines fraction with the formation of bed forms:

$$E_{remob} = p_{fines} \cdot \gamma \cdot \rho_s \cdot (1 - n) \cdot \frac{d\eta}{dt} \tag{4.3}$$

where:
p_{fines} = fines percentage in the seabed [-]
γ = remobilisation efficiency factor, ranges between 0 and 1 [-]
ρ_s = density of solids in the seabed [kg/m3]
n = porosity [-]

The time-dependent change in bedform height is computed using the Soulsby et al. (2012) model:

$$\frac{d\eta}{dt} = \frac{\beta}{T_e}(\eta_{eq} - \eta) \tag{4.4}$$

where:
η = time-dependent bedform height [m]
T_e = characteristic timescale for bedform formation [s]
β = rate of change coefficient [-]
η_{eq} = equilibrium bedform height [m]

Both the relaxation timescale (T_e/β) and the equilibrium bedform height (η_{eq}) depend on hydrodynamic forcing, through a representative bed shear stress (τ). Full details of the Soulsby *et al.* 2012 model and required input are provided in Appendix A.

Combining Equation (4.3) and Equation (4.4) leads to the following formulation for E_{remob}:

$$E_{remob} = p_{fines} \cdot \gamma \cdot \rho_s \cdot (1-n) \cdot \frac{\beta}{T_e}(\eta_{eq} - \eta) \tag{4.5}$$

The parameters and fluxes of the buffer model and our bedform release model are comparable, see Table 4.1. For example, the thickness of the buffer layer (d_2) roughly corresponds to the maximum ripple height during a storm (η_{storm}). Furthermore, the aggregated resuspension parameter M_2 is proportional to the total seabed volume put into motion during a storm. Vice versa, the buffer model provides a framework for aggregating complex seabed dynamics. We will use the latter to describe the remobilisation efficiency factor (γ) in the following section.

Table 4.1.: Buffer model parameters and how these relate to the novel bedform release parameters

Description	**Buffer model (van Kessel *et al.* 2011)**	**Bedform release model**
Fines percentage in seabed	p_2	p_{fines}
Remobilisation rate	$M_2\left(\frac{\tau}{\tau_{cr,2}} - 1\right)^{1.5}$	$\gamma \cdot \rho_s \cdot (1-n) \cdot \frac{d\eta}{dt}$
Maximum remobilisation depth	d_2	η_{storm}

The starting point for the derivation of the bedform release model is the mechanistic burial model introduced in Chapter 3. This describes how the interaction between current-induced ripples and storm-induced megaripples leads to the deep burial of fines in the seabed (Figure 4.2), where deep burial means up to tens of centimetres. This causes fines to remain trapped within the seabed for longer periods (i.e, between storms).

Four distinct phases in the burial process are proposed in the model, forming a dynamic cycle (Hendriks *et al.* 2022). Here, we focus on phases 2 and 3 of this dynamic cycle (Figure 4.2), describing the state of the seabed during the build-up and peak of a storm.

During these phases, megaripples are formed by a combination of current- and wave-induced forcing (van der Spek *et al.* 2022, van der Werf *et al.* 2022). They are not formed instantaneously, but need time to develop (Figure 4.2 – phase 2) (Soulsby *et al.* 2012, Traykovski 2007). As they grow, they gradually release the fines buried within the seabed together with the sand. We argue that when the bedforms have reached their maximum height (Figure 4.2 – phase 3), the remobilised amount of fines also reaches its maximum and that further erosion stops.

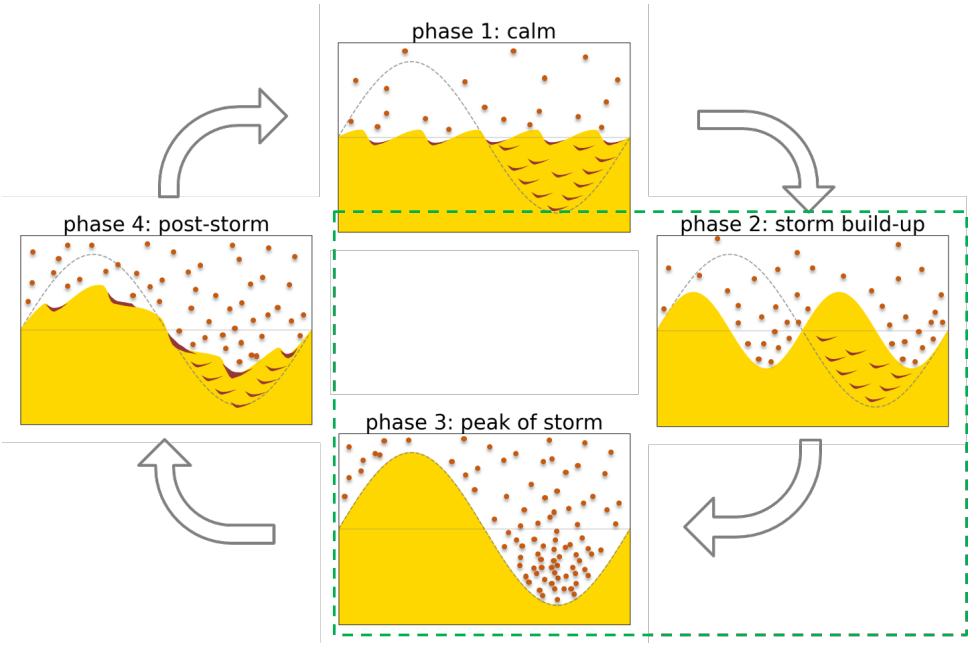

Figure 4.2.: Conceptual burial model introduced in Chapter 3. The green dashed rectangle indicates the phases examined in this Chapter, i.e., phase 2 and 3.

We quantify this with three components: (1) sand volume mobilised during a storm; (2) the mass of fines per unit volume of the seabed, i.e. the fines fraction; (3) a factor quantifying the stochastic nature (i.e. uncertainty) of the presence of fines in the seabed and bedform development. Each of these components is described below.

(1) The sand volume mobilised during a storm is assessed using the time-dependent ripple model of Soulsby *et al.* (2012), as provided in Appendix A. Essentially, their model is formulated as a simple differential equation describing relaxation towards an equilibrium bedform height. The mobilised volume is proportional to the bedform height if we assume that the megaripples are uniformly distributed over the seabed.

(2) The fines mass per seabed unit volume, i.e., the fines fraction, relates the remobilised sand volume to the fines mass flux. In the case of a sandy substrate with a gran-

ular skeleton, the fines are found within the pores of the skeleton only. If their solids density is equal to that of the sand, the fines mass per unit volume is given by:

$$m_{fines} = p_{fines} \cdot (1 - n) \cdot \rho_s \tag{4.6}$$

where:
m_{fines} = fines mass per seabed volume [kg/m^3]
p_{fines} = fines fraction [-]
n = porosity [-]
ρ_s = density of solids in the seabed [kg/m^3]

We assume that the composition of the sand-mud mixture does not influence sand erosion rates, which holds when p_{fines} is smaller than 13% (van Ledden *et al.* 2004, Winterwerp *et al.* 2021). These fines percentages are rarely exceeded in the southern North Sea (Chapter 2 and references therein).

(3) The third and final element of our bedform release model is a factor quantifying the stochastic nature (i.e. uncertainty) of fines presence in the seabed and bedform development. Figure 4.3 conceptually shows the different aspects of this uncertainty, complementing the simplified sketch of Figure 4.1b.

The first aspect is the large spatial variation in fines presence in the seabed (indicated by the brown lenses in Figure 4.3). In Chapter 3 we showed how the actual fines percentage in the seabed varies strongly down to the meso (metres) and micro (centimetre) scale. This is caused by the stochastic nature of bedform formation and migration, which leads to an irregular distribution of fines within the seabed, both horizontally and vertically.

The second aspect is similar to the formation and migration of megaripples. On the scale of single megaripples, remobilisation depends on where these megaripples will actually develop (Figure 4.3). Whether their troughs coincide with where the fines are buried depends on chance. However, when these megaripples migrate they will mobilise larger parts of the seabed, thereby reducing the uncertainty of fines being remobilised.

These stochastic processes can be parameterised with a remobilisation efficiency factor (γ) when the spatial domain of analysis is large enough – here we propose a 100x100 m^2 domain. Hereby, γ aggregates the spatial heterogeneity in fines percentage and megaripple formation, with its value varying between 0 and 1. If the megaripple troughs align perfectly with where the fines are buried up to a certain depth (η_{storm}), γ equals 1. Vice versa, if the troughs only mobilise parts of the seabed without fines, γ will equal 0 (van Kessel and Vanlede 2009, Winterwerp *et al.* 2021).

4.3. DATA AND METHODS

This section describes the dataset of Witbaard *et al.* 2013 and how we analysed it to study fine sediment dynamics during and after storms. This dataset contains both SSC time series and other elements required to test the bedform release model presented in the previous section.

The bedform release model (Figure 4.1b) revolves around the formation of storm-induced megaripples. Hence, to test it, we need to identify storms in the dataset. Fur-

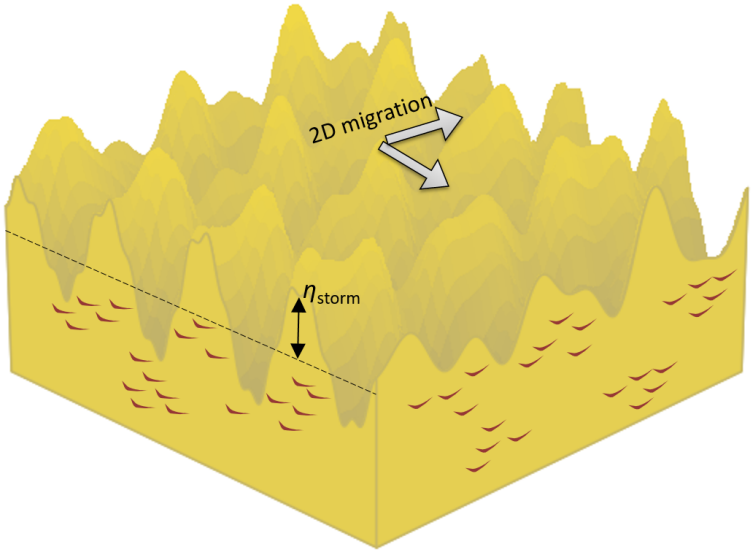

Figure 4.3.: Sketch showing two-dimensional megaripple variations and difference in fines presence. Horizontal scale : meters, vertical scale tens of centimeters. Brown patches indicate fines in the seabed, which are drawn as concave-up lenses further to the burial model (Chapter 3).

thermore, the dataset should be long enough to distinguish between the different phases of the dynamic cycle in Figure 4.2. As the formation of megaripples is driven by waves and currents, we need a measure for both their intensity. Furthermore, we need to know whether large-scale bedforms actually develop on the seabed. All these aspects are discussed in the following sections.

4.3.1. STUDY SITE AND MEASUREMENT SET UP

The study site is located on the lower shoreface of the Holland coast, 1 km offshore of Egmond aan Zee. Therefore, we refer to it as the Egmond site. It is located in the far-field region of the Rhine Region of Freshwater Influence (ROFI), and periodically experiences weak stratification (Rijnsburger *et al.* 2016, van der Hout *et al.* 2015). The seabed is mostly sandy, with a median grain size (d_{50}) of 200-250 μm (Witbaard *et al.* 2016).

The Egmond site is located 20 km north of the port of IJmuiden. Approximately 1 MT of dredged fine sediment is disposed directly north of the harbour entrance channel annually (Winterwerp 2001). This disposal location is located 15 km south of the Egmond site, and the fines deposited there will eventually reach the study site as the residual transport direction of fines along the Dutch coast is in northern direction (de Boer *et al.* 2009).

From February 2011 until October 2012, a measurement frame (i.e., the lander) was

deployed at a ~10 m deep location off the coast (52°38.249′N 04°36.294′E – Figure 4.4) Witbaard *et al.* 2015. The lander was equipped with a set of sensors measuring tidal currents, water pressure, turbidity, temperature, salinity, and fluorescence. Here, we only elaborate on the measurements of tidal currents, water pressure, and turbidity.

Tidal currents were measured every 10 min at 15 cm above the seabed with a Nortek Vector ADV. Every 10 minutes, the ADV recorded a burst of 2 minutes with a frequency of 1 Hz. The water pressures were measured by the ADV on an identical time interval at 30 cm above the bed. The ADV measured the distance to the seabed at the start and end of each burst, thus detecting the formation and/or migration of bedforms.

Simultaneous measurements of optical backscatter (OBS) and fluorescence were made at four heights above the seabed, i.e. 30, 80, 140 and 200 cm, using ALEC Compact-CLW's (`http://ocean.jfe-advantech.co.jp`). To convert the turbidity data from the OBS to SSC, all ALEC sensors were calibrated in the lab over a range of SSC by Witbaard *et al.* (2015).

The site was visited every 3 to 6 weeks to service the lander and to collect sediment samples from four locations around the platform (Figure 4.4). In 2011 and 2012, the site was visited 19 times in total. During each site visit, at least two boxcorer samples were collected at each location. If a boxcorer sample was of sufficient quality, i.e. with an undisturbed surface layer and more than 10 cm high, small sub-samples were taken for grain size analysis. In 2011, only the top 5 cm was subsampled. In 2012, both the upper 5 cm and the lower 5 cm (5-10 cm below the seabed surface) were subsampled. These subsamples were frozen and then transported (Witbaard *et al.* 2015).

4.3.2. DATA PROCESSING

HYDRODYNAMIC AND SSC DATA

Hydrodynamic conditions are derived from the ADV data. Here, we distinguish between tidal currents, wave height, and wave period.

Tidal current data were preprocessed by van der Hout *et al.* 2017. For this study, we transformed the velocities from global East-North-Up coordinates to alongshore and cross-shore currents, by rotating them by 6° in clockwise direction.

The water pressure was recorded by the ADV. The pressure fluctuations were translated into wave heights using linear wave theory. The two-minute bursts are split into two time series of one minute. After detrending, a spectrum is determined for each minute. The spectra are averaged over an hour, implying 12 spectra per hour. The wave spectra are used to deduce the significant wave height (H_{m0}) and the wave period (T_{m02}). The zeroth, first, and second order moments of the wave spectrum (*m0*, *m1*, *m2*, respectively) are used to compute these properties, according to Madsen *et al.* (1988):

$$H_{m0} = 4\sqrt{m0} \tag{4.7}$$

$$T_{m02} = \sqrt{\frac{m0}{m2}} \tag{4.8}$$

The SSC data were preprocessed by van der Hout *et al.* (2017). These ten-minute filtered data were smoothed by applying a two-hour wide moving average.

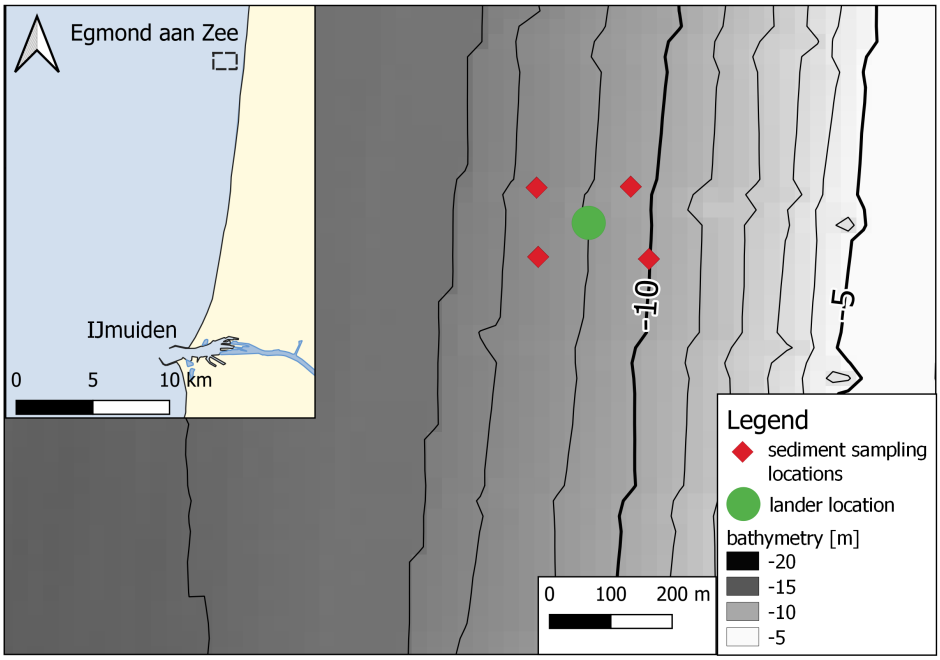

Figure 4.4.: Egmond study site, indicating the lander and sediment sampling locations. Bathymetry from NLHO Digital Terrain Model, based on bathymetric surveys from 2009, 2012 and 2014 (NLHO and Deltares, 2019). The dashed box in the inset indicates the location of the lander along the North Holland coast. All bed levels are referenced to the Dutch Ordnance level (NAP, Nieuw Amsterdams Peil).

SEDIMENT SAMPLES FROM THE SEABED

The sediment samples collected with the boxcorer were transported to the NIOZ laboratory in frozen condition. There, they were first freeze dried for 48 h and then thoroughly homogenised. From these samples, a subsample was taken for the actual analyses. This subsample was first sieved over a 2 mm mesh and then transferred to a measurement tube, which was shaken for 30 seconds to produce a homogeneous suspension, see Witbaard *et al.* (2013).

This suspension was analysed with a *Beckman Coulter LS 13 320*, to determine its grain size distribution. This instrument determines the grain size distribution by laser diffraction, yielding the volume percentage of different size classes. The size class of particles smaller than 63 μm is referred to as fines. We do not distinguish between clay and silt fractions, as the larger mudflocs were broken during treatment. Similarly to Callesen *et al.* (2018) and Hendriks *et al.* (2020), we assume that volume percentages are representative of mass percentages.

BED ELEVATION

The local bed elevation represents the formation and/or migration of bedforms and is calculated from the distance to the seabed as recorded by the ADV. The distance to the seabed is filtered in two steps. First, all zeros (erroneous data) are removed from the dataset. Subsequently, a 3-hour moving median is computed for the time series. Values that deviate more than 40 mm from this median are removed from the dataset. The local bed elevation is computed by subtracting the mean distance to the bed during the first day of each three-to-six week deployment. As a final step, the sign of the time series is reversed, so a positive bed elevation corresponds to local deposition and negative values to local erosion.

IDENTIFYING STORM PERIODS IN THE DATASET

To analyse the effect of storms on SSC, we identified storm events in the data set. For this, we used the computed significant wave height (H_{m0}) defined in Section 4.3.2. We consider a period as a storm when the peak H_{m0} exceeds 0.8 m, which is consistent with van der Hout (2024). Furthermore, there should be a clear response in SSC beyond regular tidal behaviour. From these storm periods, we selected individual storms that do not occur shortly after another storm or during a sustained stormy period. This condition was assessed using SSC time series, ensuring that the pre-storm SSC peaks did not exceed 200 mg/l (Schmidt 2021).

4.3.3. ESTIMATING THE TOTAL SUSPENDED MASS AND REMOBILISATION FLUX

To test the bedform release model (Section 4.2), we compute the cumulative remobilisation flux (ΣE_{remob}) for each storm and compare it to the total maximum suspended sediment mass during a storm ($M_{sus,storm}$). We therefore assume that the rate of change in the measured suspended sediment mass during storms depends only on remobilisation. During the considered short period, we neglect deposition (and subsequent burial) and transport gradients, allowing us to describe the change in suspended matter per unit area (M_{sus}) as:

$$\frac{\mathrm{d}M_{sus}}{\mathrm{d}t} = E_{remob} \tag{4.9}$$

M_{sus} is defined by:

$$M_{sus}(t) = \int_{z_{nb}}^{z_{surf}} c(z,t)\mathrm{d}z \tag{4.10}$$

where:
c (z,t) = SSC as a function of height above the bed and time [kg / m^3];
z_{nb} = a reference height near the seabed = 0.1 m
z_{surf} = a reference height near the water surface = 10.0 m

Following from Equation (4.9), we define ($M_{sus,storm}$) as:

$$M_{sus,storm} = M_{sus,onset} + \Sigma E_{remob} \tag{4.11}$$

where:
$M_{sus,onset}$ = total suspended matter at the storm onset [kg / m^2]

and where:

$$\Sigma E_{remob} = \int_{t_{onset}}^{t_{peak}} E_{remob} \mathrm{d}t \tag{4.12}$$

t_{onset} = the onset of the storm
t_{peak} = the moment when M_{sus} reaches its maximum

To obtain $c(z)$, we extrapolate the measured smoothed SSC time series. For each time step in the dataset, we check if SSC was measured correctly at more than 2 heights. If so, SSC values are log-transformed, and a linear regression is computed based on the non-zero SSC values. If this regression has a negative slope, the fit is extrapolated from z_{nb} to z_{surf}. M_{sus} is then found by integrating $c(z)$. To find $M_{sus,storm}$, we compute M_{sus} over the course of a storm and subtract $M_{sus,onset}$.

The cumulative remobilisation flux (E_{remob}) is computed by quantifying Equation (4.5). In order to do so, time-dependent ripple heights ($\frac{d\eta}{dt}$) are computed using the Soulsby *et al.* (2012) model (Appendix A). For this model, we need to provide both hydrodynamic input and ripple predictors. The hydrodynamic input consists of the wave height (H_{m0}), the wave period (T_{m02}) and the depth-averaged tidal current magnitude (U). The wave height and wave period are defined in Equation (4.7) and Equation (4.8), respectively.

U is computed from the ADV timeseries, assuming a logarithmic velocity profile. First, u_* is computed using:

$$u(z) = \frac{u_*}{\kappa} \ln\left(\frac{z}{z_0}\right) \tag{4.13}$$

where:
z = height above the seabed of the ADV measurement volume = 0.15 [m]
κ = von Karman constant = 0.4 [-]
z_0 = roughness height = $\frac{k_s}{30}$
k_s = Nikuradse roughness height = $1 \cdot 10^{-3}$ [m]

After obtaining u_*, we reconstruct the logarithmic velocity profile over the full water depth using Equation (4.13). Averaging over the depth leads to U. Finally, we take its absolute value ($|U|$) as input for the ripple model.

For the provided ripple predictors, we distinguish between predictors for current-dominated and wave-dominated conditions. The current-dominated predictor is taken from Baas *et al.* (2000). For wave-dominated conditions, a wide range of predictors exist. We compared four different predictors, being: Traykovski (2007) – TR07, Traykovski (2007) as implemented by Marten (2010) – MN10, Soulsby and Clarke (2005) – SW05 and Wiberg and Harris (1994) – WH94. The full details of these predictors are given in Appendix A.

Eventually, we compute the cumulative remobilisation flux (ΣE_{remob}) :

$$\Sigma E_{remob} = p_{fines} \cdot \gamma \cdot \rho_s \cdot (\eta_{storm} - \eta_c) \tag{4.14}$$

where:
η_{storm} = the maximum storm-induced ripple height [m]
η_c = the current-induced ripple height [m]

The median fines percentages from the sediment samples are used (Section 4.3.1). We used a weighted average to interpolate the fines percentage (p_{fines}) between the sediment sampling dates. The values of the other applied parameters are given in Table 4.2.

Table 4.2.: Parameter values used for quantifying ΣE_{remob}

Parameter	Value [unit]
γ	0.5 [-]
ρ_s	2650 [kg m^{-3}]
n	0.4 [-]

4.4. RESULTS

4.4.1. IDENTIFIED STORMS

Twelve individual storms were identified in the dataset using the definitions of Section 4.3.2 (Schmidt 2021, van der Hout 2024). Table 4.3 lists the selected storms, including peak wave heights and wind characteristics for these periods.

According to the definition in Section 4.3.2, each storm has a peak H_{m0} that is larger than 0.8 m. Most of these storms are from the north-westerly to south-westerly quadrant. They are spread fairly well throughout the year (Figure 4.5a), both including summer and winter conditions. In November and December 2011, a succession of storms occurred, but none of them could be classified as an individual storm. Hence, no storms from these months were included in the analysis.

The duration of most storms was approximately one week, varying from 4 to 11 days. Generally, pre-storm SSC is re-established within several days to a week after the storm peak. This will be discussed in more detail in Section 4.4.4.

Table 4.3.: Individual storms identified in the dataset

Storm number	Start date	End date	Peak H_{m0} [m] at Egmond site
#1	25-02-2011	03-03-2011	1.54
#2	07-03-2011	18-03-2011	1.60
#3	31-03-2011	04-04-2011	0.83
#4	04-04-2011	09-04-2011	0.93
#5	26-08-2011	05-09-2011	1.39
#6	04-10-2011	10-10-2011	2.52
#7	16-10-2011	24-10-2011	1.82
#8	14-01-2012	18-01-2012	1.11
#9	03-03-2012	18-03-2012	0.93
#10	15-05-2012	19-05-2012	1.37
#11	06-06-2012	16-06-2012	1.95
#12	09-07-2012	14-07-2012	1.08

4.4.2. SEDIMENT DATA

The fines percentages as obtained from the boxcorer data are shown in Figure 4.5b. These are grouped by sampling date in the box plots. In 2011, only the upper 5 cm within the seabed was sampled, while in 2012 additional samples were taken 5-10 cm below the seabed surface.

More than 95% of the sediment samples contained fines. The median fines percentage of the upper layer varies moderately with time, between 2 – 9%, though no clear seasonal trend is visible.

For the lower layer, this varied between 2 and 5%. The percentages of the lower layer follow the same trend as those of the upper layer. Generally, vertical variations in the fines percentages appear to be limited for the 5-cm layer thicknesses.

The horizontal variations in fines percentage are more pronounced. They reach maxima of approximately 30%, while the 75th percentile generally does not exceed 10% (Figure 4.5b). Fines percentages vary both between stations and between samples collected at the same station. This implies that fines percentages vary on the scale of metres, i.e. the positioning accuracy of the vessel and boxcorer deployment, to hundreds of metres. These strong spatial gradients have been explained in Chapter 3.

4.4.3. SSC DYNAMICS BEFORE, DURING AND AFTER STORMS

Two storms are selected to explain the behaviour of the SSC dynamics before, during and after a storm. These are storms #2 and #5, which took place in March 2011 and August 2011, respectively (Table 4.3). For both storms, we plot SSC, wave characteristics, bed elevation, and computed ripple heights in Figure 4.5. The subplots in the left column (Figure 4.5a, c, e, g and i) correspond to storm #2 while the subplots in the right column (Figure 4.5b, d, f, h and j) correspond to storm #5.

In the days prior to each storm, we observe similar behaviour. SSC is low in both cases, even at 30 cm above the seabed (SSC1 in Figure 4.5 a, b). Wave heights are generally low during these days (Figure 4.5 c, d) and the seabed level hardly varies (Figure 4.5 e, f). The predicted ripple heights (Figure 4.5 g, h) are equal to the predicted equilibrium ripple height for current-dominated conditions ($\eta_{eq,current}$ = 18 mm).

However, there is one major difference between the two considered storms. Storm #5 was preceded by more than two weeks of calm weather (Figure 4.5a), while storm #2 was preceded by storm #1 (Table 4.3). The latter took place approximately one week before the onset of storm #2, and SSC returned to pre-storm conditions in between. Although it is not certain whether the short succession of these two storms has had an effect, it is good to be aware of it when interpreting the results.

During storm #2, the wave height develops in two steps, first peaking at 0.7 m and then peaking at approximately 1.5 m the day after. SSC peaks during both occasions, although the second peak in SSC is more pronounced (Figure 4.6 a, c, e, g). This peak occurs half a day after the maximum wave heights have been reached. It then takes 3 to 4 days before SSC returns to pre-storm levels, which corresponds to previous observations (Flores *et al.* 2017, Hendriks *et al.* 2022, van der Hout *et al.* 2017). The observed bed elevation decreases strongly around the storm peak and subsequently increases by 50 mm. After the storm, there is hardly any variation in bed elevation. This is likely due to the low flow velocities after the storm, which do not exceed the critical threshold of motion, which is indicated with the dashed line in Figure 4.6c.

The predicted ripple heights (Figure 4.6i) increase strongly when the wave height exceeds 1 m (Figure 4.5e). Ripple maxima are predicted to lie between 50 and 60 mm. All ripple heights then gradually decrease as the wave height decreases. The predicted ripple heights agree with the observed changes in bed elevation ($z_{max} - z_{min}$) (Figure 4.6g and h), both in terms of magnitude and their temporal development.

During storm #5, the wave height gradually increases, reaching a peak of almost 1.5 m. SSC begins to increase when the wave heights have reached their maximum (Figure 4.6b, d). The SSC peak occurs at the maximum wave height. Afterwards, SSC then returns to pre-storm levels in 5 to 6 days. The bed elevation shows pronounced fluctuations during the storm. It first increases by 50 mm during storm build-up, decreases by 80 mm during

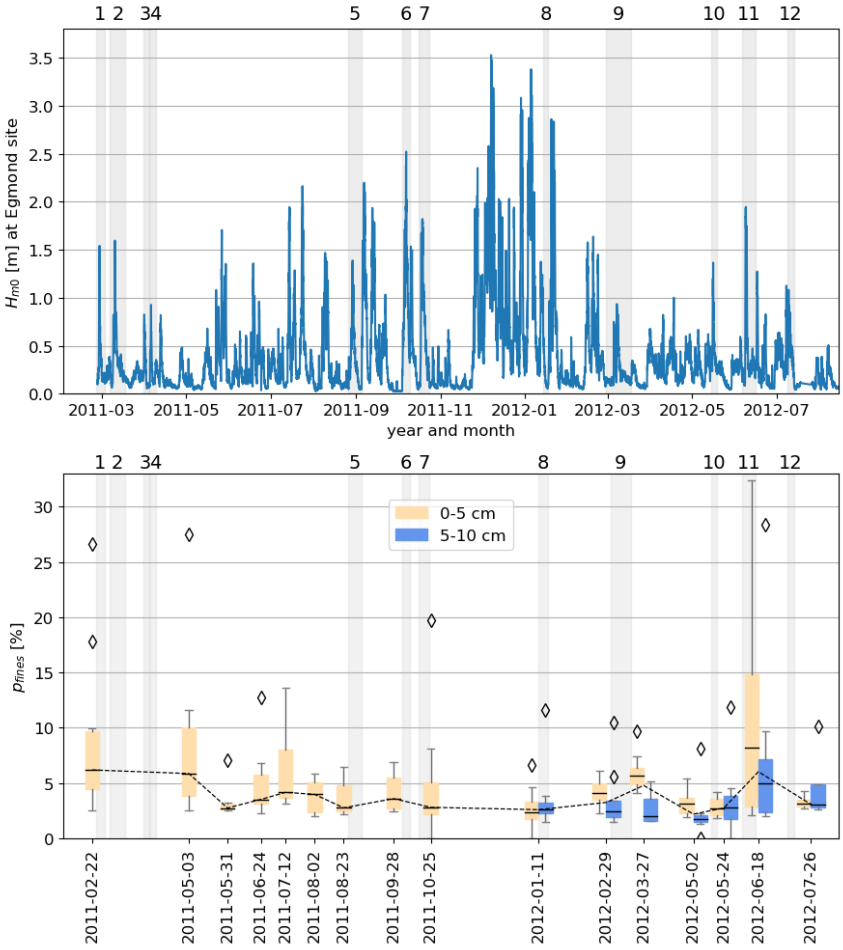

Figure 4.5.: a) H_{m0} at the Egmond site during the full measurement period. The identified storm periods are indicated with the grey hatch and labelled with their storm number (Table 4.3). b) Fines percentage of sediment samples, grouped in boxplot per sampling date. Samples from upper and lower layer are indicated with orange and blue boxes, respectively. The dashed black line indicates the weighted average between sampling dates. The box for each date extends from the first quartile (Q1) to the third quartile (Q3) of the data, with a line at the median. The whiskers extend from the box to the furthest data point lying within 1.5x the inter-quartile range (IQR) from the box (Hunter 2007). The diamonds indicate data points outside this range.

the storm peak, and shortly thereafter increases again. The rapid decrease in bed level coincides with the SSC peak. Afterwards, the bed elevation varies by 10-20 mm during

several successive tidal cycles. Again, the ripple predictors predict a strong increase in bedform height when the wave height exceeds 1 m, reaching up to 80 mm. In the days after the storm, they gradually decreased to the current-dominated ripple height of 18 mm.

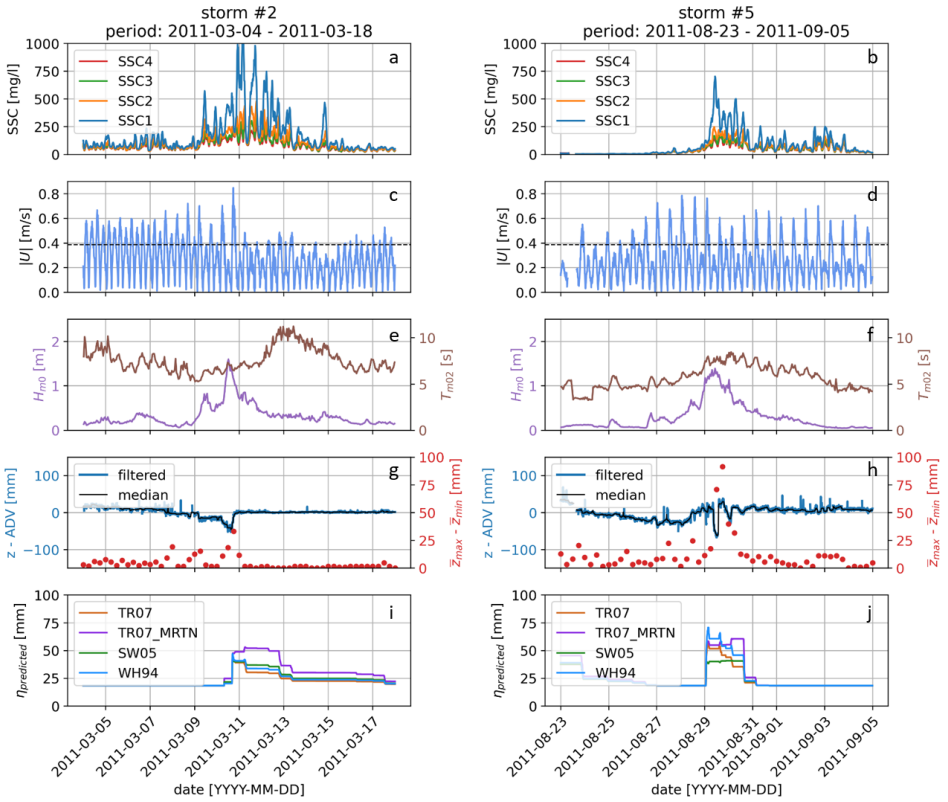

Figure 4.6.: SSC, tidal current, wave height and period, seabed elevation and predicted ripple height for two individual storms in 2011. (a, c, e, g, i) Storm #2 in March 2011. (b, d, f, h, j) Storm #5 in August 2011. The dashed line in subplots c and d indicates the threshold of motion for sand based on the Shields criterion for a median grain size of 250 μm. Predicted ripple heights based on four predictors: TR07 (Traykovski 2007), MN10 (Marten 2010), SW05 (Soulsby and Clarke 2005) and WH94 Wiberg and Harris 1994.

4.4.4. TIMESCALES FOR REMOBILISATION AND SSC DECAY

In addition to the detailed analysis of the behaviour observed during storm #2 and #5, we investigated the timescales related to remobilisation and subsequent decay in SSC for all

twelve storms. These timescales may provide us with further insight into the dominant processes.

First, we compute the remobilisation timescale. We define this as the timelag between the occurrence of the wave height peak and two local SSC maxima. The first is the maximum SSC at 30 cm above the bed (SSC1 in Figure 4.6), while the second is the maximum total suspended mass ($M_{sus,storm}$) (Section 4.3.3). Both are taken from the SSC data, and are correlated, as $M_{sus,storm}$ is estimated from SSC at all four measurement heights. A positive timelag means that these suspended matter maxima occurred after the wave height peak.

The SSC peaks for all twelve storms occur during or after the wave height peak (Figure 4.7 – solid bars). The smallest timelag is observed for storm #5, where the SSC peak coincides with the maximum wave height (see Figure 4.6b, d). The longest timelags occur during storms #9 and #12, with timelags of 4.5 and 3.5 days, respectively. The timelags for all other storms range from 0 to 2 days.

For most storm periods, maximum $M_{sus,storm}$ is reached after the wave height peak (Figure 4.7 – hatched bars). Storm #1 appears to be the outlier in this analysis, as it is the only storm with a negative timelag to maximum $M_{sus,storm}$. Of the other eleven storms, the maximum $M_{sus,storm}$ usually takes place within two days after the storm peak. The longest timelags again occur during storms #9 and #12. For storm #9, this could be explained by the long sustained period of high SSC, where the final peak was slightly higher than the previous peaks. Storm #12 showed rather different behaviour, as SSC only started to increase after the storm waned. Furthermore, near-bed concentrations for this storm exceeded 2000 mg/L, which is considerably higher than for the other storms.

For each storm, the maxima in SSC and $M_{sus,storm}$ occur within 2 days of each other, with the majority occurring less than half a day apart. For 8 out of 12 storms, peak SSC precedes maximum $M_{sus,storm}$. The mean timelag for both approaches is roughly the same at approximately 31 hours. That these two approaches yield a similar result suggests that the approach is fairly robust even though we are considering maximum values.

The timelag of 0 to 2 days for most storms suggests that fines are remobilised locally and then resuspended, and not advected from distant concentrated sources.

Furthermore, this analysis shows that SSC does not react instantaneously when a storm takes place. There are two possible explanations for this behaviour. The first is prompted by our conceptual remobilisation model. It takes waves multiple hours to build up the larger bedforms and for these bedforms to migrate. The second possible explanation is provided by the remobilisation formulation of the two-layer buffer model (Equation (4.2)). As long as the bed shear stress (τ) exceeds the critical bed shear stress ($\tau_{cr,2}$), remobilisation continues. And as long as remobilisation exceeds deposition (D), the total suspended mass will keep on increasing.

The second timescale describes the decay in SSC after a storm. Assuming that tidal currents can resuspend all readily available fines, a decay in SSC means that fines are no longer present on the seabed. Thus, SSC decay serves as a key indicator for fines burial: the more efficient the burial, the shorter the decay timescale. We define it as the half-life of the storm-induced SSC, which is determined by fitting an exponential function to the SSC peaks at 0.3 m above the bed during the decay period:

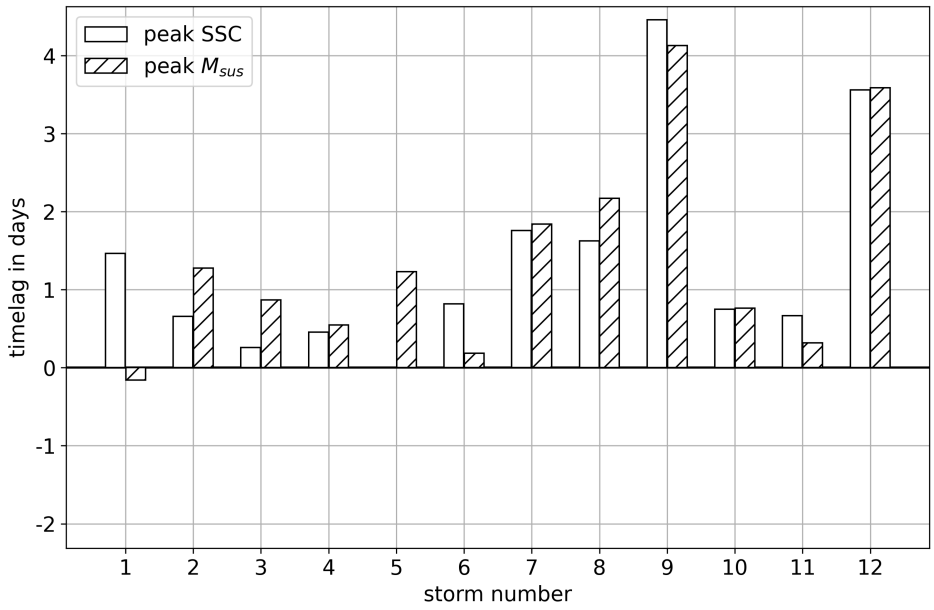

Figure 4.7.: Timelag between peak wave height and suspended matter maxima. For the latter, we consider both the SSC peak at 30cm above the bed (solid white bars) and the total suspended matter peak (hatched bars).

$$c(t) = c_0 e^{-\lambda t} \quad \text{and} \quad \tau_{0.5} = \frac{\ln(2)}{\lambda} \tag{4.15}$$

where:
c (t) = SSC peak at time t [mg/l]
c_0 = maximum SSC during the storm [mg/l]
t = elapsed time since maximum SSC [days]

The peaks are selected from the period between the maximum SSC and when concentrations return to pre-storm conditions. The latter are reached when SSC remains below 200 mg/l again during an entire tidal cycle (12.5 hours), which is the same as the pre-storm threshold used for identifying storm periods (Section 4.3.2). From this period, we select the SSC peaks during each half-tidal cycle.

To illustrate this procedure, Figure 4.8a shows the selected SSC peaks for storm #5 and the fit applied to these data. The white dot indicates the maximum SSC value during this storm. The peak during each half-tidal cycle is indicated with a small black dot.

Using this approach, we identified the half-life in SSC for each storm and summarised the results in Figure 4.8b. This histogram divides all storms into separate bins according to their half-life. It shows that for most storms, this timescale is between 0.5-1.5 days. Two storms (#4 and #13) exhibited a decay period of less than a day. For storm #4, this

was caused by low SSC throughout this period. For storm #13, it was caused by the aforementioned maximum SSC that exceeded 2500 mg/L. Storms with a half-life of more than 1.5 days (#7 and #12) are characterised by a prolonged period of high wave heights. This wave activity likely remobilised the fines for multiple days, allowing the tidal currents to keep them suspended.

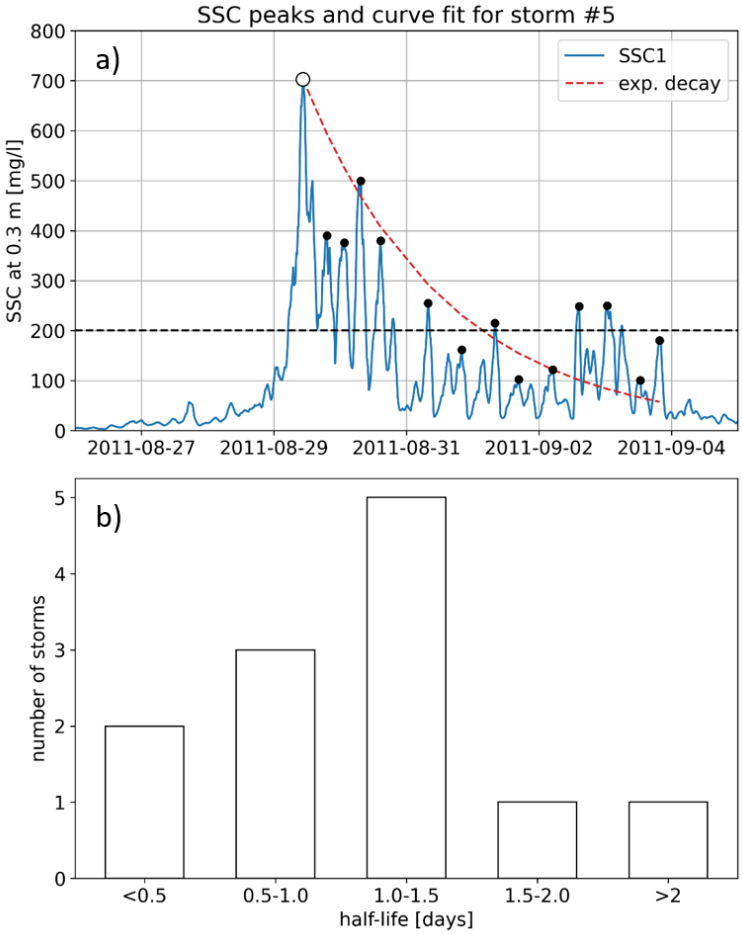

Figure 4.8.: (a) Example of storm #5 illustrating how decay period is defined and estimated. This is the period from storm peak (white dot) until peak SSC falls below 200 mg/l (black and white cross-hatched dot). (b) Histogram of SSC half-life during the selected storms.

4.4.5. TOTAL SUSPENDED SEDIMENT MASS DURING STORMS

The final step in our analysis is to validate whether the bedform release model provides a reliable estimate for the cumulative remobilisation flux during a storm. Using the approach described in Section 4.3.3, we estimate the maximum suspended mass from the measured SSC ($M_{sus,storm}$) and from the cumulative remobilisation flux (ΣE_{remob}) for each individual storm.

Figure 4.9 shows the result of this analysis. In each subplot, $M_{sus,storm}$ is plotted on the x-axis, while $E_{remob,storm}$ is plotted on the y-axis. The four subplots correspond to the four applied ripple predictors (listed in Table A.2). Dashed line indicates exact agreement between $M_{sus,storm}$ and $E_{remob,storm}$.

For six storms, $M_{sus,storm}$ remains below 1 kg/m^2, while another five do not exceed 2 kg/m^2. The storm with the highest $M_{sus,storm}$ is storm #9, as the total suspended matter reaches approximately 3 kg/m^2.

The four different ripple predictors show considerably different results. Using the TR07 or WH94 predictor leads to substantial variation in computed masses (top left and bottom right plot in Figure 4.9). The SW05 ripple predictor leads to the smallest variation in the computed masses, with $E_{remob,storm}$ only just exceeding 1 kg/m^2 for two storms (lower left plot in Figure 4.9). The MN10 predictor leads to a moderate variation in $E_{remob,storm}$.

The root-mean squared error (RMSE) for the applied predictors tells a similar story. The RMSE is highest for the WH94 predictor, followed by TR07. This is due to an overestimation of the suspended mass. In contrast, the SW05 generally underestimates the suspended mass, but as this only leads to small deviations between $M_{sus,storm}$ and $E_{remob,storm}$, the RMSE is already substantially lower. The MN10 predictor has the lowest RMSE and thus performs best for these storms. So, given all the uncertainties and assumptions used to estimate these total masses, remobilisation from the seabed is predicted fairly well by the time-dependent ripple model.

Interestingly, all four predictors strongly underestimated the suspended mass of storm 9. None of them predicts a suspended mass greater than 1 kg / m^2, while $M_{sus,storm}$ was the highest for this storm. Interestingly, this was also the storm with the longest time-lag between the peak wave height and suspended matter maxima (Figure 4.7. This long time lag suggests that the SSC is less influenced by the instantaneous forcing. Other processes than local resuspension might therefore play a role for this storm. If we exclude it, the RMSE decreases for each predictor. However, their relative performance does not change.

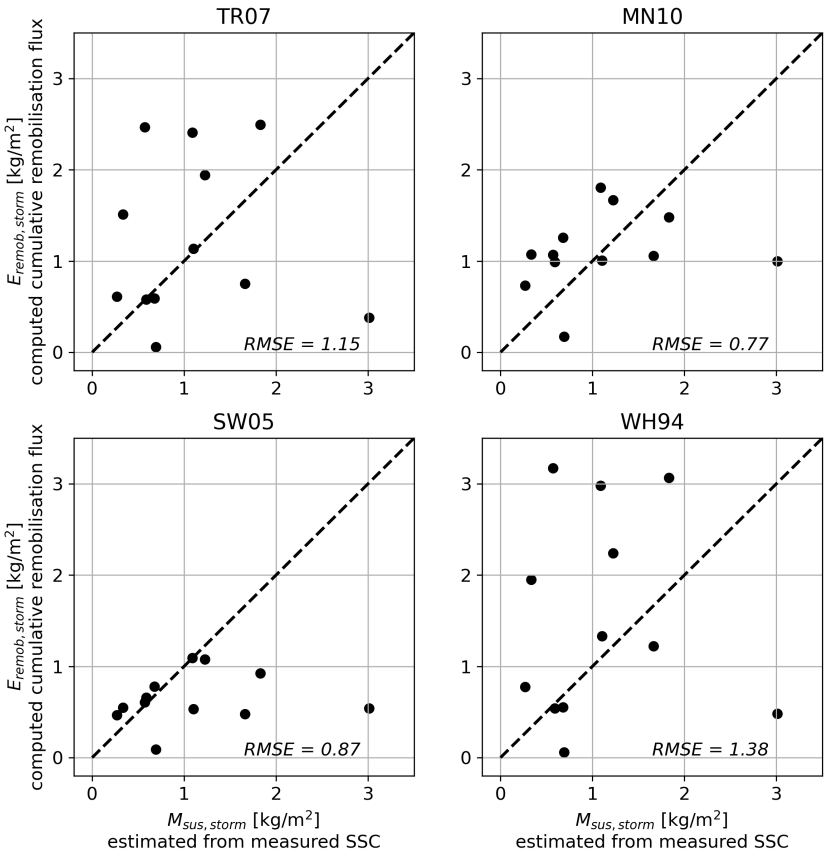

Figure 4.9.: Maximum suspended sediment mass per unit area, estimated from measured SSC and cumulative remobilisation flux. For the remobilisation flux approach, four ripple predictors were applied: TR07 (Traykovski 2007), MN10 (Marten 2010), SW05 (Soulsby and Clarke 2005) and WH94 (Wiberg and Harris 1994). Dashed line indicates exact agreement between $M_{sus,storm}$ and $E_{remob,storm}$.

4.5. DISCUSSION

In the previous section, we presented an analysis of the increase in SSC during storms and the gradual decay afterwards, based on the dataset of Witbaard *et al.* (2013). We analysed the general patterns in SSC during twelve storms and presented the involved timescales. Finally, we provided an estimate of the amount of fines remobilised from the seabed.

In this section, we discuss how these timescales and magnitudes relate to previous studies on sediment dynamics in the Dutch Coastal Zone. Furthermore, we discuss the bedform release model presented in Section 4.2 and how it can provide guidance when modelling the remobilisation of fines. This enables us to relate our findings to modelling practice and provide a wider outlook.

4.5.1. TIMESCALES

REMOBILISATION TIMESCALE

The remobilisation timescale was defined as the time interval between the maximum wave heights and the highest SSC peak during a storm (Figure 4.7). SSC increases steadily during storms, but it takes time before they reach their maximum value. For most storms, this timescale varies between zero and two days (Figure 4.7), with maxima of approximately four days for 2 of the 12 storms.

These timescales are consistent with the observations of Kleinhans *et al.* (2005) and Flores *et al.* (2017). They both observed storm-induced SSC peaks within 1 to 2 days after maximum wave heights were reached. Their study sites lie closer to the river Rhine outflow, at Noordwijk aan Zee and the Sand Engine, respectively. The offshore distance is comparable for all three datasets and ranges from 1 to 2 kilometres. The observations presented in Chapter 3 show similar behaviour.

The observed timelags can partially be explained by the time it takes for wave-induced bedforms to adjust to the governing hydrodynamics. Figure 4.6 shows that the measured bed elevation and the computed ripple heights exhibit a small timelag compared to the wave heights. During storms, wave-induced ripples require several hours to adjust to the governing wave conditions. This is observed not only for the two storms shown in Figure 4.6, but also for most other storms. Hence, the delay in SSC peaks cannot be explained entirely by just this adjustment period.

Another probable explanation for these timelags is the advection of fines to the study site. Here, we should distinguish between alongshore and cross-shore fluxes. If the timelag is due to alongshore advection, the sources of fines should be located within several kilometres of the site. As fines are spread heterogeneously in the seabed (see Figure 4.5b), fines that are remobilised near the location of the lander can be advected. Another possible process is cross-shore advection, leading to an accumulation fines in the nearshore zone (i.e. less than 2 km offshore). However, previous research shows contrasting observations. Cross-shore transport in onshore direction was observed by van der Hout *et al.* 2015 for calm conditions, while Flores *et al.* 2017 observed offshore transport during storm conditions.

The final possible cause is how a storm develops once it has reached its peak. When the wave heights during a storm decrease rapidly after its peak, bedform migration will be limited, and thus limit additional remobilisation. The observed timelag will then be short. If wave heights decrease slowly, the wave-induced bedforms are likely to migrate substantially, thereby remobilising additional fines. This leads to an ongoing increase of SSC within days after the storm peak.

Since the aforementioned processes operate on a similar timescale, we cannot determine which process is dominant based on the current analysis.

DECAY TIMESCALE

For the decay timescale, we defined the half-life of the storm-induced SSC. For most storms, this ranged from 0.5 to 2 days. This means that it may take up to three or four days for the SSC to reach pre-storm levels, depending on the maximum SSC during a storm.

During these decay periods, SSC is still high, though the hydrodynamic forcing is often comparable to pre-storm conditions. This asymmetric response of SSC to hydrodynamic forcing, i.e., hysteresis, was previously observed and was related to the local availability of fine sediment (Eleveld *et al.* 2008, Stanev *et al.* 2009, Suijlen and Duin 2001, van der Hout *et al.* 2017). Our bedform release model qualitatively links this hysteresis to remobilisation of fines from the seabed. This further elucidates the effect of water-bed exchange on SSC throughout the Dutch Coastal Zone, and implies that observed SSC cannot be interpreted as an instantaneous response to occurring bed shear stress.

These observations corroborate the explanatory burial model of Chapter 3. There we proposed that the interaction between storm-induced megaripples and current-induced ripples is primarily responsible for the burial of fines in the sandy seabed. After storms wane, the megaripples are gradually flattened by current-induced ripples, and fines are buried in the former troughs of the megaripples. Hence, bedform height gradually decreases in the wake of storms, which may take days. Furthermore, SSC steadily decreases as fines are buried within the seabed and cannot be easily resuspended by the tidal currents. For the burial of fines after a storm, we suggested a timescale of approximately a week.

The gradual decrease in bedform height is supported by the measured bed elevation (Figure 4.6e,f) and corroborated by the predicted ripple heights (Figure 4.6g,h). However, for this dataset, it seems to be taking place within several days rather than a week. Thus, the burial process may take place on a shorter timescale than we proposed in Chapter 3.

4.5.2. MAGNITUDE OF SSC INCREASE

When the upper strata of the seabed are mobilised during storms, the fines present in this part of the seabed are eroded along with the sand. This assumes that all fines are remobilised from this part of the seabed, thus depleting the supply of fines. Thus, the seabed is regularly depleted from fines. Even when average fines percentages are in the order of 2-5%, a succession of storms can deplete all the fines from the seabed (see Chapter 3 and references therein).

However, this depletion is partly a matter of scale. As Figure 4.3 shows, both megaripple dimensions and fines presence vary substantially, even on a centimetre to decimetre scale. So, while part of the upper seabed strata may contain little to no fines, fines may still be present several metres away or in the lower strata. This strong heterogeneity in fines presence is confirmed by the sediment data (Figure 4.5b). Where fines are momentarily buried in the seabed depends on the succession of burial and remobilisation in the previous months to years, and even on older geological deposits.

In our analysis, we assumed that the total suspended sediment mass mainly depends on the processes of remobilisation and resuspension, not taking lateral gradients into

account. This is justified based on previous studies van der Hout *et al.* 2017. If this can be applied to a wider area, the total suspended sediment mass depends on the storm-induced bedform height (η_{storm}), the remobilisation efficiency factor (γ) and the amount of fines currently available in the seabed. As we readily discussed the last factor, we will only discuss the first two here. Time-dependent bedform height (η) can be adequately predicted by the time-dependent ripple model of Soulsby *et al.* (2012). However, the computed ripple heights did vary substantially for the set of predictors used in this study, up to 5 cm for several storms. The Marten (2010) ripple predictor provided the most accurate estimate for the remobilisation flux (Figure 4.9).

The remobilisation efficiency factor (γ) lumps different uncertainties in the remobilisation process into a single parameter. We set it to 0.5 (Table 4.1), assuming that all fines present in the seabed are remobilised where storm-induced megaripple troughs form. We did not explicitly account for inhomogeneity in the seabed when setting this value for γ. This inhomogeneity could lead to a higher or lower value for γ. Another factor affecting the value of γ is bedform migration. If this is taken into account, γ should be increased.

4.5.3. GUIDANCE FOR MODELLING

We have compared the proposed remobilisation flux with measured SSC and have interpreted the parameters that influence it (Section 4.4.5 and Section 4.5.2). As a final step, we discuss how the bedform release model can provide guidance to select the appropriate parameter settings for the buffer model of van Kessel *et al.* (2011).

Both formulations were presented in Section 4.2, here we repeat them for convenience:

$$E_{buffer} = p_2 M_2 \left(\frac{\tau}{\tau_{cr,2}} - 1 \right)^{1.5} \tag{4.16}$$

$$E_{remob} = p_{fines} * \gamma * \rho_s * (1 - n) * \frac{d\eta}{dt} \tag{4.17}$$

We apply the parameter settings for E_{remob} as presented in Section 4.3.3. We assume that wave forcing is dominant and neglect the bed shear stress due to currents. Furthermore, we use a constant fines fraction (p_2) of 5% for both methods. For the buffer model, we set the resuspension parameter (M_2) to $1{\cdot}10^{-2}$ kg/m^{2}s, which is the van Rijn pick-up parameter for fine sand for a d_{50} of 250 μm (van Rijn 2007). We note that this value for (M_2) is at least one to several orders of magnitude larger than values commonly applied in North Sea sediment modelling (van Kessel *et al.* 2011, van Maren *et al.* 2020).

As discussed in Section 4.2, the change in ripple height ($\mathrm{d}\eta/\mathrm{d}t$) in E_{remob} depends on two terms: (1) the difference between equilibrium ripple height (η_{eq}) and actual ripple height (η) and (2) a relaxation timescale (T_e/β). Both η_{eq} and (T_e/β) can be rewritten to depend solely on the wave-induced bed shear stress (τ_w). Thus, we can directly compare the predicted remobilisation flux for both methods as a function of τ_w.

For E_2, we compute the flux using two critical bed shear stresses,i.e. a $\tau_{cr,2}$ of 0.17 and 1.0 Pa. E_2 depends substantially on $\tau_{cr,2}$, over the entire range of τ_w, since the calculated fluxes are an order of magnitude apart (Figure 4.10). The lower value for $\tau_{cr,2}$ corresponds to the Shields criterion for incipient motion θ_{cr} for fine sand ($d_{50} = 250\mu m$),

while the higher value is often used to model the dynamics of fine sediment in sandy shelf seas (e.g. van Kessel *et al.* 2011, van Maren *et al.* 2020). For a sandy seabed composed mainly of fine sand, the latter falls well within the megaripple domain (Brakenhoff *et al.* 2020,Kleinhans 2005). This means that in fine sediment modelling, it is implicitly assumed that substantial remobilisation of fines only takes place when megaripples are formed on the seabed.

For E_{remob}, the relevant variable is the difference between the equilibrium ripple height and the actual ripple height ($\eta_{eq} - \eta(t)$). If we assume that the minimum value for ηt is the current-induced ripple height η_c, we can compute a maximum remobilisation rate $E_{remob,max}$ for each value of τ_w, through:

$$E_{remob,max} = p_{fines} * \gamma * \rho_s * (1-n) * \frac{\beta}{T_e}(\eta_{eq} - \eta_c) \tag{4.18}$$

4

This results in the green line in Figure 4.10. The values for $E_{remob,max}$ generally fall between the values of E_2 values. However, they are substantially larger than E_2 if $\tau_{cr,2}$is set to 1.0 Pa (Figure 4.10). This means that, in principle, the remobilisation rate predicted by the bedform release model is larger. However, E_{remob} will gradually decrease over the course of a storm, whereas E_2 remains constant with constant τ_w. As the bedforms gradually adjust to the hydrodynamic forcing, the difference between the equilibrium bedform height (η_{eq}) and the actual bedform height ($\eta(t)$) decreases. To illustrate this, we included the 50% value of $E_{remob,max}$. Even when bed shear stresses increase, the smaller difference between η_{eq} and $\eta(t)$) will dominate.

Modelling the dynamics of fine sediment dynamics requires not only the prescription of the erosion formulation but also the definition of the layer from which erosion can take place. In most numerical models, an active layer is considered with inactive layers below (van der Molen *et al.* 2009, Wiberg *et al.* 1994). The most straightforward solution is to set a constant and uniform thickness (van Kessel *et al.* 2011). However, if bedforms determine the erosion rates, as indicated above, the thickness of the active layer should also change with the forcing. This implies that short intense storms will mobilise sediment from deeper strata and thereby lead to more erosion of fines than longer milder storms. Further exploration in numerical tests is needed to determine the impact of these mechanisms.

4.6. CONCLUSIONS

The goal of this chapter was to quantify how fast and how much fine sediment is remobilised during storms and to determine the underlying mechanisms. To this end, we analysed the long-term dataset of Witbaard *et al.* (2013). From this dataset, we selected twelve isolated storms, for which we investigated storm-related timescales and magnitude of the SSC increase.

Fines are only remobilised when storms are able to mobilise substantial parts of the sandy seabed. The maximum SSC is reached within several days after the peak in wave height. Fines then remain in the water column between one and six days before the return to pre-storm conditions. This leads to an asymmetric response of SSC to hydrodynamic forcing.

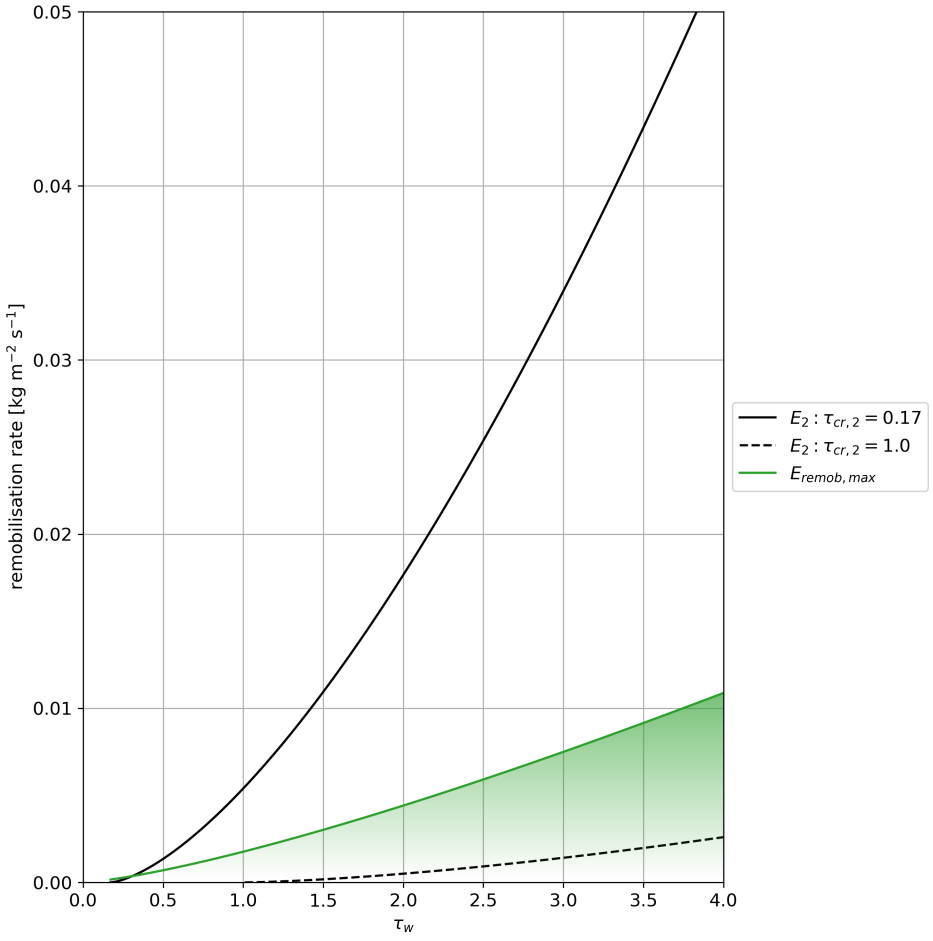

Figure 4.10.: Remobilisation flux estimated using the formulation from the two-layer buffer model (E_2) indicated by the solid and dashed black line; and the flux $E_{remob,max}$ as deduced from the bedform release model (solid green line) The colour gradient underneath this curve indicates a decrease in the difference between η_{eq} and $\eta(t)$.

To quantify the magnitude in SSC increase, we introduced a novel process-based formulation, which describes the remobilisation of fines from the sandy seabed. This bedform release model relates remobilisation of fines to the formation and migration of megaripples on the seabed. The latter is modelled using the time-dependent ripple model of Soulsby *et al.* (2012), for which multiple ripple predictors can be used. The predicted remobilisation was then compared to the total fines mass suspended during storms. Generally, the predicted and observed remobilisation agreed well. Applying the

Marten (2010) ripple predictor in our bedform release model led to the best fit with the experimental data.

The proposed bedform release model provides guidance for setting parameters for water-seabed exchange models for fine sediment modelling. To illustrate this, we compared remobilisation rates predicted by the bedform release model with the two-layer buffer model of van Kessel *et al.* (2011). Provided with the same set of parameters, they predict similar remobilisation rates. The bedform release model can contribute to a better understanding of the exchange of fines with a sandy seabed. Improving this understanding is essential as it enables us to more accurately predict the effect of human interferences on the southern North Sea.

5

SYNTHESIS

The North Sea is one of the world's busiest coastal seas. Apart from its economic importance, we must realise that the North Sea plays a vital role as habitat for a wide variety of marine species. To understand how human activities affect this ecosystem, we must understand their impact on key physical processes. The transport of fine sediment throughout the North Sea is such a process, and one of the main unknowns related to it was the exchange of fine sediment between the water column and the mostly sandy seabed.

Therefore, the main objective of this dissertation was to find out *"How the seabed - water column exchange of fine sediment affects the distribution of fines in the southern North Sea"*. In this chapter, we provide answers to the questions related to this objective (Section 5.1). Once we have answered these questions, we reflect on our research methods and what it means for measuring, modelling, and monitoring of fine sediment dynamics (Section 5.2). Section 5.2 is finalised by providing recommendations for future research in Section 5.2.3. Eventually, we discuss how this research contributes to the major developments currently taking place in the southern North Sea: the energy, food, and nature transitions (Section 5.3).

5.1. CONCLUSIONS

The seabed and the water column form a coupled system, where fine sediment is exchanged regularly. This leads to memory effects, as observations of sediment — both suspended and in the seabed — result from past events, both in the recent and more distant past.

On the short term, i.e., on a scale of days to weeks, storm timing strongly affects the amount of suspended fines (Chapter 3). Only once fines have been remobilised from the seabed, will hydrodynamic processes like tides and baroclinic forcing drive their transport throughout the system. Over longer timescales (months to years), hydrodynamic events govern the burial and remobilisation of fines. Together with the supply of fines, these processes determine the amount of fines buried within in the sandy seabed. On a seasonal scale, a succession of storms may lead to a locally depleted seabed (Chapter 3). During successive calm periods, the fines stock in the seabed is built up once again (Chapter 4).

Research question 1: Where are fines found in the seabed of the southern North Sea?

We focused on the Dutch Coastal Zone (DCZ) of the southern North Sea, where the seabed is predominantly sandy and contains a fines fraction of approximately 1-10%. Importantly, fines are not uniformly distributed in the seabed but show strong spatial gradients. We identified three spatial scales on which their presence varies: the macro, meso, and micro scale (Figure 5.1).

To explain this distribution, we developed a conceptual framework. This consists of three components: (1) sources of fines; (2) transport pathways from these sources; and (3) accumulation potential. The latter reflects whether a location is calm enough for fines to accumulate. It thereby implicitly expresses the balance between burial and remobilisation at a given location. All three components must be considered to understand the

distribution of fines.

On the macro scale, fines are primarily concentrated in a 20-kilometer-wide band along the Dutch coast. This is consistent with previous studies (Eisma 1968, van Alphen 1987a) which suggests that on a decadal time scale, the distribution of fines on a macro scale is relatively stable. Although there is ample accumulation potential beyond 20 km offshore — such as in the troughs of the tidal sand waves (Figure 2.10) — fines are virtually absent in this area. We therefore conclude that, on the macro scale, fines presence is mainly governed by sources and the transport pathways from these sources. Upstream changes in either component may affect downstream areas on a scale of tens of kilometres or even further.

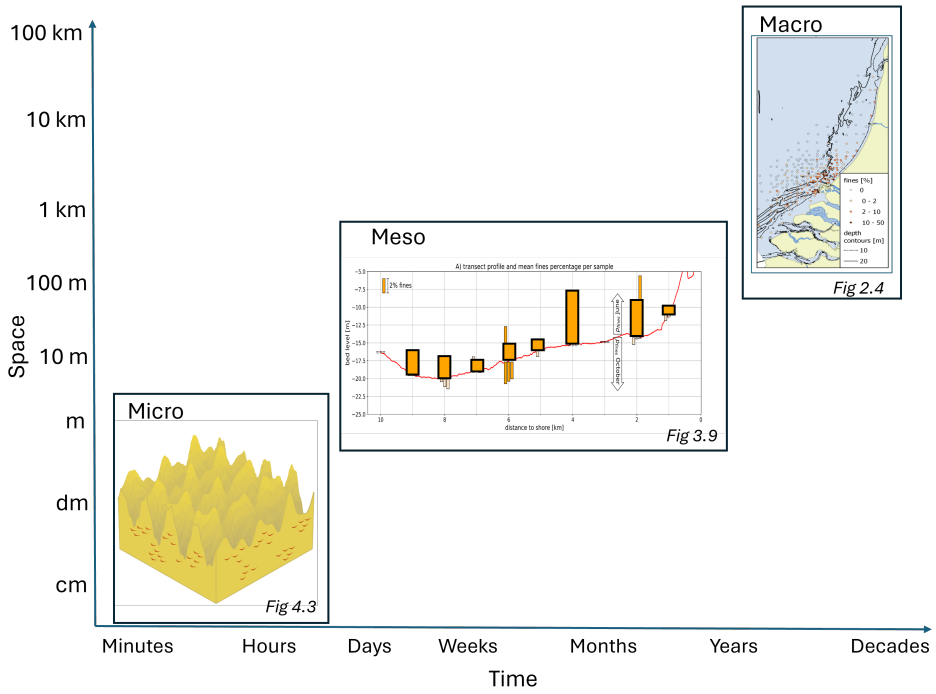

Figure 5.1.: Presence of fines in the southern North Sea bed on distinct spatial and temporal scales. Presence on the macro scale is mainly governed by sources and transport pathways, while on the meso scale, accumulation potential plays a more dominant role. On the micro scale, the distribution is determined by small-scale burial processes.

Building on the macro-scale patterns, we examined fines distribution on the meso scale. Here, fines percentages of 10-20% are concentrated within 2-3 km of the shore near the Rhine outflow. These deposits are mostly temporary, as waves regularly remobilise the upper parts of the seabed. Other local maxima in fines (up to 20%) occur near sites where dredged sediment is spread and in former tidal channels of closed estuaries

(Chapter 2).

On the micro scale, the distribution of fines distribution remains highly variable. This variability likely originates from burial processes, which introduce vertical variation at the centimetre scale and horizontal variation at the decimetre scale (Figure 5.1).

In the DCZ, large-scale human interventions clearly influence fines distribution. Our conceptual framework can be used to explain these effects, by identifying which of its three components is affected by an intervention:

(1) Human-induced sources of fines mainly originate from the spreading of dredged (fine) sediment (Hendriks and Schuurman 2017) and sand mining (Spearman *et al.* 2011).

(2) Transport pathways are only altered if human interventions affect large-scale hydrodynamic patterns, such as tidal currents or density gradients. In the DCZ, only large-scale interventions, such as the closure works in the Southwestern delta (Elias *et al.* 2017) or Maasvlakte 2 (MV2), have had such effects.

(3) Accumulation potential is affected when a location becomes more sheltered or more exposed. Over the past decade, the construction of MV2 has notably affected accumulation potential in two key areas. South of MV2, ongoing fines accumulation from the earlier closure of the Haringvliet estuary (Elias *et al.* 2017, van Heteren 2002) intensified further. Additionally, accumulation potential increased sharply in the deep sand mining pit created for MV2 (Chapter 2). Recent studies indicate similar behaviour in shallower sand mining pits, where fines percentages are elevated relative to surrounding areas (Witbaard and Craeymeersch 2023, Leewis *et al.* 2024).

Research question 2: How and when are fines temporarily buried in the seabed?

Storms remobilise fines from the seabed, leading to increased suspended sediment concentrations (SSC) across the southern North Sea (Suijlen and Duin 2001, cf. Chapter 4). SSC returns to pre-storm levels within days to a week, which is driven by the temporary burial of fines. This burial process thus operates on a similar timescale as the SSC decrease. Based on previous research (e.g. Kleinhans *et al.* 2005), we identified bedform migration as the only viable burial mechanism for the southern North Sea within a week after a storm.

We developed a mechanistic description of fines burial (Chapter 3), consisting of a four-phase dynamic cycle. All of these phases are related to the occurrence of storms. Remobilised fines will eventually settle on the sandy seabed. The interaction between bedforms of different scales is then crucial for burial. As storm-induced megaripples adjust to calmer conditions, current-induced ripples bury fines in their (former) troughs.

This process explains the burial of fines into the seabed for depths of up to 10-15 cm and a large variability in fines presence. Horizontal variation corresponds to megaripple lengths (decimetres to metres), while vertical variation corresponds to ripple height

(centimetres). Sediment cores and images of the upper seabed strata (Chapter 3) corroborate this description, showing fines in distinct horizontal and vertical patches. Temporal variations in fines percentage suggest occasional seabed depletion, resulting in supply-limited conditions.

Burial effectivity and the associated timescale depend on the ratio between storm intensity and current magnitude. Weak tidal currents prevent sand mobilisation, while strong currents shorten the burial time window. Optimal burial conditions are likely to be found in between, with timescales ranging from days to about a week.

Research question 3: Under which conditions are fines remobilised from the seabed and how long do they remain in the water column thereafter?

Fines are only remobilised when storms are able to form megaripples on the seabed, thereby mobilising substantial parts of the sandy seabed. This process triggers a rapid increase in SSC, which reaches its maximum within one to several days after the wave height peak. Fines remain suspended for one to six days before SSC returns to pre-storm conditions, resulting in an asymmetric SSC response to hydrodynamic forcing.

To quantify the increase in SSC, we propose a new conceptual formulation based on the mechanistic description of Chapter 3. This bedform release model directly relates remobilisation to the formation of storm-induced bedforms. To model ripple dynamics, we applied the time-dependent model of Soulsby *et al.* (2012), which allows for multiple ripple predictors.

We validated the model against observations from a 21-month in situ dataset (Witbaard *et al.* 2013). The modelled values agreed well with the observations, and the Marten (2010) ripple predictor showed the best agreement.

The process-based bedform release model clarifies the physical basis of existing erosion formulations and guides the interpretation and calibration of their aggregated parameters. For example, comparing our model with the van Kessel *et al.* (2011) two-layer buffer model revealed similar remobilisation rates, though standard parameter settings for large-scale models show some discrepancies.

5.2. REFLECTION AND OUTLOOK

5.2.1. REFLECTION ON RESEARCH METHODS

We analysed data from various sources, including readily available sediment data and numerical model output (Chapter 2), newly collected field data (Chapter 3), and a long-term time series (Chapter 4). Although the data analysed in Chapter 2 and Chapter 4 were originally collected for other purposes, they were instrumental for our research. The newly collected data presented in Chapter 3 required considerable effort and investment.

Reusing existing data (Chapter 2, Chapter 4) was only possible as these data followed the FAIR principles (Findable, Accessible, Interoperable, and Reusable). The benefits of FAIR data are clear, and it should be straightforward and rewarding for researchers to adopt these practices. Providing training, assistance, and incentives to individual researchers is essential to encourage them to follow these principles.

The analysed datasets varied not only in source but also in spatial and temporal coverage. While the sediment data from Chapter 2 covered most of the DCZ, the data from Chapter 3 and Chapter 4 were both collected at sites offshore of Egmond aan Zee. The campaigns presented in Chapter 3 particularly focused on high-resolution in-situ measurements at this location. This focus enabled us to repeat measurements, revealing substantial temporal and spatial variability in fines presence (e.g., Figure 3.9, Figure 4.5). These insights were made possible by the combined use of the SPI camera and NIOZ Multi Corer (Figure 3.5). Without these combined measurements, we would not have been able to uncover the small-scale processes that lead to the burial of fines. Naturally, focusing our efforts on this particular study site raises the question of whether these results are applicable to other parts of the southern North Sea, or more generally, other coastal seas. Focusing on the underlying physical processes and translating these into a conceptual framework proved to be essential for making these results more widely applicable.

Most of our research relied on in-situ measurements. While the techniques themselves were established, their combined application across multiple spatial and temporal scales proved instrumental in uncovering key processes governing fine sediment dynamics.

5.2.2. IMPLICATIONS FOR MEASUREMENTS, MONITORING AND MODELLING

We discovered significant spatial and temporal variation in fines presence in both the seabed and water column. How can we leverage these insights to improve the measurements, monitoring, and modelling of fine sediment?

Selecting appropriate temporal and spatial resolutions for field observations is crucial, and our research provides guidance. The dominant hydrodynamic forcing occurs on a scale of hours to days (Chapter 3 and Chapter 4). Point measurements can quantify such temporal processes (Chapter 4), but a theoretical or conceptual framework is necessary to generalise such observations. Synoptic measurements, such as remotely sensed data, provide valuable information on spatial variation, although they may be affected by the system's strong memory effects (e.g., Brandao *et al.* 2023).

Due to their spatial variation, it may be challenging to predict the exact fines percentage in the upper seabed strata. Statistical approaches to estimate the probability of encountering fines in the seabed seem more valuable, either through geostatistical methods (Stephens and Diesing 2015) or physics-based classifications (Chapter 2). Furthermore, duplicates (e.g. multiple sediment cores taken close together) may offer valuable information, as they provide average fines percentages and allow for quantifying spatial variability (Chapter 3).

Due to the pronounced variation in fines presence, drawing statistically significant conclusions about human interventions requires numerous observations over multiple years (Borst *et al.* 2013, Blaas and van den Boogaard 2006). This may be further complicated by multiple human interventions taking place in each other's vicinity or because of long-lasting effects. Awareness of which interventions occurred where and when is essential (Chapter 2). Furthermore, combining field observations with numerical modelling may prove to be particularly useful here. Modelling can be used to isolate the

effect of a single intervention, while field observations are essential for validating those models.

Finally, we learned that the burial process operates on a substantially smaller scale than hydro-morphological model grid size. Hence, small-scale variations in fines presence cannot be represented in model outcome. The only way to represent this on the level of single grid cells is by introducing additional variation in the seabed stratigraphy. More importantly, parameterisations should aim at correctly representing large-scale patterns of fines in the seabed, considering the temporal and spatial variations of wave- and current-induced bed shear stress.

5.2.3. RECOMMENDATIONS FOR FURTHER RESEARCH

The findings of this research highlight several opportunities for further research into fine sediment transport in the southern North Sea. Follow-up studies should aim at integrating knowledge from different disciplines, as fine sediment dynamics lie at the intersection between hydrodynamics, morphodynamics, sedimentology and marine ecology.

The main uncertainty related to the exchange of fines between the water column and seabed lies in the evolution of the sandy seabed. More specifically, we recommend investigating how small-scale bedforms develop in both time and space. In Chapter 3 we demonstrated how the interaction between bedforms of different scales leads to the burial of fines in the sandy seabed. To quantify this burial flux (Figure 3.14), the rate at which storm-induced megaripples are flattened by current-induced ripples needs to be determined. This requires translating sedimentological concepts, such as phase diagrams (e.g., Brakenhoff *et al.* 2020) or bedding sequences (e.g., Reineck and Singh 1980), to quantitative fluxes on the scale of (mega-) ripples. Research on hummocky cross-stratification (e.g. Passchier and Kleinhans 2005) is a good starting point, as this bedding sequence is storm-induced and consists of a mixture of fines and sand. Furthermore, recent research by Lichtman *et al.* (2018) unveiled how small percentages of fines may already affect the formation and migration of bedforms on intertidal flats. It remains to be explored whether these effects play a similar role in subtidal environments.

In our analyses, we have implicitly assumed that the properties of fine sediment do not change during and after deposition. The main assumption is that the critical shear stress for the soft layer of fines (i.e, the fluffy layer) on top of the seabed is always lower than the critical shear stress of fine sand (Chapter 3). This holds if the fines layer remains unconsolidated. If the fines can actually consolidate, their critical shear stress may increase substantially (Terwindt and Breusers 1972). This depends on several factors, such as the time since deposition, layer thickness and the ambient hydrodynamics while the sediment is deposited on the bed (Tran and Strom 2019). In energetic, sandy environments, consolidation does not seem likely, but this assumption warrants further investigation.

To further improve our understanding of fine sediment fluxes in the southern North Sea, we need accurate estimates of the main sources and sinks within the system. These sources and sinks dictate the alongshore sediment flux (van Alphen 1990). In turn, this alongshore flux is used for calibrating numerical models (de Kok 1996, Gerritsen *et al.* 2001, van Kessel *et al.* 2011) and as input for sediment budgets of estuaries and tidal basins adjacent to the North Sea (van Kessel and Vanlede 2009, Colina Alonso *et al.* 2024). Accurate estimates are crucial, given the contribution of fines on sedimentation rates

(e.g., van Maren *et al.* 2015, Colina Alonso *et al.* 2021).

One substantial but uncertain source is the flux of fines entering the southern North Sea through the Dover Strait (van Alphen 1990, Fettweis *et al.* 2007. The most accurate estimate of this flux is provided by Fettweis *et al.* (2007), who set it at 22-31 MT/year. However, a recent study of sediment provenance has shown that the suspended material in the Belgian and Dutch coastal zones originates mainly from Holocene deposits off the Belgian coast (Adriaens *et al.* 2018). This casts considerable doubt on the dominance of the Dover Strait flux and thus its magnitude. Accurately quantifying this flux is therefore essential for constructing a reliable fine sediment budget for the southern North Sea.

Ultimately, and preferably sooner rather than later, the aforementioned knowledge should be integrated into marine governance. Achieving this requires collaboration not only across scientific disciplines, but also across the science-policy interface. As the next and final section will show, such collaborations are more relevant than ever for safeguarding a healthy North Sea ecosystem.

5.3. IMPLICATIONS FOR TRANSITIONS ON THE NORTH SEA

This dissertation advances our understanding of how human interventions influence fine sediment dynamics in the southern North Sea and how these changes may, in turn, affect ecosystem functioning. Such insights are urgently needed as three major transitions are currently taking place on the North Sea: the energy transition, the food transition and the nature transition (OFL 2020). Meanwhile, other human activities such as maintenance dredging, shipping, and sand mining will continue to take place and will likely intensify (Stolk and Dijkshoorn 2009).

Hence, it would be an omission to focus solely on these transitions, without accounting for the ongoing human activities. These activities already have clear effects on the ecosystem, both directly (e.g., Witbaard and Craeymeersch 2023) and indirectly, through the changes in fine sediment dynamics (see Chapter 2). Even when interventions took place decades ago, they can still affect both the physical system and the ecosystem, as these need time to adjust and recover (e.g., de Jong 2016).

These persisting and emerging human activities increase the complexity of the North Sea system. This complexity makes it more difficult to ensure a healthy ecosystem, as there may be unforeseen or compounding effects. Conceptual frameworks, such as the one presented in Chapter 2, are essential tools for quantifying individual and compounding effects, particularly as pressures continue to mount.

This is emphasized by recent assessments, which show that cumulative pressures from human activities affect the marine ecosystem and biodiversity of the North Sea in significant and measurable ways. According to OSPAR, the net effect of these pressures has resulted in a 'not good' environmental status for many common species, as well as for threatened and declining species (OSPAR 2023). This appears to conflict with the ambitious goals of the energy transition.

Since the early 2010s, the main driver for developments on the North Sea is the transition from fossil fuels to renewable energy. The countries bordering the North Sea have large ambitions: from a currently installed capacity of 25 GW, they aim to increase this capacity to 76 GW in 2030 and on to 260 GW in 2050 (North Sea Energy Cooperation

2022). To put this into perspective, this would mean that in 2050, 25% of the Dutch sector of the North Sea would be an offshore wind farm (OWF). This already leads to a "race for space" in the southern North Sea. Apart from these spatial constraints, this will affect the ecosystem directly and indirectly.

A direct effect of OWFs is that they will lead to a local decrease in fishing intensity, as OWFs will be closed for any kind of fisheries. Most notably, this means bottom-trawling will effectively cease in OWFs, which theoretically leads to less disturbance of the seabed and thus better development of benthic communities. Furthermore, this will lead to less resuspension of fine sediment and therefore a decrease in turbidity. Both effects would benefit the ecosystem. However, it is not yet clear if the fishing activity that took place within OWFs will cease altogether or will take place elsewhere, resulting in more intense fishing in other areas (Van Hoey *et al.* 2021).

In addition to these direct ecological effects, OWFs may also have significant indirect impacts. Multiple studies have shown that the large-scale development of offshore wind will lead to changes in stratification throughout the southern North Sea (Carpenter *et al.* 2016, Floeter *et al.* 2017, Dorrell *et al.* 2022, Zijl *et al.* 2023). Although this will not directly change the availability of fine sediment, it will affect its transport. These changes may alter fine sediment transport pathways,

These developments stress the need for integrated, science-based management of the North Sea. In response, researchers and policy makers are increasingly focused on ensuring that the combined effect of all human activities does not exceed the "ecological carrying capacity" of the North Sea (OFL 2020). Multi-year research programmes such as the *Ecological Programme Offshore Wind* (Wozep) and *Nature Strengthening and Species Protection Monitoring Survey* (MONS) seek to understand how the ecosystem is affected by human interventions, and how these effects can be minimised or mitigated (van Nieuwpoort *et al.* 2023, Asjes *et al.* 2021). As the ecosystem and the physical environment are coupled, the insights from this dissertation provide essential input for such research programmes.

As many economic activities depend on a healthy ecosystem, protecting the North Sea may be seen as a pragmatic choice. It is up to us to leverage this with our ideals of what the North Sea should look like. There is only one North Sea, and its future depends on the choices we make today.

REFERENCES

[1] R. Adriaens, E. Zeelmaekers, M. Fettweis, E. Vanlierde, J. Vanlede, P. Stassen, J. Elsen, J. Środoń, and N. Vandenberghe. "Quantitative clay mineralogy as provenance indicator for recent muds in the southern North Sea". In: *Marine Geology* 398 (Apr. 2018), pp. 48–58. ISSN: 0025-3227. DOI: 10.1016/J.MARGEO.2017.12.011. URL: https://www.sciencedirect.com/science/article/pii/S0025322717301123?via%3Dihub.

[2] J. N. Aldridge, M. J. N. Bergman, T. Bolam, J. A. Craeymeersch, and S. Degraer. *Structure and dynamics of the North Sea benthos*. 2007. ISBN: 8774820583.

[3] Alkyon. *PMR monitoring natuurcompensatie Voordelta. Perceel 4, abiotiek. Beschrijving aanpak modelsimulaties, calibratie en validatie*. Tech. rep. Emmeloord, The Netherlands, 2010.

[4] C. L. Amos, A. J. Bowen, D. A. Huntley, J. T. Judge, and M. Z. Li. "Ripple migration and sand transport under quasi-orthogonal combined flows on the Scotian Shelf". In: *Journal of Coastal Research* 15.1 (1999), pp. 1–14. ISSN: 07490208.

[5] Carl L. Amos, M. Z. Li, and K. S. Choung. "Storm-generated, hummocky stratification on the outer-Scotian Shelf". In: *Geo-Marine Letters* 16.2 (1996), pp. 85–94. ISSN: 02760460. DOI: 10.1007/BF02202602.

[6] Edward J. Anthony and Troels Aagaard. "The lower shoreface: Morphodynamics and sediment connectivity with the upper shoreface and beach". In: *Earth-Science Reviews* 210 (Nov. 2020). ISSN: 00128252. DOI: 10.1016/j.earscirev.2020.103334.

[7] Kenneth R. N. Anthony, Peter V. Ridd, Alan R. Orpin, Piers Larcombe, and Janice Lough. "Temporal variation of light availability in coastal benthic habitats: Effects of clouds, turbidity, and tides". In: *Limnology and Oceanography* 49.6 (Nov. 2004), pp. 2201–2211. ISSN: 00243590. DOI: 10.4319/lo.2004.49.6.2201. URL: http://doi.wiley.com/10.4319/lo.2004.49.6.2201.

[8] Arcadis. *PMR monitoring natuurcompensatie Voordelta. Perceel 4, Abiotiek. Validatierapport voor de simulaties Juni 2004 t/m December 2012*. Tech. rep. 2014, p. 678.

[9] Arcadis and Deltares. *WAQUA-IN-SIMONA: Kustzuid and Kustgrof model results*. 2019.

[10] J Asjes, H Merkus, O G Bos, J Steenbergen, S Stuijfzand, I van Splunder, T Van Kooten, S Rivero, and G A J Vis. *Monitoring en Onderzoek Natuurversterking en Soortenbescherming (MONS)*. Tech. rep. The Hague, The Netherlands: Overlegorgaan Fysieke Leefomgeving, 2021, p. 190.

[11] D. W.T. Au, C. A. Pollino, R. S.S. Wu, P. K.S. Shin, S. T.F. Lau, and J. Y.M. Tang. "Chronic effects of suspended solids on gill structure, osmoregulation, growth, and triiodothyronine in juvenile green grouper Epinephelus coioides". In: *Marine Ecology Progress Series* 266 (2004), pp. 255–264. ISSN: 01718630. DOI: 10.3354/meps266255.

[12] J. H. Baas, R. L. van Dam, and J. E.A. Storms. "Duration of deposition from decelerating high-density turbidity currents". In: *Sedimentary Geology* 136.1-2 (2000), pp. 71–88. ISSN: 00370738. DOI: 10.1016/S0037-0738(00)00088-9.

[13] Meinte Blaas and H. van den Boogaard. *Statistical methods to assess the impact of MV2 on SPM along the Dutch coast*. Tech. rep. The Hague, Netherlands: WL | Delft Hydraulics, 2006, p. 79.

[14] Frank Detlef Bockelmann, Walter Puls, Ulrike Kleeberg, Dagmar Müller, and Kay Christian Emeis. "Mapping mud content and median grain-size of North Sea sediments – A geostatistical approach". In: *Marine Geology* 397.September 2017 (2018), pp. 60–71. ISSN: 00253227. DOI: 10.1016/j.margeo.2017.11.003. URL: https://doi.org/10.1016/j.margeo.2017.11.003.

[15] Wil Borst and Onno van Tongeren. *Memo silt contents boxcore samples benthos*. Tech. rep. Rotterdam: Port of Rotterdam Authority, 2012, pp. 1–13.

[16] Wil Borst and Tiedo Vellinga. "The Monitoring Programme for the Maasvlakte 2 - Construction at the Port of Rotterdam". In: *Terra et Aqua* 129 (2012), pp. 16–29.

[17] Wil Borst, Tiedo Vellinga, and Onno Van Tongeren. "The Monitoring Programme for the Maasvlakte 2 Construction at the Port of Rotterdam - Part II". In: *Terra et Aqua* 130 (2013), pp. 20–32.

[18] Laura Brakenhoff, Maarten Kleinhans, Gerben Ruessink, and Maarten van der Vegt. "Spatio-temporal characteristics of small-scale wave–current ripples on the Ameland ebb-tidal delta". In: *Earth Surface Processes and Landforms* 45.5 (2020), pp. 1248–1261. ISSN: 10969837. DOI: 10.1002/esp.4802.

[19] I. L.S. Brandao, J. van der Molen, and D. van der Wal. "Effects of offshore wind farms on suspended particulate matter derived from satellite remote sensing". In: *Science of The Total Environment* 866 (Mar. 2023), p. 161114. ISSN: 0048-9697. DOI: 10.1016/J.SCITOTENV.2022.161114.

[20] Simon-Philippe Breton and Geir Moe. "Status, plans and technologies for offshore wind turbines in Europe and North America". In: *Renewable Energy* 34.3 (Mar. 2009), pp. 646–654. ISSN: 0960-1481. DOI: 10.1016/J.RENENE.2008.05.040. URL: https://www.sciencedirect.com/science/article/pii/S0960148108002243#fig1.

[21] Daryl Burdon, Suzanne J. Boyes, Michael Elliott, Katie Smyth, Jonathan P. Atkins, Richard A. Barnes, and Rüdiger K. Wurzel. "Integrating natural and social sciences to manage sustainably vectors of change in the marine environment: Dogger Bank transnational case study". In: *Estuarine, Coastal and Shelf Science* 201 (Feb. 2018), pp. 234–247. ISSN: 02727714. DOI: 10.1016/j.ecss.2015.09.012.

[22] Ruth Callaway, Georg H. Engelhard, John Dann, John Cotter, and Heye Rumohr. “A century of North Sea epibenthos and trawling: Comparison between 1902-1912, 1982-1985 and 2000”. In: *Marine Ecology Progress Series* 346.August 2007 (2007), pp. 27–43. ISSN: 01718630. DOI: 10.3354/meps07038.

[23] Ingeborg Callesen, Hannes Keck, and Thorbjørn Joest Andersen. “Particle size distribution in soils and marine sediments by laser diffraction using Malvern Mastersizer 2000—method uncertainty including the effect of hydrogen peroxide pretreatment”. In: *Journal of Soils and Sediments* 18.7 (2018), pp. 2500–2510. ISSN: 16147480. DOI: 10.1007/s11368-018-1965-8.

[24] Elisa Capuzzo, Christopher P. Lynam, Jon Barry, David Stephens, Rodney M. Forster, Naomi Greenwood, Abigail McQuatters-Gollop, Tiago Silva, Sonja M. van Leeuwen, and Georg H. Engelhard. “A decline in primary production in the North Sea over 25 years, associated with reductions in zooplankton abundance and fish stock recruitment”. In: *Global Change Biology* 24.1 (Jan. 2018), e352–e364. ISSN: 1365-2486. DOI: 10.1111/GCB.13916. URL: https://onlinelibrary.wiley.com/doi/full/10.1111/gcb.13916.

[25] Elisa Capuzzo, David Stephens, Tiago Silva, Jon Barry, and Rodney M. Forster. “Decrease in water clarity of the southern and central North Sea during the 20th century”. In: *Global Change Biology* 21.6 (June 2015), pp. 2206–2214. ISSN: 1354-1013. DOI: 10.1111/gcb.12854. URL: https://onlinelibrary.wiley.com/doi/10.1111/gcb.12854.

[26] Jeffrey R. Carpenter, Lucas Merckelbach, Ulrich Callies, Suzanna Clark, Lidia Gaslikova, and Burkard Baschek. “Potential impacts of offshore wind farms on North Sea stratification”. In: *PLoS ONE* 11.8 (Aug. 2016). ISSN: 19326203. DOI: 10.1371/JOURNAL.PONE.0160830.

[27] C. Cheng. “Biogeomorphological aspects within tidal sand wave fields”. PhD thesis. Ghent University, 2021. URL: https://research.wur.nl/en/publications/biogeomorphological-aspects-within-tidal-sand-wave-fields-doctora.

[28] Chiu Hwa Cheng, Karline Soetaert, and Bas Wijnand Borsje. “Sediment characteristics over asymmetrical tidal sand waves in the Dutch north sea”. In: *Journal of Marine Science and Engineering* 8.6 (2020). ISSN: 20771312. DOI: 10.3390/JMSE8060409.

[29] A. Colina Alonso, D. S. van Maren, E. P.L. Elias, S. J. Holthuijsen, and Z. B. Wang. “The contribution of sand and mud to infilling of tidal basins in response to a closure dam”. In: *Marine Geology* 439 (Sept. 2021), p. 106544. ISSN: 0025-3227. DOI: 10.1016/J.MARGEO.2021.106544.

[30] Ana Colina Alonso, Dirk Sebastiaan van Maren, Albert Peter Oost, Peter Esselink, Robert Lepper, Frank Kösters, Jesper Bartholdy, Allert Imre Bijleveld, and Zheng Bing Wang. “A mud budget of the Wadden Sea and its implications for sediment management”. In: *Communications Earth & Environment 2024 5:1* 5.1 (Mar. 2024), pp. 1–9. ISSN: 2662-4435. DOI: 10.1038/s43247-024-01315-9. URL: https://www.nature.com/articles/s43247-024-01315-9.

[31] Irene Colosimo, Paul L.M. de Vet, Dirk S. van Maren, Ad J.H.M. Reniers, Johan C. Winterwerp, and Bram C. van Prooijen. "The impact of wind on flow and sediment transport over intertidal flats". In: *Journal of Marine Science and Engineering* 8.11 (2020), pp. 1–26. ISSN: 20771312. DOI: 10.3390/jmse8110910.

[32] Katherine Cronin and Meinte Blaas. *Maasvlakte 2 and fine sediment fluxes towards the Wadden Sea*. Tech. rep. Delft, The Netherlands: Deltares, 2015, p. 32.

[33] J.M. Damen, Thaiënne A G P van Dijk, and Suzanne J. M. H. Hulscher. "Spatially Varying Environmental Properties Controlling Observed SandWave Morphology". In: *Journal of Geophysical Research: Earth Surface* 123 (2018), pp. 983–1008. DOI: 10.1002/2014JF003418.Received. URL: https://doi.org/10.1002/2017JF004322.

[34] J. H. Damveld, K. J. van der Reijden, C. Cheng, L. Koop, L. R. Haaksma, C. A.J. Walsh, K. Soetaert, B. W. Borsje, L. L. Govers, P. C. Roos, H. Olff, and S. J.M.H. Hulscher. "Video Transects Reveal That Tidal Sand Waves Affect the Spatial Distribution of Benthic Organisms and Sand Ripples". In: *Geophysical Research Letters* 45.21 (Nov. 2018), pp. 837–11. ISSN: 1944-8007. DOI: 10.1029/2018GL079858. URL: https://onlinelibrary.wiley.com/doi/full/10.1029/2018GL079858.

[35] P.J.T. Dankers. *The intrusion of fine suspended sediment into a sandy sediment bed. A literature review*. Tech. rep. Delft, The Netherlands: Delft University of Technology, 2005, p. 41.

[36] Gerben J. de Boer, Julie D. Pietrzak, and Johan C. Winterwerp. "SST observations of upwelling induced by tidal straining in the Rhine ROFI". In: *Continental Shelf Research* 29.1 (2009), pp. 263–277. ISSN: 02784343. DOI: 10.1016/j.csr.2007.06.011.

[37] S.J. de Groot. "The impact of laying and maintenance of offshore pipelines on the marine environment and the North Sea fisheries". In: *Ocean Management* 8.1 (June 1982), pp. 1–27. ISSN: 0302-184X. DOI: 10.1016/0302-184X(82)90011-7.

[38] Maarten Fije de Jong. "The ecological effects of deep sand extraction on the Dutch continental shelf". PhD thesis. Wageningen University, 2016. ISBN: 9789462576834.

[39] J.M. de Kok. "A two-layer model of the Rhine plume". In: *Journal of Marine Systems* 8.3-4 (Sept. 1996), pp. 269–284. ISSN: 0924-7963. DOI: 10.1016/0924-7963(96)00010-3. URL: https://www.sciencedirect.com/science/article/pii/0924796396000103?via%3Dihub.

[40] Lynyrd de Wit, A. M. Talmon, and C. van Rhee. "3D CFD simulations of trailing suction hopper dredger plume mixing: A parameter study of near-field conditions influencing the suspended sediment source flux". In: *Marine Pollution Bulletin* 88.1-2 (Nov. 2014), pp. 47–61. ISSN: 0025-326X. DOI: 10.1016/J.MARPOLBUL.2014.08.043.

[41] Jeroen De Reu, Jean Bourgeois, Machteld Bats, Ann Zwertvaegher, Vanessa Gelorini, Philippe De Smedt, Wei Chu, Marc Antrop, Philippe De Maeyer, Peter Finke, Marc Van Meirvenne, Jacques Verniers, and Philippe Crombé. "Application of the topographic position index to heterogeneous landscapes". In: *Geomorphology* 186 (2013), pp. 39–49. DOI: 10.1016/j.geomorph.2012.12.015. URL: http://dx.doi.org/10.1016/j.geomorph.2012.12.015.

[42] S Degraer, V Van Lancker, T A G P Van Dijk, S N R Birchenough, B De Witte, M Elliott, S Le Bot, H Reiss, V Stelzenmüller, S Van Gaever, E Balian, D Cox, F Hernandez, G Lacroix, H Lindeboom, J Reubens, and K Soetaert. "Interdisciplinary science to support North Sea marine management: lessons learned and future demands". In: *Hydrobiologia* Special Is.NORTH SEA OPEN SCIENCE CONFERENCE (2019), pp. 1–11. ISSN: 1573-5117. DOI: 10.1007/s10750-019-04109-9. URL: https://doi.org/10.1007/s10750-019-04109-9.

[43] S. Degraer, E. Verfaillie, W. Willems, E. Adriaens, M. Vincx, and V. Van Lancker. "Habitat suitability modelling as a mapping tool for macrobenthic communities: An example from the Belgian part of the North Sea". In: *Continental Shelf Research* 28.3 (Feb. 2008), pp. 369–379. ISSN: 0278-4343. DOI: 10.1016/J.CSR.2007.09.001. URL: https://www.sciencedirect.com/science/article/pii/S0278434307002671.

[44] Robert M. Dorrell, Charlie J. Lloyd, Ben J. Lincoln, Tom P. Rippeth, John R. Taylor, Colm cille P. Caulfield, Jonathan Sharples, Jeff A. Polton, Brian D. Scannell, Deborah M. Greaves, Rob A. Hall, and John H. Simpson. "Anthropogenic Mixing in Seasonally Stratified Shelf Seas by Offshore Wind Farm Infrastructure". In: *Frontiers in Marine Science* 9 (Mar. 2022), p. 830927. ISSN: 22967745. DOI: 10.3389/FMARS.2022.830927/PDF. URL: www.frontiersin.org.

[45] D Eisma. "Composition, origin and distribution of Dutch coastal sands between Hoek van Holland and the island of Vlieland." English. PhD thesis. Rijksuniversiteit Groningen, 1968. URL: http://catalog.hathitrust.org/api/volumes/oclc/23627619.html.

[46] D Eisma. "Supply and Deposition of Suspended Matter in the North Sea". In: *Holocene Marine Sedimentation in the North Sea Basin*. Ed. by S-D Nio, R.T.E Shuttenhelm, and T.C.E. van Weering. Blackwell Publishing Ltd., 1981, pp. 415–428. ISBN: 9781444303759. DOI: 10.1002/9781444303759.ch29. URL: http://dx.doi.org/10.1002/9781444303759.ch29.

[47] D Eisma, R Johnston, and J I G Cadogan. "The North Sea: An Overview [and Discussion]". In: *Philosophical Transactions of the Royal Society of London. B, Biological Sciences* 316.1181 (Sept. 1987), 461 LP –485.

[48] Marieke A. Eleveld, Reinold Pasterkamp, Hendrik J. van der Woerd, and Julie D. Pietrzak. "Remotely sensed seasonality in the spatial distribution of sea-surface suspended particulate matter in the southern North Sea". In: *Estuarine, Coastal and Shelf Science* 80.1 (Oct. 2008), pp. 103–113. ISSN: 02727714. DOI: 10.1016/j.ecss.2008.07.015. URL: https://linkinghub.elsevier.com/retrieve/pii/S027277140800276X.

[49] Steve Elgar, Britt Raubenheimer, and R Guza. "Quality control of acoustic Doppler velocimeter data in the surfzone". In: *Measurement Science and Technology* 16 (Aug. 2005), p. 1889. DOI: 10.1088/0957-0233/16/10/002.

[50] Edwin P.L. Elias, Ad J.F. van der Spek, and Marian Lazar. "The 'Voordelta', the contiguous ebb-tidal deltas in the SW Netherlands: Large-scale morphological changes and sediment budget 1965-2013; Impacts of large-scale engineering". In: *Geologie en Mijnbouw/Netherlands Journal of Geosciences* 96.3 (2017), pp. 233–259. ISSN: 15739708. DOI: 10.1017/njg.2016.37.

[51] Kay Christian Emeis, Justus van Beusekom, Ulrich Callies, Ralf Ebinghaus, Andreas Kannen, Gerd Kraus, Ingrid Kröncke, Hermann Lenhart, Ina Lorkowski, Volker Matthias, Christian Möllmann, Johannes Pätsch, Mirco Scharfe, Helmuth Thomas, Ralf Weisse, and Eduardo Zorita. "The North Sea — A shelf sea in the Anthropocene". In: *Journal of Marine Systems* 141 (Jan. 2015), pp. 18–33. ISSN: 0924-7963. DOI: 10.1016/J.JMARSYS.2014.03.012. URL: https://www.sciencedirect.com/science/article/pii/S0924796314000724#f0005.

[52] Paul L.A. Erftemeijer, Bernhard Riegl, Bert W. Hoeksema, and Peter A. Todd. "Environmental impacts of dredging and other sediment disturbances on corals: A review". In: *Marine Pollution Bulletin* 64.9 (2012), pp. 1737–1765. ISSN: 0025326X. DOI: 10.1016/j.marpolbul.2012.05.008. URL: http://dx.doi.org/10.1016/j.marpolbul.2012.05.008.

[53] Karel Essink. "Ecological effects of dumping of dredged sediments; Options for management". In: *Volume 5, Issue 1, Pages 69 - 80* 5.1 (1999), pp. 69–80. ISSN: 14000350. DOI: 10.1007/BF02802741.

[54] P. Feldens, K. Schwarzer, D. Sakuna, W. Szczuciński, and P. Sompongchaiyakul. "Sediment distribution on the inner continental shelf off Khao Lak (Thailand) after the 2004 Indian Ocean tsunami". In: *Earth, Planets and Space* 64.10 (2012), pp. 875–887. ISSN: 18805981. DOI: 10.5047/eps.2011.09.001.

[55] R I Ferguson and M Church. "A Simple Universal Equation for Grain Settling Velocity". In: *Journal of Sedimentary Research* 74.6 (Nov. 2004), pp. 933–937. ISSN: 1527-1404. DOI: 10.1306/051204740933. URL: https://doi.org/10.1306/051204740933.

[56] Rocío Fernandez, Jim Best, and Fabián López. "Mean flow, turbulence structure, and bed form superimposition across the ripple-dune transition". In: *Water Resources Research* 42.5 (2006), pp. 1–17. ISSN: 00431397. DOI: 10.1029/2005WR004330.

[57] Michael Fettweis, Frederic Francken, Dries van den Eynde, Toon Verwaest, Job Janssens, and Vera van Lancker. "Storm influence on SPM concentrations in a coastal turbidity maximum area with high anthropogenic impact (southern North Sea)". In: *Continental Shelf Research* 30.13 (July 2010), pp. 1417–1427. ISSN: 0278-4343. DOI: 10.1016/J.CSR.2010.05.001.

[58] Michael Fettweis, Jean-Sébastien Houziaux, Isabelle Du Four, Vera Van Lancker, Cecile Baeteman, Mieke Mathys, Dries Van den Eynde, Frederic Francken, and Stanislas Wartel. “Long-term influence of maritime access works on the distribution of cohesive sediments: analysis of historical and recent data from the Belgian nearshore area (southern North Sea)”. In: *Geo-Marine Letters* 29.5 (2009), pp. 321–330. ISSN: 1432-1157. DOI: 10.1007/s00367-009-0161-7. URL: https://doi.org/10.1007/s00367-009-0161-7.

[59] Michael Fettweis, Jaak Monbaliu, Matthias Baeye, Bouchra Nechad, and Dries Van den Eynde. “Weather and climate induced spatial variability of surface suspended particulate matter concentration in the North Sea and the English Channel”. In: *Methods in Oceanography* 3-4.November (2012), pp. 25–39. ISSN: 22111220. DOI: 10.1016/j.mio.2012.11.001. URL: http://dx.doi.org/10.1016/j.mio.2012.11.001.

[60] Michael Fettweis, Bouchra Nechad, and Dries Van den Eynde. “An estimate of the suspended particulate matter (SPM) transport in the southern North Sea using SeaWiFS images, in situ measurements and numerical model results”. In: *Continental Shelf Research* 27.10-11 (June 2007), pp. 1568–1583. ISSN: 0278-4343. DOI: 10.1016/J.CSR.2007.01.017.

[61] Michael Fettweis, Rolf Riethmüller, Romaric Verney, Marius Becker, Joan Backers, Matthias Baeye, Marion Chapalain, Styn Claeys, Jan Claus, Tom Cox, Julien Deloffre, Davy Depreiter, Flavie Druine, Götz Flöser, Steffen Grünler, Frédéric Jourdin, Robert Lafite, Janine Nauw, Bouchra Nechad, Rüdiger Röttgers, Aldo Sottolichio, Tom van Engeland, Wim Vanhaverbeke, and Hans Vereecken. “Uncertainties associated with in situ high-frequency long-term observations of suspended particulate matter concentration using optical and acoustic sensors”. In: *Progress in Oceanography* 178.August (2019), p. 102162. ISSN: 00796611. DOI: 10.1016/j.pocean.2019.102162. URL: https://doi.org/10.1016/j.pocean.2019.102162.

[62] Michael Fettweis and Dries Van den Eynde. “The mud deposits and the high turbidity in the Belgian–Dutch coastal zone, southern bight of the North Sea”. In: *Continental Shelf Research* 23.7 (May 2003), pp. 669–691. DOI: 10.1016/S0278-4343(03)00027-X. URL: https://linkinghub.elsevier.com/retrieve/pii/S027843430300027X.

[63] Rebecca Fisher, Clair Stark, Peter Ridd, and Ross Jones. “Spatial patterns in water quality changes during dredging in tropical environments”. In: *PLoS ONE* 10.12 (2015), pp. 1–22. ISSN: 19326203. DOI: 10.1371/journal.pone.0143309.

[64] Jens Floeter, Justus E.E. van Beusekom, Dominik Auch, Ulrich Callies, Jeffrey Carpenter, Tim Dudeck, Sabine Eberle, André Eckhardt, Dominik Gloe, Kristin Hänselmann, Marc Hufnagl, Silke Janßen, Hermann Lenhart, Klas Ove Möller, Ryan P. North, Thomas Pohlmann, Rolf Riethmüller, Sabrina Schulz, Stefan Spreizenbarth, Axel Temming, Bettina Walter, Oliver Zielinski, and Christian Möllmann. “Pelagic effects of offshore wind farm foundations in the stratified North Sea”. In: *Progress in Oceanography* 156 (Aug. 2017), pp. 154–173. ISSN: 00796611. DOI: 10.1016/J.POCEAN.2017.07.003.

[65] Raúl P Flores, Sabine Rijnsburger, Alexander R. Horner-Devine, Alejandro J Souza, and Julie D Pietrzak. "The impact of storms and stratification on sediment transport in the Rhine region of freshwater influence". In: *Journal of Geophysical Research: Oceans* 122.5 (May 2017), pp. 4456–4477. ISSN: 2169-9275. DOI: 10.1002/2016JC012362. URL: https://agupubs.onlinelibrary.wiley.com/doi/10.1002/2016JC012362.

[66] Caroline Gautier and Sofia Caires. "Operational wave forecasts in the Southern North Sea". In: *E-Proceedings of the 36th IAHR World Congress*. The Hague, Netherlands, 2015, pp. 2–5.

[67] Joseph D Germano, Donald C Rhoads, Raymond M Valente, Drew a Carey, and Martin Solan. "The use of Sediment Profile Imaging (SPI) for environmental impact assessments and monitoring studies: lessons learned from the past four decades". In: *Oceanography and Marine Biology: An Annual Review* 49 (2011), pp. 235–298. ISSN: 0078-3218. DOI: 10.1201/b11009.

[68] H Gerritsen, J.G Boon, T van der Kaaij, and R.J Vos. "Integrated Modelling of Suspended Matter in the North Sea". In: *Estuarine, Coastal and Shelf Science* 53.4 (Oct. 2001), pp. 581–594. DOI: 10.1006/ecss.2000.0633.

[69] Derek Goring and Vladimir Nikora. "Despiking Acoustic Doppler Velocimeter Data". In: *Journal of Hydraulic Engineering-asce - J HYDRAUL ENG-ASCE* 128 (Jan. 2002). DOI: 10.1061/(ASCE)0733-9429(2002)128:1(117).

[70] Gerhard Graf and Rutger Rosenberg. "Bioresuspension and biodeposition: a review". In: *Journal of Marine Systems* 11.3-4 (June 1997), pp. 269–278. DOI: 10.1016/S0924-7963(96)00126-1. URL: https://linkinghub.elsevier.com/retrieve/pii/S0924796396001261.

[71] Bart Grasmeijer, Bas Huisman, Arjen Luijendijk, Reinier Schrijvershof, Jebbe van der Werf, Firmijn Zijl, Harry de Looff, and Wout de Vries. "Modelling of annual sand transports at the Dutch lower shoreface". In: *Ocean & Coastal Management* 217 (Feb. 2022), p. 105984. ISSN: 0964-5691. DOI: 10.1016/J.OCECOAMAN.2021.105984.

[72] Junke Guo. "Simple and explicit solution of wave dispersion equation". In: *Coastal Engineering* 45.2 (Apr. 2002), pp. 71–74. ISSN: 0378-3839. DOI: 10.1016/S0378-3839(02)00039-X.

[73] Laura Florentina Gușatu, Stefano Menegon, Daniel Depellegrin, Christian Zuidema, André Faaij, and Claudia Yamu. "Spatial and temporal analysis of cumulative environmental effects of offshore wind farms in the North Sea basin". In: *Scientific Reports 2021 11:1* 11.1 (May 2021), pp. 1–18. ISSN: 2045-2322. DOI: 10.1038/s41598-021-89537-1. URL: https://www.nature.com/articles/s41598-021-89537-1.

[74] W. D. Harrison, D. Musgrave, and W. S. Reeburgh. "A wave-induced transport process in marine sediments". In: *Journal of Geophysical Research* 88.C12 (1983), p. 7617. ISSN: 0148-0227. DOI: 10.1029/JC088iC12p07617. URL: http://doi.wiley.com/10.1029/JC088iC12p07617.

[75] C Heip, D Basford, J A Craeymeersch, J M Dewarumez, J Dörjes, P de Wilde, G Duineveld, A Eleftheriou, P M J Herman, U Niermann, P Kingston, A Künitzer, E Rachor, H Rumohr, K Soetaert, and T Soltwedel. "Trends in biomass, density and diversity of North Sea macrofauna". In: *ICES Journal of Marine Science* 49.1 (Feb. 1992), pp. 13–22. ISSN: 1054-3139. URL: http://dx.doi.org/10.1093/icesjms/49.1.13.

[76] E. Hendriks, B. C. van Prooijen, C. H. Cheng, S. G.J. Aarninkhof, J. C. Winterwerp, and K. E. Soetaert. "An explanatory model for the burial of fines in the sandy seabed of the southern North Sea". In: *Marine Geology* 454 (Dec. 2022), p. 106953. ISSN: 0025-3227. DOI: 10.1016/J.MARGEO.2022.106953.

[77] H.C.M. Hendriks and F.P. Schuurman. *Modellering alternatieve loswal locaties*. Tech. rep. Delft, The Netherlands: Deltares and RoyalHaskoning/DHV, 2017, p. 54.

[78] H.C.M. Hendriks, B.C. van Prooijen, S.G.J. Aarninkhof, and J.C. Winterwerp. "How human activities affect the fine sediment distribution in the Dutch Coastal Zone seabed". In: *Geomorphology* 367 (2020), p. 107314. ISSN: 0169555X. DOI: 10.1016/j.geomorph.2020.107314. URL: https://doi.org/10.1016/j.geomorph.2020.107314.

[79] Rik Houthuys, Alain Trentesaux, and Peter De Wolf. "Storm influences on a tidal sandbank's surface (Middelkerke Bank, southern North Sea)". In: *Marine Geology* 121 (1994), pp. 23–41.

[80] M. Huettel, W. Ziebis, and S. Forster. "Flow-induced uptake of particulate matter in permeable sediments". In: *Limnology and Oceanography* 41.2 (Mar. 1996), pp. 309–322. ISSN: 00243590. DOI: 10.4319/lo.1996.41.2.0309. URL: http://doi.wiley.com/10.4319/lo.1996.41.2.0309.

[81] Markus Huettel and Antje Rusch. "Transport and degradation of phytoplankton in permeable sediment". In: *Limnology and Oceanography* 45.3 (May 2000), pp. 534–549. DOI: 10.4319/lo.2000.45.3.0534. URL: https://aslopubs.onlinelibrary.wiley.com/doi/10.4319/lo.2000.45.3.0534.

[82] Suzanne J. M. H. Hulscher and G. Matthijs van den Brink. "Comparison between predicted and observed sand waves and sand banks in the North Sea". In: *Journal of Geophysical Research: Oceans* 106.C5 (May 2001), pp. 9327–9338. ISSN: 0148-0227. DOI: 10.1029/2001JC900003. URL: https://agupubs.onlinelibrary.wiley.com/doi/10.1029/2001JC900003.

[83] J D Hunter. "Matplotlib: A 2D Graphics Environment". In: *Computing in Science & Engineering* 9.3 (2007), pp. 90–95. ISSN: 1558-366X VO - 9. DOI: 10.1109/MCSE.2007.55.

[84] J Huthnance. "Physical oceanography of the North Sea". In: *Ocean and Shoreline Management* 16.3-4 (1991), pp. 199–231. DOI: 10.1016/0951-8312(91)90005-M. URL: http://www.sciencedirect.com/science/article/pii/095183129190005M%20https://linkinghub.elsevier.com/retrieve/pii/095183129190005M.

[85] Pat J. Iampietro, Rikk G. Kvitek, and Erica Morris. “Recent Advances in Automated Genus-specific Marine Habitat Mapping Enabled by High-resolution Multibeam Bathymetry”. In: *Marine Technology Society Journal* 39 (2005), pp. 83–93.

[86] Georg Irion and Volker Zollmer. “Clay mineral associations in fine-grained surface sediments of the North Sea”. In: *Journal of Sea Research* 41.1-2 (1999), pp. 119–128. URL: http://www.sciencedirect.com/science/article/B6VHH-3VX90DP-B/2/e24e1a3f54421a9aec6a10c342aec6f9.

[87] MI Jennes and G.C.A. Duineveld. “Effects of tidal currents on chlorophyll a content of sandy sediments in the southern North Sea”. In: *Marine Ecology Progress Series* 21 (1985), pp. 283–287. DOI: 10.3354/meps021283. URL: http://scholar.google.com/scholar?hl=en&btnG=Search&q=intitle:Effects+of+tidal+currents+on+chlorophyll+a+content+of+sandy+sediments+in+the+southern+North+Sea#0%20http://www.int-res.com/articles/meps/21/m021p283.pdf.

[88] Ross Jones, Rebecca Fisher, Clair Stark, and Peter Ridd. “Temporal patterns in seawater quality from dredging in tropical environments”. In: *PLoS ONE* 10.10 (2015), pp. 1–25. ISSN: 19326203. DOI: 10.1371/journal.pone.0137112.

[89] L. Kamp-Nielsen, J. E. Vermaat, I. Wesseling, J. Borum, and O. Geertz-Hansen. “Sediment properties along gradients of siltation in south-east Asia”. In: *Estuarine, Coastal and Shelf Science* 54.1 (2002), pp. 127–137. ISSN: 02727714. DOI: 10.1006/ecss.2001.0822.

[90] Ioannis Karakassis, Manolis Tsapakis, Christopher J. Smith, and Heye Rumohr. “Fish farming impacts in the Mediterranean studied through sediment profiling imagery”. In: *Marine Ecology Progress Series* 227 (2002), pp. 125–133. ISSN: 01718630. DOI: 10.3354/meps227125.

[91] Chang S. Kim and Hak-Soo Lim. “Sediment dispersal and deposition due to sand mining in the coastal waters of Korea”. In: *Continental Shelf Research* 29.1 (Jan. 2009), pp. 194–204. ISSN: 0278-4343. DOI: 10.1016/J.CSR.2008.01.017. URL: https://www.sciencedirect.com/science/article/pii/S0278434308000320#fig6.

[92] R R Kirby, Gregory Beaugrand, J A Lindley, A J Richardson, M Edwards, and P C Reid. “Climate effects and benthic-pelagic coupling in the North Sea. Climate effects and benthic-pelagic coupling in the”. In: *Mar Ecol Prog Ser* 330 (2007), pp. 31–38. URL: www.int-res.com.

[93] John T. O. Kirk. *Light and photosynthesis in aquatic ecosystems*. Cambridge: Cambridge University Press, 1994. ISBN: 9780511623370. DOI: 10.1017/CBO9780511623370. URL: http://ebooks.cambridge.org/ref/id/CBO9780511623370.

[94] M G Kleinhans. “Phase diagrams of bed states in steady, unsteady, oscillatory and mixed flows”. In: *EU SANDPIT*. Ed. by Leo C. van Rijn, Richard L Soulsby, Piet Hoekstra, and Alan G. Davies. Utrecht, The Netherlands, 2005. Chap. Paper Q, Q1–Q16.

[95] M.G. Kleinhans, O Montfort, P J T Dankers, L C Van Rijn, and W Bonne. “Mud dynamics on the shoreface and upper shelf, {Noordwijk, The Netherlands}”. In: *Sandpit project* 5.October (2005), Q1–Q16.

[96] Maarten G. Kleinhans and Bart T. Grasmeijer. “Bed load transport on the shoreface by currents and waves”. In: *Coastal Engineering* 53.12 (Dec. 2006), pp. 983–996. ISSN: 03783839. DOI: 10.1016/J.COASTALENG.2006.06.009. URL: http://www.coastalresearch.nl.

[97] Leo Koop, Karin J. van der Reijden, Sebastiaan Mestdagh, Tom Ysebaert, Laura L. Govers, Han Olff, Peter M.J. Herman, Mirjam Snellen, and Dick G. Simons. “Measuring Centimeter-Scale Sand Ripples Using Multibeam Echosounder Backscatter Data from the Brown Bank Area of the Dutch Continental Shelf”. In: *Geosciences 2020, Vol. 10, Page 495* 10.12 (Dec. 2020), p. 495. ISSN: 2076-3263. DOI: 10.3390/GEOSCIENCES10120495. URL: https://www.mdpi.com/2076-3263/10/12/495/htm%20https://www.mdpi.com/2076-3263/10/12/495.

[98] Erik Kristensen, Gil Penha-Lopes, Matthieu Delefosse, Thomas Valdemarsen, Cintia O. Quintana, and Gary T. Banta. “What is bioturbation? The need for a precise definition for fauna in aquatic sciences”. In: *Marine Ecology Progress Series* 446 (Feb. 2012), pp. 285–302. ISSN: 0171-8630. DOI: 10.3354/MEPS09506. URL: https://www.int-res.com/abstracts/meps/v446/p285-302/.

[99] R. W P M Laane, H. L A Sonneveldt, A. J. Van Der Weyden, J. P G Loch, and G. Groeneveld. “Trends in the spatial and temporal distribution of metals (Cd, Cu, Zn and Pb) and organic compounds (PCBs and PAHs) in Dutch coastal zone sediments from 1981 to 1996: A model case study for Cd and PCBs”. In: *Journal of Sea Research* 41.1-2 (1999), pp. 1–17. DOI: 10.1016/S1385-1101(98)00038-0.

[100] P. Le Hir, Y. Monbet, and F. Orvain. “Sediment erodability in sediment transport modelling: Can we account for biota effects?” In: *Continental Shelf Research* 27.8 (May 2007), pp. 1116–1142. ISSN: 02784343. DOI: 10.1016/j.csr.2005.11.016. URL: https://linkinghub.elsevier.com/retrieve/pii/S0278434307000076.

[101] Pascal Lecroart, Sabine Schmidt, Pierre Anschutz, and Jean Marie Jouanneau. “Modeling sensitivity of biodiffusion coefficient to seasonal bioturbation”. In: *Journal of Marine Research* 65.3 (2007), pp. 417–440. ISSN: 00222402. DOI: 10.1357/002224007781567630.

[102] L. Leewis, L.M. van Son, and L. Lubos. *Zand uit Zee chronosequentie: Rapportage Boxcore-campagne*. Tech. rep. Amsterdam, The Netherlands: Eurofins AquaSense, 2024, p. 127. URL: https://zanduitzee.nl/bibliotheek/@296149/leewis-son-lubos-2024-chronosequentie-rapportage/.

[103] Michael Z. Li and Carl L. Amos. “Field observations of bedforms and sediment transport thresholds of fine sand under combined waves and currents”. In: *Marine Geology* 158.1-4 (1999), pp. 147–160. ISSN: 00253227. DOI: 10.1016/S0025-3227(98)00166-2.

[104] Ian D. Lichtman, Jaco H. Baas, Laurent O. Amoudry, Peter D. Thorne, Jonathan Malarkey, Julie A. Hope, Jeffrey Peakall, David M. Paterson, Sarah J. Bass, Richard D. Cooke, Andrew J. Manning, Alan G. Davies, Daniel R. Parsons, and Leiping Ye. "Bedform migration in a mixed sand and cohesive clay intertidal environment and implications for bed material transport predictions". In: *Geomorphology* 315 (2018), pp. 17–32. ISSN: 0169555X. DOI: 10.1016/j.geomorph.2018.04.016. URL: https://doi.org/10.1016/j.geomorph.2018.04.016.

[105] Ole Secher Madsen, Ying-Keung Poon, and Hans Graber. "Spectral Wave Attenuation by Bottom Friction: Theory". In: *Coastal Engineering 1988*. Proceedings. Dec. 1988, pp. 492–504. ISBN: 9780872626874. DOI: doi:10.1061/9780872626874.035. URL: https://doi.org/10.1061/9780872626874.035.

[106] S. Marmin, J. C. Dauvin, and P. Lesueur. "Collaborative approach for the management of harbour-dredged sediment in the Bay of Seine (France)". In: *Ocean and Coastal Management* 102.PA (2014), pp. 328–339. ISSN: 09645691. DOI: 10.1016/j.ocecoaman.2014.10.012. URL: http://dx.doi.org/10.1016/j.ocecoaman.2014.10.012.

[107] K. V. Marten. "Field Observation and Modelling of Near-shore Sediment Transport Processes". PhD thesis. Bangor University, UK, 2010.

[108] A. J. Martin. "Flaser and wavy bedding in ephemeral streams: A modern and an ancient example". In: *Sedimentary Geology* 136.1-2 (2000), pp. 1–5. ISSN: 00370738. DOI: 10.1016/S0037-0738(00)00085-3.

[109] A W Martinius and J H van den Berg. *Atlas of sedimentary structures in estuarine and tidally-influenced river deposits of the Rhine-Meuse-Scheldt system: their application to the interpretation of analogous outcrop and subsurface depositional systems*. English. Ed. by Robert T. Buller. 1st. Houten, the Netherlands: EAGE Publications BV, 2011, p. 298. ISBN: 9789073834118.

[110] R.R. McCandliss, S.E. Jones, M. Hearn, R. Latter, and C.F. Jago. "Dynamics of suspended particles in coastal waters (southern North Sea) during a spring bloom". In: *Journal of Sea Research* 47.3-4 (2002), pp. 285–302. ISSN: 13851101. DOI: 10.1016/S1385-1101(02)00123-5.

[111] I. N. McCave, R. J. Bryant, H. F. Cook, and C. A. Coughanowr. "Evaluation of a laser-diffraction-size analyzer for use with natural sediments". In: *Journal of Sedimentary Research* 56.4 (July 1986), pp. 561–564. ISSN: 1527-1404. DOI: 10.1306/212F89CC-2B24-11D7-8648000102C1865D.

[112] Patrick McLaren and Richard Powys. *Sediment transport pathways in the Eems estuary*. Tech. rep. Cambridge, UK: GeoSea Consulting Ltd., 1991, p. 82.

[113] S. R. McLean, J. M. Nelson, and S. R. Wolfe. "Turbulence structure over two-dimensional bed forms: Implications for sediment transport". In: *Journal of Geophysical Research: Oceans* 99.C6 (June 1994), pp. 12729–12747. ISSN: 0148-0227. DOI: 10.1029/94JC00571. URL: http://doi.wiley.com/10.1029/94JC00571%20https://agupubs.onlinelibrary.wiley.com/doi/10.1029/94JC00571.

[114] Julia P. McManus and David Prandle. “Development of a model to reproduce observed suspended sediment distributions in the southern North Sea using Principal Component Analysis and Multiple Linear Regression”. In: *Continental Shelf Research* 17.7 (June 1997), pp. 761–778. ISSN: 0278-4343. DOI: 10.1016/S0278-4343(96)00057-X. URL: https://www.sciencedirect.com/science/article/pii/S027843439600057X.

[115] Saulo Meirelles, Martijn Henriquez, Alejandro J. Souza, Alexander R. Horner-Devine, Julie D. Pietrzak, Sabine Rijnsburg, and Marcel J.F. Stive. “Small Scale Bedform Types off the South-Holland Coast”. In: *Journal of Coastal Research* 1.75 (Mar. 2016), pp. 423–426. ISSN: 15515036. DOI: 10.2112/SI75-085.1/29687/SMALL-SCALE-BEDFORM-TYPES-OFF-THE-SOUTH-HOLLAND.

[116] Jack J. Middelburg, Karline Soetaert, and Peter M.J. Herman. “Empirical relationships for use in global diagenetic models”. In: *Deep Sea Research Part I: Oceanographic Research Papers* 44.2 (Feb. 1997), pp. 327–344. ISSN: 0967-0637. DOI: 10.1016/S0967-0637(96)00101-X.

[117] Maynard Nichols, Robert J. Diaz, and Linda C. Schaffner. “Effects of hopper dredging and sediment dispersion, chesapeake bay”. In: *Environmental Geology and Water Sciences* 15.1 (Jan. 1990), pp. 31–43. ISSN: 0099-0094. DOI: 10.1007/BF01704879. URL: http://link.springer.com/10.1007/BF01704879.

[118] NLHO and Deltares. *Netherlands Hydrographic Office bathymetric data*. 2019.

[119] North Sea Energy Cooperation. *Joint Statement on the North Seas Energy Cooperation – 12 Sept 2022*. Tech. rep. December 2021. Dublin, Ireland: North Sea Energy Cooperation, 2022, pp. 1–6. URL: https://circabc.europa.eu/ui/group/9198696f-e42c-4a88-b4f1-7a1788eb9b7c/library/082173b4-8d19-4c4b-aaa4-7612daf879c0/details.

[120] OFL. *The North Sea Agreement*. Tech. rep. The Hague, The Netherlands: Overlegorgaan Fysieke Leefomgeving, 2020, p. 52. DOI: 10.1093/nq/s12-xii.249.52f.

[121] OSPAR. *OSPAR Quality Status Report: Synthesis Report. 10. Regional Summaries: Pressures and Biodiversity at the Level of the OSPAR Regions*. 2023. URL: https://oap.ospar.org/en/ospar-assessments/quality-status-reports/qsr-2023/synthesis-report/regional-summaries/.

[122] L. Otto, J.T.F. Zimmerman, G.K. Furnes, M. Mork, R. Saetre, and G. Becker. “Review of the physical oceanography of the North Sea”. In: *Netherlands Journal of Sea Research* 26.2-4 (Nov. 1990), pp. 161–238. ISSN: 0077-7579. DOI: 10.1016/0077-7579(90)90091-T. URL: https://www.sciencedirect.com/science/article/pii/007775799090091T.

[123] S Passchier and M G Kleinhans. “Observations of sand waves, megaripples, and hummocks in the Dutch coastal area and their relation to currents and combined flow conditions”. In: *Journal of Geophysical Research: Earth Surface* 110.F4 (Dec. 2005). ISSN: 01480227. DOI: 10.1029/2004JF000215. URL: http://doi.wiley.com/10.1029/2004JF000215.

[124] R.S. Piekhaar and M.W. Kort. *Haringvliet monding – Sedimentatieonderzoek 1970–1981*. Tech. rep. The Hague, Netherlands: Rijkswaterstaat Deltadienst, 1983.

[125] Gerjan Piet, Fiona Culhane, Ruud Jongbloed, Leonie Robinson, Bob Rumes, and Jacqueline Tamis. "An integrated risk-based assessment of the North Sea to guide ecosystem-based management". In: *Science of The Total Environment* 654 (Mar. 2019), pp. 694–704. ISSN: 0048-9697. DOI: 10.1016/J.SCITOTENV.2018.11.001. URL: https://www.sciencedirect.com/science/article/pii/S004896971834347X.

[126] Julie D. Pietrzak, Gerben J. de Boer, and Marieke A. Eleveld. "Mechanisms controlling the intra-annual mesoscale variability of SST and SPM in the southern North Sea". In: *Continental Shelf Research* 31.6 (Apr. 2011), pp. 594–610. ISSN: 0278-4343. DOI: 10.1016/J.CSR.2010.12.014.

[127] Pieter Provoost, Ulrike Braeckman, Dirk Van Gansbeke, Leon Moodley, Karline Soetaert, Jack J. Middelburg, and Jan Vanaverbeke. "Modelling benthic oxygen consumption and benthic-pelagic coupling at a shallow station in the southern North Sea". In: *Estuarine, Coastal and Shelf Science* 120 (Mar. 2013), pp. 1–11. ISSN: 0272-7714. DOI: 10.1016/J.ECSS.2013.01.008.

[128] Denise J Reed, Ann C Hijuelos, and Sarah M Fearnley. "Ecological Aspects of Coastal Sediment Management in the Gulf of Mexico". In: *Journal of Coastal Research* (May 2012), pp. 51–65. ISSN: 0749-0208. DOI: 10.2112/SI{_}60{_}6. URL: http://www.jcronline.org/doi/abs/10.2112/SI_60_6.

[129] H.E. Reineck and F. Wunderlich. "Classification and Origin of Flaser and Lenticular Bedding". In: *Sedimentology* 11.1-2 (1968), pp. 99–104. ISSN: 13653091. DOI: 10.1111/j.1365-3091.1968.tb00843.x.

[130] Hans-Erich Reineck and Indra B Singh. *Depositional sedimentary environments with reference to terrigenous clastics*. English. 2nd. Heidelberg, Germany: Springer Berlin, 1980, p. 551. ISBN: 9783540101895. URL: https://doi.org/10.1007/978-3-642-81498-3.

[131] DC Rhoads and JD Germano. "Characterization of Organism-Sediment Relations Using Sediment Profile Imaging: An Efficient Method of Remote Ecological Monitoring of the Seafloor (Remots™ System)". In: *Marine Ecology Progress Series* 8 (1982), pp. 115–128. ISSN: 0171-8630. DOI: 10.3354/meps008115. URL: papers2://publication/uuid/BC2F905F-9B3B-4B37-9084-16C3FD977064%20http://www.int-res.com/articles/meps/8/m008p115.pdf.

[132] Rijkswaterstaat. *Economic activities on Netherlands Continental Shelf*. 2019.

[133] Sabine Rijnsburger, Carola M. van der Hout, Onno van Tongeren, Gerben J. de Boer, Bram C. van Prooijen, Wil G. Borst, and Julie D. Pietrzak. "Simultaneous measurements of tidal straining and advection at two parallel transects far downstream in the Rhine ROFI". In: *Ocean Dynamics* 66.5 (2016), pp. 719–736. ISSN: 16167228. DOI: 10.1007/s10236-016-0947-x. URL: http://dx.doi.org/10.1007/s10236-016-0947-x.

[134] Adriaan Rijnsdorp, Jan Jaap Poos, Floor J. Quirijns, Reinier HilleRisLambers, Jan W. De Wilde, and Willem M. Den Heijer. “The arms race between fishers”. In: *Journal of Sea Research* 60.1-2 (Jan. 2008), pp. 126–138. ISSN: 1385-1101. DOI: 10.1016/J.SEARES.2008.03.003. URL: https://www.sciencedirect.com/science/article/pii/S1385110108000178.

[135] James R. Robbins, Phil J. Bouchet, David L. Miller, Peter G.H. Evans, James Waggitt, Alex T. Ford, and Sarah A. Marley. “Shipping in the north-east Atlantic: Identifying spatial and temporal patterns of change”. In: *Marine Pollution Bulletin* 179.December 2021 (2022), p. 113681. ISSN: 18793363. DOI: 10.1016/j.marpolbul.2022.113681. URL: https://doi.org/10.1016/j.marpolbul.2022.113681.

[136] A. Romero-Ramirez, A. Grémare, M. Desmalades, and J. C. Duchêne. “Semi-automatic analysis and interpretation of sediment profile images”. In: *Environmental Modelling and Software* 47 (2013), pp. 42–54. ISSN: 13648152. DOI: 10.1016/j.envsoft.2013.04.008. URL: http://dx.doi.org/10.1016/j.envsoft.2013.04.008.

[137] Sally Rouse, Andronikos Kafas, Rui Catarino, and Hayes Peter. “Commercial fisheries interactions with oil and gas pipelines in the North Sea: considerations for decommissioning”. In: *ICES Journal of Marine Science* 75.1 (July 2017), pp. 279–286. ISSN: 1054-3139. DOI: 10.1093/icesjms/fsx121. URL: https://doi.org/10.1093/icesjms/fsx121.

[138] R M Salden. *Een model voor het transport van slib in de Nederlandse kustzone. Een hulpmiddel bij scenario studies naar kustuitbreidingsplannen*. Tech. rep. Working kdocument RIKZ/OS-98.119X. RIKZ, 1998.

[139] W Salomons and W D Eysink. “Pathways of mud and particulate trace metals from rivers to the southern North Sea”. In: *Holocene marine sedimentation in the North Sea Basin*. Vol. 5. Blackwell, Oxford, 1981, pp. 429–450.

[140] Felipe Sanchez, Björn Nykvist, Olle Olsson, and Linus Linde. “Lessons from oil and gas transitions in the North Sea”. In: (2023). DOI: 10.51414/SEI2023.041. URL: https://www.sei.org/publications/lessons-oil-gas-transitions-north-sea/.

[141] Lawrence P. Sanford. “Modeling a dynamically varying mixed sediment bed with erosion, deposition, bioturbation, consolidation, and armoring”. In: *Computers and Geosciences* 34.10 (2008), pp. 1263–1283. ISSN: 00983004. DOI: 10.1016/j.cageo.2008.02.011.

[142] Anneliese K Schmidt. “The effect of storms on fine sediment dynamics in the Dutch Coastal Zone”. PhD thesis. Delft University of Technology, 2021.

[143] Reinier Schrijvershof, Laura Brakenhoff, and Bart Grasmeijer. *Hydrodynamics and bedforms on the Dutch lower shoreface*. Tech. rep. Delft, The Netherlands: Deltares, 2019, p. 58.

[144] J.H. Simpson. “Physical processes in the ROFI regime”. In: *Journal of Marine Systems* 12.1-4 (Aug. 1997), pp. 3–15. ISSN: 0924-7963. DOI: 10.1016/S0924-7963(96)00085-1. URL: https://www.sciencedirect.com/science/article/pii/S0924796396000851.

[145] John H. Simpson, Wim G. Bos, Florian Schirmer, Alejandro J. Souza, Thomas P Rippeth, Sarah E Jones, and David Hydes. “Periodic stratification in the Rhine ROFI in the North Sea”. In: *Oceanologica Acta* 16.1 (1993), pp. 23–32. URL: http://archimer.ifremer.fr/doc/00099/21050/.

[146] R. L. Soulsby, R. J.S. Whitehouse, and K. V. Marten. “Prediction of time-evolving sand ripples in shelf seas”. In: *Continental Shelf Research* 38 (2012), pp. 47–62. ISSN: 02784343. DOI: 10.1016/j.csr.2012.02.016. URL: http://dx.doi.org/10.1016/j.csr.2012.02.016.

[147] R.L. Soulsby and S. Clarke. *Bed Shear-stresses Under Combined Waves and Currents on Smooth and Rough Beds*. Tech. rep. Wallingford, UK: HR Wallingford, 2005, p. 55.

[148] Richard Soulsby. *Dynamics of marine sands : a manual for practical applications*. English. London: Thomas Telford, 1997. ISBN: 9780727725844.

[149] A.J. Souza and J.H. Simpson. “The modification of tidal ellipses by stratification in the Rhine ROFI”. In: *Continental Shelf Research* 16.8 (July 1996), pp. 997–1007. ISSN: 0278-4343. DOI: 10.1016/0278-4343(95)00042-9. URL: https://www.sciencedirect.com/science/article/pii/0278434395000429?via%3Dihub.

[150] J.R. Spearman, A. De Heer, S.G.J. Aarninkhof, and M. Van Koningsveld. “Validation of the TASS system for predicting the environmental effects of trailing suction hopper dredgers”. 2011. URL: https://repository.tudelft.nl/islandora/object/uuid:6f32ee7a-a54c-4286-995d-53126e5e2323?collection=research.

[151] Emil Vassilev Stanev, Mikhail Dobrynin, Andrey Pleskachevsky, Sebastian Grayek, and Heinz Günther. “Bed shear stress in the southern North Sea as an important driver for suspended sediment dynamics”. In: *Ocean Dynamics* 59.2 (2009), pp. 183–194. ISSN: 1616-7228. DOI: 10.1007/s10236-008-0171-4. URL: http://dx.doi.org/10.1007/s10236-008-0171-4.

[152] Nathalie A. Steins, Jeroen A. Veraart, Judith E.M. Klostermann, and Marnix Poelman. “Combining offshore wind farms, nature conservation and seafood: Lessons from a Dutch community of practice”. In: *Marine Policy* 126 (Apr. 2021), p. 104371. ISSN: 0308-597X. DOI: 10.1016/J.MARPOL.2020.104371.

[153] David Stephens and Markus Diesing. “Towards quantitative spatial models of seabed sediment composition”. In: *PLoS ONE* 10.11 (2015), pp. 1–23. ISSN: 19326203. DOI: 10.1371/journal.pone.0142502.

[154] Ad Stolk and Chris Dijkshoorn. “Sand extraction Maasvlakte 2 Project: License , Environmental Impact Assessment and Monitoring”. In: *European Marine Sand and Gravel Group - a wave of opportunities for the marine aggregates industry, EMSAGG Conference, 7-8 May 2009* May (2009), pp. 7–8.

[155] J M Suijlen and R N M Duin. *Variability of near-surface total suspended matter concentrations in the Dutch coastal zone of the North Sea*. Tech. rep. December. The Hague, The Netherlands: National Institute for Coastal, Marine Management/RIKZ Directorate General of Public Works, and Water Management, 2001, p. 86. URL: http://resolver.tudelft.nl/uuid:af202f38-7574-4913-9036-ab5b12496ff0.

[156] Andrew B. Sutherland and Judy L. Meyer. "Effects of increased suspended sediment on growth rate and gill condition of two southern Appalachian minnows". In: *Environmental Biology of Fishes* 80.4 (2007), pp. 389–403. ISSN: 03781909. DOI: 10.1007/s10641-006-9139-8.

[157] D.H. Swart. "Offshore Sediment Transport and Equilibrium Beach Profiles." PhD thesis. Delft University of Technology, 1974, p. 302.

[158] Hitoshi Tanaka and To Van Dang. "Geometry of Sand Ripples due to Combined Wave-Current Flows". In: *Journal of Waterway, Port, Coastal, and Ocean Engineering* 122.6 (Nov. 1996), pp. 298–3000. DOI: 10.1061/(ASCE)0733-950X(1996)122:6(298). URL: https://doi.org/10.1061/(ASCE)0733-950X(1996)122:6(298).

[159] J H J Terwindt and H.N.C. Breusers. "Experiments on the Origin of Flaser, Lenticular and Sand-Clay Alternating Bedding". In: *Sedimentology* 19.1-2 (1972), pp. 85–98. ISSN: 13653091. DOI: 10.1111/j.1365-3091.1972.tb00237.x.

[160] Duc Tran and Kyle Strom. "Floc sizes and resuspension rates from fresh deposits: Influences of suspended sediment concentration, turbulence, and deposition time". In: *Estuarine, Coastal and Shelf Science* 229 (Nov. 2019), p. 106397. ISSN: 0272-7714. DOI: 10.1016/J.ECSS.2019.106397.

[161] Peter Traykovski. "Observations of wave orbital scale ripples and a nonequilibrium time-dependent model". In: *Journal of Geophysical Research: Oceans* 112.6 (2007), pp. 1–19. ISSN: 21699291. DOI: 10.1029/2006JC003811.

[162] Nieves G. Valiente, Gerd Masselink, Tim Scott, Daniel Conley, and Robert Jak McCarroll. "Role of waves and tides on depth of closure and potential for headland bypassing". In: *Marine Geology* 407 (Jan. 2019), pp. 60–75. ISSN: 0025-3227. DOI: 10.1016/J.MARGEO.2018.10.009. URL: https://www.sciencedirect.com/science/article/pii/S0025322718302342#!.

[163] J. S. L. J. van Alphen. *Slibvoorkomens landwaarts 10m lijn tussen Terheijde en Noordwijk*. Tech. rep. Rijswijk, The Netherlands: Rijkswaterstaat, Directie Noordzee, 1987, pp. 1–17.

[164] J. S. L. J. van Alphen. *Slibvoorkomens op het Nederlands en Belgisch deel van het Continentaal Plat*. Tech. rep. Rijswijk, The Netherlands: Rijkswaterstaat, Directie Noordzee, 1987, pp. 1–19.

[165] J.S.L.J. van Alphen. "A mud balance for Belgian-Dutch coastal waters between 1969 and 1986". In: *Netherlands Journal of Sea Research* 25.1-2 (May 1990), pp. 19–30. DOI: 10.1016/0077-7579(90)90005-2. URL: https://linkinghub.elsevier.com/retrieve/pii/0077757990900052.

[166] Elisabeth H S van Duin, Gerard Blom, F Johannes Los, Robert Maffione, Richard Zimmerman, Carl F Cerco, Mark Dortch, and Elly P H Best. "Modeling underwater light climate in relation to sedimentation, resuspension, water quality and autotrophic growth". In: *Hydrobiologia* 444.1 (2001), pp. 25–42. ISSN: 1573-5117. DOI: 10.1023/A:1017512614680. URL: http://dx.doi.org/10.1023/A:1017512614680.

[167] W. van Gerwen, B. W. Borsje, J. H. Damveld, and S. J.M.H. Hulscher. "Modelling the effect of suspended load transport and tidal asymmetry on the equilibrium tidal sand wave height". In: *Coastal Engineering* 136.January (2018), pp. 56–64. ISSN: 03783839. DOI: 10.1016/j.coastaleng.2018.01.006. URL: https://doi.org/10.1016/j.coastaleng.2018.01.006.

[168] Sytze van Heteren. *Analyse van slibdikte in de monding van het Haringvliet*. Tech. rep. Utrecht, The Netherlands: Netherlands Insitute of Applied Geoscience TNO – National Geological Survey, 2002, p. 15.

[169] Gert van Hoey, Steven Degraer, and Magda Vincx. "Macrobenthic community structure of soft-bottom sediments at the Belgian Continental Shelf". In: *Estuarine, Coastal and Shelf Science* 59.4 (Apr. 2004), pp. 599–613. ISSN: 0272-7714. DOI: 10.1016/J.ECSS.2003.11.005. URL: https://www.sciencedirect.com/science/article/pii/S0272771403003238#FIG7.

[170] T van Kessel and J Vanlede. *Impact of harbour basins on mud dynamics Scheldt estuary*. Tech. rep. Delft and Antwerp: Deltares and Flanders Hydraulics, 2009, p. 29.

[171] Thijs van Kessel, Aukje Spruyt-de Boer, Jebbe van der Werf, Lucca Sittoni, Bram van Prooijen, and Han Winterwerp. "Bed module for sand-mud mixtures". In: (2012), p. 129.

[172] Thijs van Kessel, Han Winterwerp, Bram Van Prooijen, Mathijs Van Ledden, and Wil Borst. "Modelling the seasonal dynamics of SPM with a simple algorithm for the buffering of fines in a sandy seabed". In: *Continental Shelf Research* 31.10 SUPPL. (2011). DOI: 10.1016/j.csr.2010.04.008.

[173] Mathijs van Ledden, Zheng-Bing Wang, Han Winterwerp, and Huib de Vriend. "Sand-mud morphodynamics in a short tidal basin". In: *Ocean Dynamics* 54.3-4 (July 2004), pp. 385–391. ISSN: 1616-7341. DOI: 10.1007/s10236-003-0050-y. URL: http://link.springer.com/10.1007/s10236-003-0050-y.

[174] Mathijs van Ledden and Han Winterwerp. *A simple 1DV model to assess the effect of water-bed exchange processes on the dispersion of fines in the North Sea released during sand mining*. Tech. rep. Royal Haskoning, 2005, pp. 1–10.

[175] D. S. van Maren, T. van Kessel, K. Cronin, and L. Sittoni. "The impact of channel deepening and dredging on estuarine sediment concentration". In: *Continental Shelf Research* 95 (Mar. 2015), pp. 1–14. ISSN: 0278-4343. DOI: 10.1016/J.CSR.2014.12.010.

[176] D. S. van Maren, J. Vroom, M. Fettweis, and J. Vanlede. “Formation of the Zeebrugge coastal turbidity maximum: The role of uncertainty in near-bed exchange processes”. In: *Marine Geology* 425.March (2020), p. 106186. ISSN: 00253227. DOI: 10.1016/j.margeo.2020.106186. URL: https://doi.org/10.1016/j.margeo.2020.106186.

[177] Dagmar van Nieuwpoort, Ingeborg van Splunder, Marije Siemensma, Martine Graafland, Maarten Platteeuw, Jos de Visser, Niels Kinneging, Aylin Erkman, Edwin Verduin, Marije Wassink, and Kees Borst. *Meerjarenprogramma Wozep 2024-2030*. Tech. rep. Rijswijk, The Netherlands, 2023.

[178] B van Prooijen, T van Kessel, and M van Ledden. “Modelling of fine sediment in a sandy environment-the coastal zone of the Netherlands”. In: *Proceedings of the Congress: International Association for Hydraulic Research*. Vol. 32. 2. Venice, Italy, 2007, p. 722.

[179] Wim van Raaphorst and Johannes F.P. Malschaert. “Ammonium adsorption in superficial North Sea sediments”. In: *Continental Shelf Research* 16.11 (1996), pp. 1415–1435.

[180] L.C. van Rijn. “Unified View of Sediment Transport by Currents and Waves. I: Initiation of Motion, Bed Roughness, and Bed-Load Transport”. In: *Journal of Hydraulic Engineering* 133.6 (June 2007), pp. 649–667. DOI: 10.1061/(ASCE)0733-9429(2007)133:6(649). URL: https://doi.org/10.1061/(ASCE)0733-9429(2007)133:6(649).

[181] Leo C. van Rijn. “Sediment Transport, Part I: Bed Load Transport”. In: *Journal of Hydraulic Engineering* 110.10 (Oct. 1984), pp. 1431–1456. ISSN: 0733-9429. DOI: 10.1061/(ASCE)0733-9429(1984)110:10(1431). URL: https://ascelibrary.org/doi/10.1061/%28ASCE%290733-9429%281984%29110%3A10%281431%29.

[182] J.W.H. van de Meene and L.C. van Rijn. “The shoreface-connected ridges along the central Dutch coast-part 2: morphological modelling”. In: *Continental Shelf Research* 20 (2000), pp. 2325–2346. ISSN: 02784343. DOI: 10.1016/S0278-4343(00)00049-2. URL: http://www.leovanrijn-sediment.com/papers/P7-2000b.pdf.

[183] Jan W.H van de Meene and Leo C. van Rijn. “The shoreface-connected ridges along the central Dutch coast — part 1: field observations”. In: *Continental Shelf Research* 20.17 (Dec. 2000), pp. 2295–2323. ISSN: 02784343. DOI: 10.1016/S0278-4343(00)00048-0. URL: https://linkinghub.elsevier.com/retrieve/pii/S0278434300000480.

[184] A. van der Giessen, W.P.M. De Ruijter, and J.C. Borst. “Three-dimensional current structure in the Dutch coastal zone”. In: *Netherlands Journal of Sea Research* 25.1-2 (May 1990), pp. 45–55. ISSN: 0077-7579. DOI: 10.1016/0077-7579(90)90007-4. URL: https://www.sciencedirect.com/science/article/pii/0077757990900074.

[185] Carola M. van der Hout. “Suspended matter transport in the coastal turbidity maximum zone along the Holland coast”. PhD thesis. Utrecht University, 2024, p. 116. ISBN: 9789062667055.

[186] Carola M. van der Hout, Theo Gerkema, Janine J. Nauw, and Herman Ridderinkhof. “Observations of a narrow zone of high suspended particulate matter (SPM) concentrations along the Dutch coast”. In: *Continental Shelf Research* 95 (Mar. 2015), pp. 27–38. ISSN: 0278-4343. DOI: 10.1016/J.CSR.2015.01.002.

[187] Carola M. van der Hout, R. Witbaard, M.J.N. Bergman, G.C.A. Duineveld, M.J.C. Rozemeijer, and T. Gerkema. “The dynamics of suspended particulate matter (SPM) and chlorophyll- a from intratidal to annual time scales in a coastal turbidity maximum”. In: *Journal of Sea Research* March (2017). ISSN: 13851101. DOI: 10.1016/j.seares.2017.04.011.

[188] M.M. Rutgers van der Loeff. “Wave effects on sediment water exchange in a submerged sand bed”. In: *Netherlands Journal of Sea Research* 15.1 (Oct. 1981), pp. 100–112. ISSN: 00777579. DOI: 10.1016/0077-7579(81)90009-0. URL: http://linkinghub.elsevier.com/retrieve/pii/0077757981900090.

[189] Johan van der Molen, Karsten Bolding, Naomi Greenwood, and David K Mills. “A 1-D vertical multiple grain size model of suspended particulate matter in combined currents and waves in shelf seas”. In: *Journal of Geophysical Research* 114.F01030 (2009). DOI: 10.1029/2008JF001150.

[190] Johan van der Molen, Piet Ruardij, and Naomi Greenwood. “A 3D SPM model for biogeochemical modelling, with application to the northwest European continental shelf”. In: *Journal of Sea Research* 127 (2017), pp. 63–81. ISSN: 13851101. DOI: 10.1016/j.seares.2016.12.003. URL: http://dx.doi.org/10.1016/j.seares.2016.12.003.

[191] Karin J. van der Reijden, Leo Koop, Sarah O’Flynn, Silvia Garcia, Oscar Bos, Christiaan van Sluis, David J. Maaholm, Peter M.J. Herman, Dick G. Simons, Han Olff, Tom Ysebaert, Mirjam Snellen, Laura L. Govers, Adriaan D. Rijnsdorp, and Ricardo Aguilar. “Discovery of Sabellaria spinulosa reefs in an intensively fished area of the Dutch Continental Shelf, North Sea”. In: *Journal of Sea Research* 144 (Feb. 2019), pp. 85–94. ISSN: 1385-1101. DOI: 10.1016/J.SEARES.2018.11.008.

[192] Ad van der Spek, Andrea Forzoni, and Tommer Vermaas. “Holocene deposits at the lower shoreface and inner shelf of the Dutch coast”. In: *Ocean & Coastal Management* 224 (June 2022), p. 106203. ISSN: 0964-5691. DOI: 10.1016/J.OCECOAMAN.2022.106203.

[193] Ad J.F. van der Spek, Jebbe J. van der Werf, Bart Grasmeijer, Albert Oost, Reinier Schrijvershof, and Tommer Vermaas. *The Kustgenese 2.0 Atlas of the Dutch Lower Shoreface*. Tech. rep. Delft, the Netherlands: Deltares, 2020, p. 86.

[194] Jebbe J. van der Werf, Reinier A. Schrijvershof, Laura B. Brakenhoff, and Bart T. Grasmeijer. “Observations of near-bed orbital velocities and small-scale bedforms on the Dutch lower shoreface”. In: *Ocean & Coastal Management* 218 (Mar. 2022), p. 106012. ISSN: 0964-5691. DOI: 10.1016/J.OCECOAMAN.2021.106012.

[195] G. Van Hoey, F. Bastardie, S. Birchenough, A. De Backer, A. Gill, S. de Koning, S. Hodgson, S. Mangi Chai, J. Steenbergen, E. Termeer, S. van den Burg, and N. Hintzen. *Overview of the effects of offshore wind farms on fisheries and aquaculture*. Tech. rep. 03. Brussels, 2021, p. 99.

[196] Els Verfaillie, Vera Van Lancker, and Marc Van Meirvenne. "Multivariate geostatistics for the predictive modelling of the surficial sand distribution in shelf seas". In: *Continental Shelf Research* 26.19 (Dec. 2006), pp. 2454–2468. DOI: 10.1016/j.csr.2006.07.028. URL: https://linkinghub.elsevier.com/retrieve/pii/S0278434306002536.

[197] M. Visser, W.P.M. de Ruijter, and L. Postma. "Distribution of suspended matter in the Dutch Coastal Zone". In: *Netherlands Journal of Sea Research* 27.2 (1991), pp. 127–143.

[198] VLIZ. *Sediment profile imaging (SPI)*. 2022. URL: https://www.vliz.be/nl/spi.

[199] N. Volkenborn, L. Polerecky, S. I.C. Hedtkamp, J. E.E. van Beusekom, and D. De Beer. "Bioturbation and bioirrigation extend the open exchange regions in permeable sediments". In: *Limnology and Oceanography* 52.5 (Sept. 2007), pp. 1898–1909. ISSN: 1939-5590. DOI: 10.4319/LO.2007.52.5.1898.

[200] D.J.R. Walstra, L.C. van Rijn, M. van Ormondt, C. Brière, and A.M. Talmon. *The Effects of Bed Slope and Wave Skewness on Sediment Transport and Morphology*. 2007. DOI: doi:10.1061/40926(239)11. URL: https://doi.org/10.1061/40926(239)11.

[201] JE Webb and J Theodor. "Irrigation of submerged marine sands through wave action". In: *Nature* 220 (1968), pp. 682–683. ISSN: 0028-0836. DOI: doi:10.1038/220682a0. URL: http://www.nature.com/nature/journal/v220/n5168/abs/220682a0.html.

[202] M. E. Wengrove, D. L. Foster, M. A. de Schipper, and T. C. Lippmann. "Wave and current ripple formation and migration during storms". In: *Proceedings of Coastal Dynamics*. Vol. 129. Helsingør, Denmark, 2017, pp. 955–965.

[203] M. E. Wengrove, D. L. Foster, T. C. Lippmann, M. A. de Schipper, and J. Calantoni. "Observations of Time-Dependent Bedform Transformation in Combined Wave-Current Flows". In: *Journal of Geophysical Research: Oceans* 123.10 (2018), pp. 7581–7598. ISSN: 21699291. DOI: 10.1029/2018JC014357.

[204] M. E. Wengrove, D. L. Foster, T. C. Lippmann, M. A. de Schipper, and J. Calantoni. "Observations of Bedform Migration and Bedload Sediment Transport in Combined Wave-Current Flows". In: *Journal of Geophysical Research: Oceans* 124.7 (2019), pp. 4572–4590. ISSN: 21699291. DOI: 10.1029/2018JC014555.

[205] P. L. Wiberg and C. K. Harris. "Ripple geometry in wave-dominated environments". In: *Journal of Geophysical Research* 99.C1 (1994), pp. 775–789. ISSN: 01480227. DOI: 10.1029/93JC02726.

[206] Patricia L. Wiberg, David E. Drake, and David A. Cacchione. “Sediment resuspension and bed armoring during high bottom stress events on the northern California inner continental shelf: measurements and predictions”. In: *Continental Shelf Research* 14.10-11 (1994), pp. 1191–1219. ISSN: 02784343. DOI: 10.1016/0278-4343(94)90034-5.

[207] J. Widdows, P. L. Friend, A. J. Bale, M. D. Brinsley, N. D. Pope, and C. E.L. Thompson. “Inter-comparison between five devices for determining erodability of intertidal sediments”. In: *Continental Shelf Research* 27.8 (2007), pp. 1174–1189. ISSN: 02784343. DOI: 10.1016/j.csr.2005.10.006.

[208] John P (John Peter) Wilson and John C Gallant. *Terrain analysis: principles and applications*. Ed. by John P (John Peter) Wilson and John C Gallant. New York ; Chichester: Wiley, 2000. ISBN: 0471321885.

[209] Margaret F. J. Wilson, Brian O’Connell, Colin Brown, Janine C. Guinan, and Anthony J. Grehan. “Multiscale Terrain Analysis of Multibeam Bathymetry Data for Habitat Mapping on the Continental Slope”. In: *Marine Geodesy* 30.1-2 (May 2007), pp. 3–35. ISSN: 0149-0419. DOI: 10.1080/01490410701295962. URL: http://www.tandfonline.com/doi/abs/10.1080/01490410701295962.

[210] J C Winterwerp and W G M van Kesteren. *Introduction to the Physics of Cohesive Sediment Dynamics in the Marine Environment*. Developments in Sedimentology. Elsevier Science, 2004. ISBN: 9780080473734. URL: https://books.google.nl/books?id=IMEGdn0FO4kC.

[211] Johan C Winterwerp, Thijs van Kessel, Dirk S van Maren, and Bram C van Prooijen. *Fine Sediment in Open Water: From Fundamentals to Modelling*. Vol. Volume 55. WORLD SCIENTIFIC, 2021, p. 644. ISBN: 978-981-12-4361-5. DOI: doi:10.1142/12473. URL: https://doi.org/10.1142/12473.

[212] Johan C. Winterwerp. *Voorstudie vermindering baggerbezwaar Voorhaven IJmuiden*. Tech. rep. Delft, the Netherlands: WL | Delft Hydraulics, 2001, p. 22. URL: http://resolver.tudelft.nl/uuid:6bedb1eb-2b15-4955-ab94-f282d51a2977.

[213] Johan C. Winterwerp. “On the sedimentation rate of cohesive sediment”. In: *Proceedings in Marine Science* 8 (2007), pp. 209–226. ISSN: 1568-2692. DOI: 10.1016/S1568-2692(07)80014-3.

[214] R Witbaard, G Duineveld, and M J N Bergman. *The final report on the growth and dynamics of Ensis directus in the near coastal zone off Egmond, in relation to environmental conditions in 2011-2012*. Tech. rep. Texel, The Netherlands: Royal Dutch Institute for Sea Research, 2013, p. 79.

[215] Rob Witbaard, Magda J.N. Bergman, Evaline van Weerlee, and Gerard C.A. Duineveld. “An estimation of the effects of Ensis directus on the transport and burial of silt in the near-shore Dutch coastal zone of the North Sea”. In: *Journal of Sea Research* (2016), pp. 1–10. ISSN: 13851101. DOI: 10.1016/j.seares.2016.12.001. URL: http://linkinghub.elsevier.com/retrieve/pii/S1385110116303501.

[216] Rob Witbaard and Johan Craeymeersch. *Littekens op de zeebodem. Een onderzoek naar de faunistische effecten op lange termijn van diepe zandwinning voor de Nederlandse kust*. Tech. rep. Texel, The Netherlands: Royal NIOZ, 2023, p. 42.

[217] Rob Witbaard, Gerard C A Duineveld, Magda J N Bergman, Hans I J Witte, Lennart Groot, and Marcel J C Rozemeijer. “The growth and dynamics of Ensis directus in the near-shore Dutch coastal zone of the North Sea”. In: *Journal of Sea Research* 95 (2015), pp. 95–105. ISSN: 13851101. DOI: 10.1016/j.seares.2014.09.008. URL: http://dx.doi.org/10.1016/j.seares.2014.09.008.

[218] Xianlong Yang, Qingyin Zhang, Xuezhang Li, Xiaoxu Jia, Xiaorong Wei, and Ming’an Shao. “Determination of Soil Texture by Laser Diffraction Method”. In: *Soil Science Society of America Journal* 79.6 (2015), pp. 1556–1566. ISSN: 1435-0661. DOI: 10.2136/sssaj2015.04.0164.

[219] F Zijl, S Laan, L Leummens, T Zijlker, Thijs van Kessel, Vincent van Zelst, Luka Jaksic, Lauriane Vilmin, L Schneider, and L van Duren. *Scenario studies on potential ecosystem effects in future offshore wind farms in the North Sea*. Tech. rep. Delft, The Netherlands: Deltares, 2023, p. 84.

A

Supporting Information for Chapter 4

A

A.1. SOULSBY ET AL. (2012) TIME-DEPENDENT RIPPLE MODEL

The Soulsby et al. (2012) model describes the temporal evolution of ripple length (λ) and height (η) using a set of simple differential equations. For the conceptual model presented in Chapter 4, we only consider ripple height. This is described by:

$$\frac{d\eta}{dt} = \frac{\beta}{T_e}(\eta_{eq} - \eta) \tag{A.1}$$

where:
η = time-dependent bedform height [m]
T_e = characteristic timescale for bedform formation [s]
β = rate of change coefficient [-]
η_{eq} = equilibrium bedform height [m]

Essentially, this equation describes the evolution of ripple height (η) over time, given a relaxation timescale (β/T_e) and an equilibrium bedform height (η_{eq}). The relaxation timescale directly depends on the hydrodynamic forcing, while the equilibrium bedform height is computed using a ripple predictor. For both, the model distinguishes between current- and wave-dominated conditions.

During each timestep (t_i), the model determines if conditions are (a) below incipient motion, (b) current-dominated or (c) wave-dominated. This is done by computing both the current-induced Shields' parameter (θ'_c), the wave-induced Shields' parameter (θ'_w) and evaluating these against the Shields criterion (θ'_{cr}). If conditions are below incipient motion, there is no change in ripple height. If conditions are current-dominated or wave-dominated, the ripple height changes if it is not yet equal to the equilibrium ripple height.

In the following sections we present the used hydrodynamic inputs and constants (A.2), computation of the Shields' parameters and how current- or wave-dominance is established (A.3), how the relaxation timescale is computed (A.4) and finally, the definition of the applied ripple predictors (A.5).

A.2. HYDRODYNAMIC INPUT AND CONSTANTS

The model uses a set of constants and hydrodynamic input parameters. The used constants are listed in Table A.1:

The hydrodynamic inputs are the radial wave frequency (ω), near-bed orbital velocity due to waves (u_w) and depth-averaged flow velocity (U). The wave-dependent parameters (ω and u_w) are defined below, together with the formulations used to compute them for our application.

$$\omega = \frac{2\pi}{T} \tag{A.2}$$

where:
T = characteristic wave period [s]

Table A.1.: Constants for the time-dependent ripple model

Constant	description
g	gravitational acceleration [m/s^2]
d_{50}	median grain size [m]
$s = \frac{\rho_s}{\rho_w}$	relative density [-]
ρ_s	sediment density [kg/m^3]
ρ_w	water density [kg/m^3]
ν	kinematic viscosity [m^2/s]

$$u_w = \frac{0.5H\omega}{\sinh(kh)} \tag{A.3}$$

where:
H = representative wave height [m]
h = water depth [m]
k = wave number [m^{-1}]

The wave number (k) is defined according to the Guo (2002) approximation of the dispersion relation:

$$k = \frac{\omega^2}{g}\left(1 - \left(e^{-\omega\left[\sqrt{\frac{h}{g}}\right]^{2.5}}\right)^{-0.4}\right) \tag{A.4}$$

The wave friction factor is determined following Swart (1974):

$$f_w = e^{\left(-5.977 + \left(5.213\left(\frac{A}{2.5d_{50}}\right)^{-0.194}\right)\right)} \tag{A.5}$$

where:
$A = \frac{u_w}{\omega}$ = the near-bed orbital excursion [m]

A.3. ESTABLISHING CURRENT- OR WAVE-DOMINANCE

The specified constants and hydrodynamic inputs are used to compute the current-induced Shields' parameter (θ'_c), the wave-induced Shields' parameter (θ'_w).

In order to do so, first the current-induced bed shear stress (τ_c) and wave-induced bed shear stress (τ_w) are computed according to Soulsby and Clarke (2005):

$$\tau_c = \rho_w C_D U^2 \tag{A.6}$$

where:
$C_D = \frac{\kappa^2}{\left(1+\ln\left(\frac{z_0}{h}\right)\right)^2}$ = the bottom friction factor [-] (Soulsby 1997)
$z_0 = \frac{d_{50}}{12}$ = bed roughness length [m]

$$\tau_w = \frac{1}{2}\rho_w f_w u_w^2 \tag{A.7}$$

The Shields parameter is then computed following:

$$\theta_c^{'} = \frac{\tau_c}{g\left(\rho_s - \rho_w\right) d_{50}} \tag{A.8}$$

$$\theta_w^{'} = \frac{\tau_w}{g\left(\rho_s - \rho_w\right) d_{50}} \tag{A.9}$$

The Shields criterion is given by:

$$\theta_{cr} = \left(\frac{0.3}{1 + 1.2D_*}\right) + \left(0.055(1 - e^{-0.02D_*})\right) \tag{A.10}$$

where D_* is the dimensionless grain size:

$$D_* = d_{50}\left(\frac{g\,(s-1)}{\nu^2}\right)^{\frac{1}{3}} \tag{A.11}$$

The wave-current dominance criterion is defined as (Marten 2010):

- if $\theta_w^{'} \geq \max\left(0.42{\theta_c^{'}}^{0.47}, 0.08\right)$, ripples are wave-dominated.
- Else, ripples are current-dominated.

A.4. COMPUTING THE RELAXATION TIMESCALE

The relaxation timescale (β / T_e) determines how fast ripples will adjust to the governing hydrodynamic conditions. This timescale differs for the current-dominated and wave-dominated conditions. For current-dominated conditions, it is defined by:

$$\beta_{\eta,c} = \frac{20\left(\theta_c^{'} - \theta_{cr}\right)^{1.5}}{2.5 + \left(\theta_c^{'} - \theta_{cr}\right)^{1.5}} \tag{A.12}$$

$$T_c = \frac{\eta_{eq,c}\lambda_{eq,c}}{\left[g(s-1)d_{50}^3\right]^{1/2}} \tag{A.13}$$

The equilibrium ripple height η_{eq}) and the ripple length (λ_{eq}) are given in Appendix A.5. For wave-dominated conditions, it is defined by:

$$T_w \equiv T \tag{A.14}$$

$$\beta_w = \frac{2.996\Psi^{1.07}}{(21700 + \Psi^{1.07})} \tag{A.15}$$

where:
$\Psi = \frac{u_w^2}{g(s-1)d_{50}}$ is the wave mobility number

A.5. PREDICTING THE EQUILIBRIUM RIPPLE HEIGHT

For both current-dominated and wave-dominated conditions, equilibrium bedform heights η_{eq} are computed using a set of predictors. For current-dominated conditions, the equilibrium height of current-induced ripples depends chiefly on the grain size (Baas *et al.* 2000):

$$\eta_{eq,c} = d_{50} 202 D_*^{-0.554} \; for 1.2 < D_* < 16 \tag{A.16}$$

For wave-dominated conditions, a wide range of wave-induced ripple predictors exist. We summarize the four predictors used in Chapter 4 in Table A.2.

Table A.2.: Wave ripple predictors used in time-dependent ripple model

source	Expression for $\lambda_{eq,w}$	Expression for $\eta_{eq,w}$
Traykovski (2007) TR_07 (assuming the peak equilibrium wave number is dominant ripple)	if $u_w \leq 4.2 w_s$: $1.5 \frac{u_w}{\omega_r}$ if $u_w > 4.2 w_s$: $\frac{4.2 w_s}{\omega_r}$	$\frac{0.25 \eta_{eq,p}}{\sqrt{\sigma (2\pi)^{1/2}}}$ where: $\eta_{eq,p} = 0.16 \lambda_{eq,w}$ $\sigma = 0.1$
Traykovski (2007) as implemented by Marten (2010) MN_10	if $u_w \leq 4.2 w_s$: $1.24 A$ if $u_w > 4.2 w_s$: $\frac{2.1 w_s}{\omega_r}$	$0.16 \lambda_{eq,w}$
Soulsby and Clarke (2005) SW_05	$\left[1 + 1.87 \times 10^{-3} \Delta Y_1\right]^{-1} A$ where: $Y_1 : 1 - \exp\left[\left(-2.0 \times 10^{-4}\right)^{1.5}\right]$	$0.15 \left[Y_2\right] \lambda_{eq,w}$ where: $Y_2 : 1 - \exp\left\{-\left(\frac{5000}{\Delta}\right)^{3.5}\right\}$
Wiberg and Harris (1994) WH_94	$0.62 A$	$0.17 \lambda_{eq,w}$

where:
w_s = settling velocity of sand [m/s]
$\Delta = \frac{A}{d_{50}}$

Dankwoord

Credo
Je mist meer
Dan je meemaakt
Helemaal
Niet erg

Martin Bril

Het laatste loodje van mijn proefschrift: tijd om terug te blikken op de voorbije jaren en om te reflecteren op de momenten dat het afronden van dit boekje ver weg leek. Maar vooral om mijn dank uit te spreken naar de mensen die op hun eigen manier hebben bijgedragen aan deze reis.

Mijn eerste woorden van dank gaan uit naar mijn begeleiders Bram, Stefan en Han. Ik ben dankbaar dat we dit traject, wat een kleine tien jaar geleden begon, samen kunnen volbrengen.

Bram, als ik terugdenk aan de afgelopen jaren dan springt boven alles je positieve energie eruit. Jouw enthousiasme, passie voor ons werk en je nieuwe ideeën werkten, en werken nog steeds, aanstekelijk. Het zeegaande onderzoek was voor ons beiden nieuw en we moesten daar onze weg in vinden. Ik ben dankbaar voor de vrijheid die je me daarin hebt gegeven en dat je me hebt gesteund op de momenten dat dat nodig was. In de afgelopen jaren stond het proefschrift meer dan eens op de waakvlam, dank voor jouw geduld hierin en het blijven aanwakkeren van dat vuurtje.

Stefan, jouw aandacht voor het grotere plaatje is van grote waarde geweest. Dat kwam vaak in de vorm van subtiele, maar beslist heldere aanwijzingen die de koers van dit proefschrift mede hebben bepaald. Tijdens de pandemie heb je altijd oog gehouden voor het welzijn van ons als promovendi. Daar ben ik je zeer dankbaar voor! Daarnaast vind ik het mooi om te zien dat je ons Waterbouw-hardloopclubje op faculteitsniveau voortzet.

Han, onze eerste kennismaking ligt al bijna 13 jaar achter ons en ik had niet kunnen voorzien waar die toe zou leiden. Wat begon bij het vak *Sediment Dynamics* mondde via een stage en afstudeerwerk uit in dit promotieonderzoek. Ik heb grote waardering voor je kritische blik, je bevlogenheid en kunde. Je aanmoedigingen om beknopt te schrijven en het proefschrift af te ronden heb ik ter harte genomen. Dank voor je oprechte interesse en alle kansen die je me geboden hebt.

Mijn onderzoek vormde onderdeel van het project SANDBOX, waarin ik naast Johan en Chiu een van de drie promovendi was. Ik heb veel van jullie geleerd als het aankomt op zandgolven en benthische ecologie, en denk met plezier terug aan onze samenwerking. Daarbij springen onze vaartochten met de RV Pelagia en Navicula er uit, als eerste kennismaking met het werk op zee. Een speciaal woord van dank voor Karline Soetaert, die ons als jonge onderzoekers het vertrouwen gaf om deze campagnes in te vullen naar ons eigen inzicht. In diezelfde adem wil ik de bemanning van deze onderzoeksschepen noemen. Bedankt voor het warme welkom en jullie harde werk om de data te verzamelen die in dit proefschrift zijn beland.

In Hoofdstuk 2 en 4 van dit proefschrift analyseren we datasets die tot stand zijn gekomen door de jarenlange inspanningen van anderen. Wil Borst en Onno van Tongeren: ik ben jullie zeer erkentelijk voor jullie inspanningen om de ecologische monitoring rond de aanleg van Maasvlakte 2 zo nauwgezet uit te voeren. Het werk dat in Hoofdstuk 2 wordt gepresenteerd was niet mogelijk geweest zonder jullie waardevolle inbreng. Voor Hoofdstuk 4 ben ik veel dank verschuldigd aan Carola van der Hout en Rob Witbaard. Jullie aanmoedigingen om met de data aan de slag te gaan en het proefschrift af te ronden waren een meer dan welkom duwtje in de rug.

Hoewel er (bijna) een volledig promotietraject past in de periode sinds ik de deur van het Waterlab achter me dicht trok, koester ik de positieve sfeer als een blijvende

herinnering. Aan mijn kamergenoten Yorick, María, Merel, Jianwei, Gonzalo en Zeinab: hoewel we allen aan verschillende onderwerpen werkten was er altijd een welgemeende interesse in elkaars werk en voelde het voor mij altijd als een fijne uitvalsbasis.

For the Waterlab as a whole, I fondly remember all the kind and talented colleagues. Thank you for the little acts of kindness that give colour to our lives. Thanks for the helping hands during field campaigns, going for early-morning or late-afternoon runs and the great discussions over a coffee or a beer. I cherish the mildly weird but equally great memories such as axe-throwing in our most beautiful Christmas sweaters, or an entire office decorated with flamingos on my 30th birthday. A big thank you to Claire, Jaap, Pieter, Andres, Nici, Victor, Liselot, Irene, Lodewijk, Stuart, Floris, Alejandra, Carine, Matt, Anne, Jill, Ana, Patricia, Clàudia, Lennart, and all the others.

Waar mijn tijd in het Waterlab eindigde, daar begonnen mijn eerste stappen als fulltime onderzoeker bij Deltares. In de jaren ervoor werkte ik er al part-time, maar begin 2021 was er maar weinig om zeker van te zijn. Dank aan Luca van Duren en Peter Herman voor het vertrouwen dat zij in mij stelden toen zij mij binnenhaalden voor een postdoc onderzoek naar de ecologische effecten van wind op zee. Die dank gaat evengoed uit naar directe collega's en leidinggevenden, die mij de ruimte gaven om dit proefschrift af te ronden.

Ik ben dankbaar voor mijn vrienden met wie ik het gelukkig ook over hele andere dingen dan de Noordzee kan hebben. Toch wel een woord van dank aan hen die me bleven vragen 'Hoe is het eigenlijk met dat proefschrift?'. Ik ben blij dat ik mijn belofte 'Het is nog niet af, maar dat komt het wel' in heb kunnen lossen.

Dank aan mijn familie en schoonfamilie, voor het fijne, warme thuis waar ik altijd op terug kan vallen. Jullie zijn en blijven op vele manieren een voorbeeld voor mij.

De laatste woorden van dit proefschrift zijn voor mijn allerliefste Stéphanie. Ons oog viel op elkaar toen ik er net mee begon, met dit onderzoek. En het geduld wat anderen met mij op moesten brengen, dat gold nog wel het meest voor jou. Ik ben zo dankbaar voor je liefde, voor hoe attent je bent en hoeveel plezier we samen hebben. De afgelopen jaren hebben ons al zoveel mooie herinneringen gebracht dat ik vol overtuiging uitkijk naar wat er komen gaat. Zo lang als het samen met jou is, dan is het goed.

Erik Hendriks
Oosterhout, 7 Januari 2026

List of Publications

Journal Articles

6. **Hendriks, E.**, Langedock, K., van Duren, L.A., Vanaverbeke, J., Boone, W., Soetaert, K. (2025) The impact of offshore wind turbine foundations on local hydrodynamics and stratification in the Southern North Sea. *Frontiers in Marine Science*. doi:10.3389/fmars.2025.1619577

5. Van der Eijk, M., Plenker, D., **Hendriks, E.**, de Wit, L. (2024) Modeling the hydrodynamic wake of an offshore solar array in OpenFOAM. *Frontiers in Energy Research*. doi:10.3389/fenrg.2024.1434356

4. **Hendriks, E.**, van Prooijen, B.C., Cheng, C.H., Aarninkhof, S.G.J., Winterwerp, J.C., Soetaert, K.E. (2022) An explanatory model for the burial of fines in the sandy seabed of the southern North Sea. *Marine Geology*. doi:10.1016/j.margeo.2022.106953

3. Pearson, S.G., Verney, R., van Prooijen, B.C., Tran, D., **Hendriks, E.**, Jacquet, M., Wang, Z.B. (2021) Characterizing the composition of sand and mud suspensions in coastal and estuarine environments using combined optical and acoustic measurements. *Journal of Geophysical Research: Oceans*. doi:10.1029/2021JC017354

2. **Hendriks, H.C.M.**, van Prooijen, B.C., Aarninkhof, S.G.J., Winterwerp, J.C. (2020) How human activities affect the fine sediment distribution in the Dutch Coastal Zone seabed. *Geomorphology*. doi:10.1016/j.geomorph.2020.107314

1. Winterwerp, J.C., Vroom, J., Wang, Z.B., Krebs, M., **Hendriks, E.**, van Maren, D.S., Schrottke, K., Borgsmüller, C., Schöl, A. (2017) SPM response to tide and river flow in the hyper-turbid Ems River. *Ocean Dynamics*. doi:10.1007/s10236-017-1043-6

Conference contributions

10. **Hendriks, E.**, Langedock, K., van Duren, L.A., Vanaverbeke, J., Boone, W., Soetaert, K. (2024) Near-field measurements around offshore wind turbines show how they enhance hydrodynamics in their direct environment. *EGU General Assembly Conference Abstracts*

9. **Hendriks, E.**, Langedock, K., van Duren, L.A., Vanaverbeke, J., Boone, W., Soetaert, K. (2024). Near-field measurements around offshore wind turbines show how they enhance hydrodynamics in their direct environment. *ASLO Aquatic Sciences Meeting 2023*

8. **Hendriks, E.**, Van Prooijen, B.C., Cheng, C.H., Aarninkhof, S.G.J., Winterwerp, J.C., Soetaert, K.E. (2021). How are fines buried in a sandy seabed? *INTERCOH 2021: 16th International Conference on Cohesive Sediment Transport Processes*

7. **Hendriks, E.**, Van Kessel, T., Vijverberg, T., Nobel, A.J., Doets, I., Klein, M.D., Sittoni, L., Uittenbogaard, R., Winterwerp, J.C. (2021). A 1DV-model for submerged density currents. *INTERCOH 2021: 16th International Conference on Cohesive Sediment Transport Processes*

6. Pearson, S.G., Verney, R., **Hendriks, E.**, Tran, D., Jacquet, M., Wang, Z.B., Van Prooijen, B.C. (2021) Characterizing the composition of suspended sand and mud suspensions in coastal environments using combined optical and acoustic measurements. *INTERCOH 2021: 16th International Conference on Cohesive Sediment Transport Processes*

5. Pearson, S.G., Verney, R., **Hendriks, E.**, Tran, D., Jacquet, M., Wang, Z.B., Van Prooijen, B.C. (2021) Characterizing the Composition of Suspended Sand and Mud Suspensions in Coastal Environments using Combined Optical and Acoustic Measurements. *Netherlands Centre for Coastal Research Conference (NCK Days) 2021*

4. **Hendriks, E.**, Van Prooijen, B. C., Cheng, C. H., Aarninkhof, S. G. J., Winterwerp, J. C., Soetaert, K. E. (2020). Towards imporving model schematisations for the burial of fines within a sandy seabed. *ECSA 58 – EMECS 13: Estuaries and coastal seas in the Anthropocene – Structure, functions, services and management*

3. **Hendriks, E.**, Van Prooijen, B.C., Aarninkhof, S.G.J., Soetaert, K.E., Winterwerp, H. (2019) Feedbacks between Fine-Grained Sediment Deposits and Bedforms in a Predominantly Sandy Seabed: Field Observations from the Southern North Sea. *Geophysical Research Abstracts, EGU General Assembly 2019*

2. **Hendriks, E.**, Van Prooijen, B.C., Winterwerp, J.C., Aarninkhof, S.G.J., Van der Hout, C. M., Witbaard, R. (2017) Response of SPM concentrations to storms in the North Sea: Investigating the water-bed exchange of fine sediments. *INTERCOH 2017: 14th International Conference on Cohesive Sediment Transport Processes*

1. **Hendriks, E.**, Van Prooijen, B.C., Winterwerp, J.C, Aarninkhof, S.G.J.(2017) Investigating the buffering of fines in a sandy sebaed: planned field measurements along the Egmond aan Zee transect. *Netherlands Centre for Coastal Research Conference (NCK Days) 2017*

About the Author

Erik Hendriks was born on January 16, 1989, in 's-Hertogenbosch, the Netherlands. He grew up in the nearby village of Vught, where he completed his primary and secondary education. In 2008, he began studying Civil Engineering at Delft University of Technology, with the goal of becoming a structural engineer. Over time, however, his interests shifted towards Hydraulic Engineering. This growing fascination led him to pursue an MSc in Hydraulic Engineering and Water Resources management at Delft University of Technology and the National University of Singapore. In his MSc thesis, he investigated how environmental factors affect the settling and self-weight consolidation of mud. Intrigued by the behaviour of these fine particles, Erik began his PhD at Delft University of Technology in 2016, while also working part-time at Deltares. Since 2021, he has been employed full-time at Deltares, where he focuses on the impact of human activities on the North Sea and its ecosystem. Erik lives in Oosterhout together with his wife. In his free time, he enjoys running, playing tennis and spending time with friends and family. As a sports and music enthusiast, he regularly attends matches and concerts.